

The role of ppGpp in E. coli cell size control

Büke, F.

DOI

[10.4233/uuid:706a49f8-f86d-49ef-aea8-22ab105b8175](https://doi.org/10.4233/uuid:706a49f8-f86d-49ef-aea8-22ab105b8175)

Publication date

2020

Document Version

Final published version

Citation (APA)

Büke, F. (2020). *The role of ppGpp in E. coli cell size control*. [Dissertation (TU Delft), Delft University of Technology]. <https://doi.org/10.4233/uuid:706a49f8-f86d-49ef-aea8-22ab105b8175>

Important note

To cite this publication, please use the final published version (if applicable).
Please check the document version above.

Copyright

Other than for strictly personal use, it is not permitted to download, forward or distribute the text or part of it, without the consent of the author(s) and/or copyright holder(s), unless the work is under an open content license such as Creative Commons.

Takedown policy

Please contact us and provide details if you believe this document breaches copyrights.
We will remove access to the work immediately and investigate your claim.

The role of ppGpp in *E. coli* cell size control

Dissertation

for the purpose of obtaining the degree of doctor

at Delft University of Technology

by the authority of the Rector Magnificus, Prof. dr. ir. T.H.J.J. van der Hagen,

Chair of the Board of Doctorates

to be defended publicly on

Wednesday 16 September 2020 at 12:30 o'clock

by

Ferhat BÜKE

Master of Science in Microbial Biotechnologies and Health

Leiden University, IBL, Netherlands

born in Bursa, Turkey

This dissertation has been approved by the co-promoters

Prof. dr. ir S. J Tans Delft University of Technology

Dr. G. E. Bokinsky Delft University of Technology

Composition of the doctoral committee

Rector magnificus chairman

Prof. dr. ir S. J Tans Delft University of Technology, promotor

Dr. G. E. Bokinsky Delft University of Technology, promotor

Independent members:

Prof. dr. ir S. J. J. Brouns Delft University of Technology

Prof. dr. M. Heinemann University of Groningen

Prof. dr. F.J. Bruggeman Vrije Universiteit Amsterdam

Prof. dr. P. R. ten Wolde AMOLF

Dr. D. E. Rozen Universteit Leiden

Reserve member:

Prof. dr. G.H. Koenderink Delft University of Technology



Keywords: Single cell, live cell microscopy, microfluidics, metabolism, regulation, *E. coli*, cell size, growth, ppGpp, Guanosine tetraphosphate,

Cover by: Ferhat Büke

Copyright © 2020 Ferhat Büke

ISBN: 978-94-6402-501-9

An electronic copy of this dissertation is available at: <http://repository.tudelft.nl/>

Table of contents

Chapter 1	Introduction.....	1
1.1	A brief history of humans and microbes.....	2
1.2	Growing and observing microbes.....	3
1.3	Reading and altering the code of life.....	4
1.4	From sequence to structure and structure to function.....	5
1.5	Regulatory loops that keep bacteria alive.....	6
Chapter 2	Stochasticity in cellular metabolism and growth: approaches and consequences.....	15
2.1	Stochasticity and metabolism.....	16
2.2	Enzyme expression generates metabolic noise.....	16
2.3	(Mis)matching pathways.....	18
2.4	Metabolism at the center.....	18
2.5	Benefits of metabolic fluctuations.....	20
2.6	An expanding array of experimental approaches.....	21
2.7	Concluding remarks.....	21
Chapter 3	ppGpp is a bacterial cell size regulator.....	27
3.1	Summary.....	28
3.2	Results.....	28
3.2.1	Ectopic control of ppGpp synthesis and hydrolysis.....	28
3.2.2	ppGpp exerts cell size control.....	28
3.2.3	ppGpp dynamically controls added cell size.....	29
3.2.4	Division accelerates transiently to achieve constant added size after induced ppGpp synthesis.....	33
3.3	Conclusions.....	35
3.4	Supplementary Information.....	36
3.5	Materials and methods.....	39

Chapter 4 Engineering a light activatable ppGpp hydrolysis enzyme..... 47

4.1 Introduction..... 48

4.2 Results..... 50

 4.2.1 Methodology of engineering and testing a light activatable ppGpp hydrolysis enzyme..... 50

 4.2.2 Variant (-3) rescues growth from ectopic ppGpp synthesis in response to light..... 51

 4.2.3 Engineering an improved variant with less activity in dark by increasing the shared helix's stability..... 54

 4.2.4 Testing the new mutants in minimal media to observe growth arrest with light on agar plates and in liquid culture..... 56

4.3 Discussion..... 57

4.4 Supplementary Information..... 60

4.5 Materials and methods..... 62

Chapter 5 Post-translational control is sufficient to coordinate membrane synthesis with growth in *Escherichia coli*..... 67

5.1 Introduction..... 68

5.2 Results..... 68

 5.2.1 The PL to biomass ratio varies inversely with μ 68

 5.2.2 Allosteric regulation of PlsB activity is sufficient to couple PL flux with μ 69

 5.2.3 Mathematical modelling supports PlsB control of steady-state PL synthesis..... 72

 5.2.4 Translation inhibition causes carbon overflow into fatty acid synthesis..... 73

 5.2.5 Moderate ppGpp concentrations regulate PlsB via post-translational control..... 75

5.3 Discussion..... 76

5.4 Supplementary Information..... 79

5.5 Materials and methods..... 86

Summary.....	95
Samenvatting.....	99
Acknowledgements.....	103
Publications.....	105
Curriculum vitae.....	106

1

Introduction

1.1 A brief history of humans and microbes

Even though the first identification of microbial life dates to late 1600s, humans have unknowingly coexisted with microbes since the first of us walked the Earth. Earliest evidence for active use of various microbes and yeast dates back to 13,000 years ago¹ which provided early humans with richer nutrients through fermentation. Conversely up until early 1900s one of the most common reasons of death were diseases transmitted by microorganisms². Thus, our relationship with microbes were complicated at best since the dawn of time.

Up until the discovery of microbial life and single cells by Antonio van Leeuwenhoek or Athanasius Kircher (debate ongoing) in late 1600s³, the basic building blocks of life were unknown. In fact, people believed that life arises from combinations of various inanimate objects, namely “spontaneous generation” and diseases were attributed to supernatural phenomena. Germ theory of disease; which is the identification of microorganisms as the cause of most diseases, had to wait till late 1800s for the work of Louis Pasteur and Robert Koch³. They also showed that fermentation was a microbial process, linking different microscopic lifeforms to macroscopic effects for the first time.

Since then we have discovered antibiotics and viral tools to fight against the “bad bacteria”^{4,5}. Methods which allowed us to enhance fermentation strains -good bacteria- led to more efficient and tastier nutrient generation^{6,7}. Furthermore, we constructed microorganisms which can produce commercial and medical compounds that they naturally could not^{8,9}. All of these were allowed by recent advances in biology, chemistry, material sciences, computational techniques and many more disciplines and a deeper understanding of the inner workings of microbial life. With these developments diseases caused by microorganisms are no longer such a large portion of deaths². Furthermore scientists are looking to utilize microbes in futuristic tasks, such as mining regolith from the surface of the moon¹⁰

In this introductory chapter we will briefly review the history and recent developments in bacterial culturing techniques which have led to the generation of microfluidic flow cells. These devices allow scientists to observe single cell dynamics without disrupting their growth by constantly supplying nutrients and removing waste. Such a device was instrumental in some of the work reviewed in chapter 2 and our research described in chapter 3. Further we will discuss how advancements in genetics, structural biology and protein engineering are allowing scientists to create proteins with functions that do not naturally occur. Our work in chapter 4 would not be possible without the modern tools to modify genetic data and the structural understanding of protein function.

1.2 Growing and observing microbes

Currently up to a trillion species of bacteria are estimated to populate the Earth¹¹. Of these, only a small fraction has been individually isolated from natural environments and grown in laboratories¹². Bacteria like all other species have evolved to survive and thrive in their natural environments. However, in order to understand how specific bacteria function in molecular detail, it is imperative to isolate a pure sample and grow it in laboratory conditions. This allows researchers to grow bacteria in large quantities and observe various functions in molecular detail.

It has been more than 200 years since the invention of agar plates by Richard Petri in Robert Koch's laboratory. Since then, they still allow scientists today to isolate individual colonies of bacteria which arise from a single cell, guaranteeing isolation. Agarose can be dissolved in water at high temperatures when cooled to room temperature, agarose polymerizes and leads to a gelatinous solid which presents a solid surface for bacteria to be grown and isolated. However, in order to grow high quantities of bacteria and isolate products, agar plates are not appropriate. This is where liquid media becomes effective.

The first method of observing single cells was used by van Leeuwenhoek himself when he looked at a drop of pond water using his microscope. Pond water is the natural growth environment of many microorganisms and thus he inadvertently used a liquid media to observe different microscopic life forms. Artificially created liquid media allow bacteria to grow to high densities. Today various different liquid media are used to grow and analyse different species of bacteria¹³. Measurements and identification of various cellular components such as DNA, protein and metabolites along with many industrial applications would not be possible without liquid growth media such as M9, MOPS or LB. Further these defined media allowed scientists to test specific nutritional requirements of bacteria shining light on their biochemistry. It was also shown that bacteria such as *E. coli* could grow under a large variety of conditions. Under favourable conditions bacteria would grow fast and if the nutrient quality is low, growth would be slower¹⁴. Utilizing only basic macro nutrients; glucose, ammonium, phosphate and sulphate along with micronutrients such as magnesium or iron, in a pH balanced environment *E. coli* can double its numbers every 45 minutes. This suggested an immense biochemical potential for *E. coli* as synthesis of a new bacteria from these simple nutrients requires thousands of different chemical reactions. In turn if a cocktail of amino acids is also added to this media, doubling time goes down to 25 minutes since bacteria spends more of its resources on growth.

Both methods above however present the bacteria with a finite source of nutrient and growing space. Therefore, after consuming the nutrients or filling the space, bacteria stop growing and enter into stationary phase¹⁵. In order to research and use bacteria as microscopic factories, bioreactors were then developed. Bioreactors are volumes of liquid media where new nutrients can be supplied at the same rate of bacterial growth. Furthermore acidity, oxygenation, waste levels and so on can be monitored

and modified to keep a constant growth environment. This allows a culture to run indefinitely as long as nutrients are supplied, and excess bacteria growth is removed. Which in turn allows continuous production of the target chemical and increases efficiency for bio-industrial purposes. Also, since the environment can be modified at the will of the researcher, various functions of bacteria can be observed under induced changes^{16–18} which could be harder or impossible to replicate using cells grown in a limited liquid environment due to time constraints.

Tiny versions of these bioreactors, generally named “microfluidic flow cells”, allow researchers to observe dynamics of individual cells under the microscope while feeding in nutrients and removing excess growth and waste. These devices are typically made out of transparent PDMS which can be poured into moulds to achieve nano to micro-meter scale features^{19,20}. After removal from the mould, PDMS device can then be attached to glass slides covalently using plasma treatment. The features can be designed to trap bacteria between the chip and the glass slide while nutrients can be pumped in and excess cells can be removed through built in flow channels. This allows for continuous growth and observations of individual bacteria throughout the experiment. Using switches prior to chip’s input, researchers can shift between different media conditions rapidly and observe the effects on the bacteria at the single cell level revealing hidden biology. Dynamical single cell measurements help characterize biological functions by observing for example correlations between bacterial growth rate and metabolism²¹ or localization of various macro-molecules²². New developments in nanoscale fabrication start to allow chips that can generate gradients²³ and dynamic incremental switches²⁴ between multiple inputs which will no doubt allow more complex experiments and increase our understanding of bacterial life.

1.3 Reading and altering the code of life

Methods to isolate and grow bacteria in large quantities allowed scientists to answer basic questions regarding the chemical composition and function of life. Identification of DNA as the hereditary material dates back to early 1900s. This was allowed by growing virulent and non-virulent Pneumococci strains to large quantities and harvesting biochemical materials. A mix of the purified DNA fraction of a virulent strain with a live non-virulent strain was shown to be virulent when either of the components by themselves were not²⁵. This proved that ability to build a capsid which led to virulence was carried by the DNA. Soon after the identification of DNA’s structure by Franklin, Watson and Crick, coining of “central dogma” linked the nucleotide sequence of DNA with amino acid sequence of proteins in 1958. It took more than a decade however for first method to sequence DNA was perfected by Sanger in 1977. He then used it to sequence the first full genome, albeit a puny bacteriophage genome with around 170.000 base pairs²⁶. In 2003 full genome of a person was sequenced after years of work and 2.7 billion dollars spent (~3.000.000.000 base pairs). Today a whole human genome costs as low as 1000 dollars to sequence with the use of modern sequencing techniques^{27,28}. This inflow of sequence information gave rise to a new

field of computational genetics which among other things revealed hereditary links between all living life forms and became one of the strongest tools to analyse life history.

Back in early 1900's, even though DNA was not known as the information carrier, researchers were already modifying it using X-Rays. Nobel prize winning work of Muller showed that hereditary information of organisms could be altered by X-Rays^{29,30}. Since then a myriad of methods were discovered to alter genetic information in a more nuanced manner. These methods either use externally built genetic sequences to be transformed into target bacteria³¹ or small alterations in bacteria's own genetic manipulation machinery to precisely control where and what will be changed^{32,33}. Methods such as Restriction Cloning, SLICE or Gibson Assembly allow scientists to build DNA sequences ranging from 10s of base pairs to hundreds of thousands. Using such techniques entire genes and even chromosomes can be built and transformed into bacteria³⁴. For example insulin was produced by the company Genentech in late 1970s by transforming human insulin gene into *E. coli*³⁵. Famously CRISPR/Cas9 system of bacteria was recently modified to precisely manipulate genetic material of living cells³⁶. Techniques developed using this allows turning on/off genes and deletions or manipulations to the genetic code in vivo. Recently even human embryos were genetically altered using a variation of the CRISPR system leading to the first genetically modified humans and a deep ethical discussion³⁷. Today a researcher can create an arbitrary combination of genes from different life forms over a single week which has been resulting in new discoveries at an increasingly faster rate.

1.4 From sequence to structure and structure to function.

Sanger's sequencing capabilities were beyond DNA, he also managed to discover the amino acid sequence of the human protein Insulin back in 1949³⁸. This was the first direct proof that proteins were sequences of amino acids. Even though it was first theorized by Astbury as early as 1930s after realizing that many proteins were denaturing into fibrous structures³⁹. In the late 1950s first structures were being resolved for haemoglobin and myoglobin⁴⁰. Today several new techniques allow for atomic scale resolution such as Cryo-EM microscopy where individual proteins are frozen and imaged with electron microscopy⁴¹, Nuclear Magnetic Resonance Spectroscopy where quantum mechanical properties of each nucleus are measured to reveal structure⁴², and x-ray crystallography where hundreds of proteins align to form a crystal which allows scientists to reconstruct structures from x-ray diffraction patterns⁴³. Today there is more than 100.000 structure entries in the protein data bank⁴⁴. Furthermore, advances in structure prediction allow scientists to estimate the structure of a protein from its sequence⁴⁰ which aids in discovering new functions and proteins from genetic sequences.

The advances in computational power, sequencing, mutagenesis and structure resolving led to the discovery of distinct functional domains in proteins. First hints that

proteins had functional domains came with the discovery of specific inhibitors that are similar in structure and chemistry to the natural substrate⁴⁵. Later specific amino acids were hypothesized to be “located at the active site” using chemical alterations to the reaction environment and observing the activity differences of enzyme⁴⁶. A general approach where mutations on single amino acids or larger alterations to gene sequences followed by activity testing, since then revealed thousands of functional domains⁴⁷ responsible for localization⁴⁸, DNA binding⁴⁹, protein-protein interactions⁵⁰, light responding⁵¹ and so on. With the increase in known sequence and structure activity information, predictive computational models helped discovering many more domains from different species’ gene sequences⁴⁰, along with different functions such as fluorescent proteins⁵².

By combining known functional domains in creative ways scientists have created a myriad of chimeric proteins and gene circuits^{53,54}. These allow distinct functions which normally do not co-occur in nature to be combined in single bacteria. For example by combining a light responding domain from a cyanobacteria with an *E.coli* kinase EnvZ in a single enzyme, researchers managed to control the kinase reaction with light⁵⁵. Later by combining other genetic elements from a phage and other bacteria in a single *E.coli* they created a genetic circuit that could detect edges on a projected image⁵⁶ a feat normally achieved by computer software. Another group created a circuit which oscillates production of two fluorophores. The colour information can then be used to estimate time the bacteria spent in a given environment such as patient gut⁵⁷. This type of research where cell’s DNA is programmed like software to achieve abstract tasks is possible through not only a deep understanding and control of each component but also modelling tools which allow calculation of the interactions. In the coming years with advances in computational tools and structural biology, we could start engineering protein structures and functions from scratch. The genetic and functional diversity on Earth is a testament to the possibilities arising from different combinations of 20 amino acids. This represents one of the biggest promises to improving humankind’s ability to conduct biochemistry.

1.5 Regulatory loops that keep bacteria alive

Understanding how bacteria work will allow us to unlock the hidden biochemical potential of bacteria for our purposes. In order to manipulate and engineer bacteria however, we first have to figure out how their systems work so that we can predict the effects of various alterations we might try. Here we discuss recent discoveries in cellular physiology and our work focusing on regulation of growth, cell size and metabolism.

In Chapter 2 we review the work that has been conducted in the past couple decades. With the advancements on single cell microscopy techniques allowing enzyme and metabolite quantification, it has been revealed that almost all processes in living cells are stochastic in nature. This “randomness” is a challenge for bacteria to overcome as fluctuations in metabolism is expected to lead to fluctuations in growth and hence

fitness. While some of this randomness allows creation of population heterogeneity and bet hedging strategies, some systems require precise control to maximize fitness. We will discuss new approaches and results which shine light onto the personalities of individual bacteria. This will reveal how recent developments in single cell imaging and culturing techniques are allowing a deeper understanding of the inner workings of life. However, this also presents a major challenge in understanding how bacteria can grow as robustly as they do.

E. coli has to produce thousands of different components in a balanced manner in order to grow and spawn two healthy daughter cells which in turn can do the same. This is a monumental task for a life form that is measured in micrometres. Because it requires the identification of the optimum concentrations and activity levels for all the cellular components under stochastic conditions. Cells mostly achieve this by means of individual feedback loops that govern each production pathway. For example production of amino acids is suppressed by the presence of excess amino acids, allowing reallocation of resources for production of other components that are lacking⁵⁸. Conversely if the bacteria experience a shortage of amino acids, this is sensed through uncharged tRNA's and leads to the activation of the Guanosine Tetra Phosphate (ppGpp) synthesis enzyme RelA. ppGpp in turn activates amino acid production genes and decreases ribosome production and transcription rates. This allows cells to limit the number of ribosomes in the face of substrate limitation and boost production of said substrates⁵⁹. If for example a specific amino acid is missing in the environment, the combination of the above two systems makes sure that only the required amino acid is synthesized by the cell. Furthermore, this system is also theorized to lead to the optimum ratio of ribosome to amino acid production under any given environment^{60,61}. The more amino acids are present in the environment the faster the bacteria can grow¹⁴ since the resources that would otherwise be spent on the production of these amino acids can be diverted to metabolism and growth. It was also observed that faster growing cells are also on average larger, another possible optimization cells undertake to house the extra production capacity.

Signalling molecule ppGpp was first discovered in 1969 by Cashel and Gallant and named as the "Magic Spot"⁶². This naming was apt as the molecule ppGpp was identified as a dark spot which appeared in chromatographs of starved bacteria. Since then it was discovered that ppGpp not only appears under extreme stress (stringent concentrations) but is also involved in regulation of growth and metabolism under different growth rates (basal concentrations)⁶³. If the environment allows for fast growth, ppGpp levels are low, on the other hand if the environment is limited and growth is slow, ppGpp levels are higher. Level of ppGpp then mostly regulates the total transcription and ribosome numbers and hence the total metabolic activity of the cell according to growth rate⁶⁴. However surprisingly ppGpp levels respond to many different stress factors such as iron⁶⁵, carbon source⁶⁶ or fatty acid limitations⁶⁷. Then up to a thousand enzyme's concentrations are altered through transcriptional regulation⁵⁹ and recently it was shown that ppGpp could bind to more than 40 enzymes

with possible direct regulatory activity⁶⁸. In this sense ppGpp acts as a balancer of metabolism at any given growth rate.

There are however more questions regarding ppGpp and its activity at the basal concentrations in single cells. Since ppGpp is a regulator with a wide range of effects, understanding how ppGpp orchestrates the cell under various conditions is instrumental in developing a full picture of bacterial physiology. While there is currently no available technique that allows quantification of ppGpp in single cells, it is important to answer if ppGpp has a role in stochasticity dampening. Even though we cannot measure ppGpp in single cells, we can alter the level of ppGpp without changing the nutrient environment by means of ectopic production of synthesis or hydrolysis enzymes^{64,69,70}. Therefore, observing single cells under shifts between different ppGpp conditions can reveal unknown functions of ppGpp. By observing phenomenology such as growth rate or cell size after a change in ppGpp levels dynamically, we can reveal information on the web of regulation of ppGpp.

Chapter 3 will discuss our work on another one of the recent discoveries in cellular physiology and its links with ppGpp. Much like many other systems, cell's size also has a stochastic nature. Divisions or DNA replication initiation can be mis-timed and force the cell to divide slightly earlier or later, leading to variations in cell size. This when unchecked would create large differences in observed cell size of a population where some are tiny and some huge. The way in which *E. coli* cells maintain size homeostasis was recently discovered to be an "Adder Mechanism" where the same length is added in each cell cycle regardless of birth size by each cell on average. However, the molecular details of the mechanism are not clear. In Chapter 3 we will present our work on ppGpp where we externally controlled its concentrations using fusion enzymes. We then observed cells' size, growth and cell cycle duration changes during shifts from one induction level to the other. This revealed functional links between ppGpp and cell size regulation machinery which is independent from ppGpp's regulation of growth rate.

Chapter 4 presents our efforts in creating a chimeric enzyme which can be activated by light. Concentrations of ppGpp are known to respond rapidly to changing environments. In order to understand the effects of this on bacteria we need to simulate such changes, however currently there are no available techniques to achieve these rapid changes without altering the growth environment. We will show how by combining a protein domain from a plant enzyme with a metabolic enzyme from a fruit fly, we managed to create a light activatable chimeric enzyme which hopefully will allow us to conduct new science. This work was possible due to decades long research into protein structure and function and we will discuss in detail how two domains can be pieced together like Lego bricks to create new function.

Chapter 5 will discuss the direct regulation of phospholipid production by ppGpp. We show that the activity of the enzyme PlsB regulates the flux through the phospholipid production pathway. This activity in turn is directly inhibited by ppGpp which allows

cells to maintain the same concentration of PlsB under slow and fast growth conditions. Having excess inactive PlsB around allows cells to rapidly respond to changes in the environment. ppGpp concentration decrease rapidly upon an increase in nutrient quality and thus cells can suddenly “turn on” their ability to produce phospholipids within minutes. This allows cells to take advantage of the improved media as soon as possible and stay competitive among other bacteria.

References

1. Liu L, Wang J, Rosenberg D, Zhao H, Lengyel G, Nadel D. Fermented beverage and food storage in 13,000 y-old stone mortars at Raqefet Cave, Israel: Investigating Natufian ritual feasting. *J Archaeol Sci Reports*. 2018;21(May):783-793. doi:10.1016/j.jasrep.2018.08.008
2. Jones DS, Podolsky SH, Greene JA. The burden of disease and the changing task of medicine. *N Engl J Med*. 2012;366(25):2333-2338. doi:10.1056/NEJMp1113569
3. Wainwright M. An alternative view of the early history of microbiology. *Adv Appl Microbiol*. 2003;52:333-355. doi:10.1016/S0065-2164(03)01013-X
4. Mohr K. History of Antibiotics Research. In: *How to Overcome the Antibiotic Crisis*. ; 2016:237-232. doi:10.1007/82_2016_499
5. Yehl K, Lemire S, Yang AC, et al. Engineering Phage Host-Range and Suppressing Bacterial Resistance through Phage Tail Fiber Mutagenesis. *Cell*. 2019;179(2):459-469.e9. doi:10.1016/j.cell.2019.09.015
6. Steensels J, Snoek T, Meersman E, Nicolino MP, Voordeckers K, Verstrepen KJ. Improving industrial yeast strains: Exploiting natural and artificial diversity. *FEMS Microbiol Rev*. 2014;38(5):947-995. doi:10.1111/1574-6976.12073
7. Parekh S, Vinci VA, Strobel RJ. Improvement of microbial strains and fermentation processes. *Appl Microbiol Biotechnol*. 2000;54(3):287-301. doi:10.1007/s002530000403
8. Ke J, Yoshikuni Y. Multi-chassis engineering for heterologous production of microbial natural products. *Curr Opin Biotechnol*. 2020;62:88-97. doi:10.1016/j.copbio.2019.09.005
9. H S. Producing high-value chemicals in Escherichia coli through synthetic biology and metabolic Engineering. In: *TU Delft University*. ; 2019:8-10. doi:10.4233/uuid
10. Dalton B, Roberto F. Lunar Regolith Biomining: Workshop Report. In: *Nasa/Cp-2008-214564*. ; 2008. <http://ntrs.nasa.gov/search.jsp?R=20090010050>.
11. Locey KJ, Lennon JT. Scaling laws predict global microbial diversity. *Proc Natl Acad Sci U S A*. 2016;113(21):5970-5975. doi:10.1073/pnas.1521291113
12. Stewart EJ. Growing unculturable bacteria. *J Bacteriol*. 2012;194(16):4151-4160. doi:10.1128/JB.00345-12

13. Elbing K, Brent R. Media Preparation and Bacteriological Tools. In: *Current Protocols in Molecular Biology*. ; 2010:219-226.
14. Ecker RE, Schaechter M. Bacterial Growth Under Conditions of Limited Nutrition. *Ann N Y Acad Sci*. 1963;102(3):549-563. doi:10.1111/j.1749-6632.1963.tb13660.x
15. Kolter R. The Stationary Phase of the Bacterial Life Cycle. *Annu Rev Microbiol*. 1993;47(1):855-874. doi:10.1146/annurev.micro.47.1.855
16. Demuth C, Varonier J, Jossen V, Eibl R, Eibl D. Novel probes for pH and dissolved oxygen measurements in cultivations from millilitre to benchtop scale. *Appl Microbiol Biotechnol*. 2016;100(9):3853-3863. doi:10.1007/s00253-016-7412-0
17. Eibl R, Kaiser S, Lombriser R, Eibl D. Disposable bioreactors: The current state-of-the-art and recommended applications in biotechnology. *Appl Microbiol Biotechnol*. 2010;86(1):41-49. doi:10.1007/s00253-009-2422-9
18. Nanchen A, Schicker A, Sauer U. Nonlinear dependency of intracellular fluxes on growth rate in miniaturized continuous cultures of *Escherichia coli*. *Appl Environ Microbiol*. 2006;72(2):1164-1172. doi:10.1128/AEM.72.2.1164-1172.2006
19. Wang P, Robert L, Pelletier J, et al. Robust growth of *Escherichia coli*. *Curr Biol*. 2010;20(12):1099-1103. doi:10.1016/j.cub.2010.04.045
20. Kaiser M, Jug F, Julou T, et al. Monitoring single-cell gene regulation under dynamically controllable conditions with integrated microfluidics and software. *Nat Commun*. 2018;9(1). doi:10.1038/s41467-017-02505-0
21. Kiviet DJ, Nghe P, Walker N, Boulineau S, Sunderlikova V, Tans SJ. Stochasticity of metabolism and growth at the single-cell level. *Nature*. 2014;514(7522):376-379. doi:10.1038/nature13582
22. Alberts B, Johnson A LJ. Visualizing Molecules in Living Cells. In: *Molecular Biology of the Cell. 4th Edition*. New York: Garland Science; 2020.
23. Lou X, Kim G, Yoon HK, Lee YEK, Kopelman R, Yoon E. A high-throughput photodynamic therapy screening platform with on-chip control of multiple microenvironmental factors. *Lab Chip*. 2014;14(5):892-901. doi:10.1039/c3lc51077h
24. Cookson S, Ostroff N, Pang WL, Volfson D, Hasty J. Monitoring dynamics of single-cell gene expression over multiple cell cycles. *Mol Syst Biol*. 2005;1(1):2005.0024. doi:10.1038/msb4100032
25. Griffith F. The significance of pneumococcal types. *J Hyg (Lond)*. 1966;64(2):129-175. doi:10.1017/S0022172400040420
26. F. SANGER, S. NICKLEN AARC. DNA sequencing with chain-terminating inhibitors. *Proc Natl Acad Sci USA*. 1977;74(12):5463-5467. doi:10.1097/00006250-199004001-00013
27. Mardis ER. A decade's perspective on DNA sequencing technology. *Nature*. 2011;470(7333):198-203. doi:10.1038/nature09796

28. Metzker ML. Sequencing technologies the next generation. *Nat Rev Genet*. 2010;11(1):31-46. doi:10.1038/nrg2626
29. Crow JF, Abrahamson S. Seventy years ago: Mutation becomes experimental. *Genetics*. 1997;147(4):1491-1496.
30. Muller HJ. Artificial transmutation of the Gene. *Science (80-)*. 1927;69(1699):84-87. doi:10.1038/285058b0
31. Cohen SN, Chang ACY, Boyer HW, Helling RB. Construction of biologically functional bacterial plasmids in vitro. *Proc Natl Acad Sci U S A*. 1973;70(11):3240-3244. doi:10.1073/pnas.70.11.3240
32. Zhang F, Wen Y, Guo X. CRISPR/Cas9 for genome editing: Progress, implications and challenges. *Hum Mol Genet*. 2014;23(R1):40-46. doi:10.1093/hmg/ddu125
33. Court DL, Sawitzke JA, Thomason LC. Genetic Engineering Using Homologous Recombination. *Annu Rev Genet*. 2002;36(1):361-388. doi:10.1146/annurev.genet.36.061102.093104
34. O'Connor M, Peifer M, Bender W. Construction of Large DNA Segments in Escherichia coli. *Science (80-)*. 1989;244(4910):1307-1312. doi:10.1016/B978-0-12-384730-0.00100-2
35. Goeddel D V., Kleid DG, Bolivar F. Expression in Escherichia coli of chemically synthesized genes for human insulin. *Proc Natl Acad Sci U S A*. 1979;76(1):106-110. doi:10.1073/pnas.76.1.106
36. Dow LE, Fisher J, O'Rourke KP, et al. Inducible in vivo genome editing with CRISPR-Cas9. *Nat Biotechnol*. 2015;33(4):390-394. doi:10.1038/nbt.3155
37. Sand M, Bredenoord AL, Jongsma KR. After the fact—the case of CRISPR babies. *Eur J Hum Genet*. 2019;27(11):1621-1624. doi:10.1038/s41431-019-0459-5
38. SANGER F. The free amino groups of insulin. *Biochem J*. 1945;39(5):507-515. doi:10.1042/bj0390507
39. ASTBURY, W. T., & WOODS HJ. The X-Ray Interpretation of the Structure and Elastic Properties of Hair Keratin. *Nature*. 1930;126(3189):913-914.
40. Wooley JC, Ye Y. A Historical Perspective and Overview of Protein Structure Prediction. In: *Computational Methods for Protein Structure Prediction and Modeling*. Springer, New York, NY; 2007:1-43.
41. Nogales E. Cryo-EM. *Curr Biol*. 2018;28(19):1127-1128. doi:10.1016/j.physbeh.2017.03.040
42. Leroy C, Bryce DL. Recent advances in solid-state nuclear magnetic resonance spectroscopy of exotic nuclei. *Prog Nucl Magn Reson Spectrosc*. 2018;109:160-199. doi:10.1016/j.pnmrs.2018.08.002
43. Huxford T. X-Ray Crystallography. *Brenner's Encycl Genet Second Ed*. 2013:366-368. doi:10.1016/B978-0-12-374984-0.01657-0

44. Berman HM, Battistuz T, Bhat TN, et al. The protein data bank. *Acta Crystallogr Sect D Biol Crystallogr.* 2002;58(6 I):899-907. doi:10.1107/S0907444902003451
45. LOEWUS MW, BRIGGS DR. The number of catalytically active sites present on the chymotrypsin molecule. *J Biol Chem.* 1952;199(2):857-864.
46. Van Eys, J., Ciotti, M. M., & Kaplan NO. Yeast alcohol dehydrogenase. *Biochim Biophys Acta.* 1957;23:581-587.
47. Janin J, Wodak SJ. Structural domains in proteins and their role in the dynamics of protein function. *Prog Biophys Mol Biol.* 1983;42(C):21-78. doi:10.1016/0079-6107(83)90003-2
48. Elmore ZC, Guillen RX, Gould KL. The kinase domain of CK1 enzymes contains the localization cue essential for compartmentalized signaling at the spindle pole. *Mol Biol Cell.* 2018;29(13):1664-1674. doi:10.1091/mbc.E18-02-0129
49. Vidangos N, Maris AE, Young A, et al. Structure, function, and tethering of DNA-binding domains in σ 54 transcriptional activators. *Biopolymers.* 2016;*(12):1082-1096. doi:10.1038/jid.2014.371
50. Rain JC, Selig L, De Reuse H, et al. The protein-protein interaction map of *Helicobacter pylori*. *Nature.* 2001;409(6817):211-215. doi:10.1038/35051615
51. Tischer D, Weiner OD. Illuminating cell signaling with optogenetic tools. *Nat Rev Mol Cell Biol.* 2014;15(8):551-558. doi:10.1016/j.pestbp.2011.02.012. Investigations
52. Prasher DC, Eckenrode VK, Ward WW, Prendergast FG, Cormier MJ. Primary structure of the *Aequorea victoria* green-fluorescent protein. *Gene.* 1992;111(2):229-233. doi:10.1016/0378-1119(92)90691-H
53. Xie M, Fussenegger M. Designing cell function: assembly of synthetic gene circuits for cell biology applications. *Nat Rev Mol Cell Biol.* 2018;19(8):507-525. doi:10.1038/s41580-018-0024-z
54. Stower H. Chimeric protein production. *Nat Rev Genet.* 2012;13(7):450-451. doi:10.1038/nrg3268
55. Levskaya, A., Chevalier, A. A., Tabor, J. J., Simpson, Z. B., Lavery, L. A., Levy, M., ... Voigt CA. Engineering *Escherichia coli* to see light. *Nature.* 2005;438(7067):441-442. doi:10.1038/438442a
56. Tabor JJ, Salis HM, Simpson ZB, et al. A Synthetic Genetic Edge Detection Program. *Cell.* 2009;137(7):1272-1281. doi:10.1016/j.cell.2009.04.048
57. Riglar DT, Richmond DL, Potvin-Trottier L, et al. Bacterial variability in the mammalian gut captured by a single-cell synthetic oscillator. *Nat Commun.* 2019;10(1):1-12. doi:10.1038/s41467-019-12638-z
58. Sander T, Farke N, Diehl C, Kuntz M, Glatter T, Link H. Allosteric Feedback Inhibition Enables Robust Amino Acid Biosynthesis in *E. coli* by Enforcing Enzyme Overabundance. *Cell Syst.* 2019;8(1):66-75.e8. doi:10.1016/j.cels.2018.12.005

-
59. Hauryliuk V, Atkinson GC, Murakami KS, Tenson T, Gerdes K. Recent functional insights into the role of (p)ppGpp in bacterial physiology. *Nat Rev Microbiol.* 2015;13(5):298-309. doi:10.1038/nrmicro3448
 60. Giordano N, Mairet F, Gouzé J-L, Geiselman J, de Jong H. Dynamical Allocation of Cellular Resources as an Optimal Control Problem: Novel Insights into Microbial Growth Strategies. *PLoS Comput Biol.* 2016;12(3):e1004802. doi:10.1371/journal.pcbi.1004802
 61. Bosdriesz E, Molenaar D, Teusink B, Bruggeman FJ. How fast-growing bacteria robustly tune their ribosome concentration to approximate growth-rate maximization. *FEBS J.* 2015;282(10):2029-2044. doi:10.1111/febs.13258
 62. Cashel M, Gallant J. Two Compounds implicated in the Function of the RC Gene of Escherichia coli. *Nature.* 1969;224:488-490. doi:10.1038/224488a0
 63. Potrykus K, Murphy H, Philippe N, Cashel M. ppGpp is the major source of growth rate control in E. coli. *Environ Microbiol.* 2011;13(3):563-575. doi:10.1111/j.1462-2920.2010.02357.x
 64. Zhu M, Dai X. Growth suppression by altered (p)ppGpp levels results from non-optimal resource allocation in Escherichia coli. *Nucleic Acids Res.* 2019;47(9):4684-4693. doi:10.1093/nar/gkz211
 65. Vinella D, Albrecht C, Cashel M, D'Ari R. Iron limitation induces SpoT-dependent accumulation of ppGpp in Escherichia coli. *Mol Microbiol.* 2005;56(4):958-970. doi:10.1111/j.1365-2958.2005.04601.x
 66. Xiao H, Kalman M, Ikehara K, Zemel S, Glaser G, Cashel M. Residual guanosine 3',5'-bispyrophosphate synthetic activity of relA null mutants can be eliminated by spoT null mutations. *J Biol Chem.* 1991;266(9):5980-5990.
 67. Seyfzadeh M, Keener J, Nomura M. spoT-dependent accumulation of guanosine tetraphosphate in response to fatty acid starvation in Escherichia coli. *Proc Natl Acad Sci U S A.* 1993;90(23):11004-11008. doi:10.1073/pnas.90.23.11004
 68. Zhang Y, Zborníková E, Rejman D, Gerdes K. Novel (p)ppGpp binding and metabolizing proteins of Escherichia coli. *MBio.* 2018;9(2):1-20. doi:10.1128/mBio.02188-17
 69. Schreiber G, Metzger S, Aizenman E, Roza S, Cashel M, Glaser G. Overexpression of the relA gene in Escherichia coli. *J Biol Chem.* 1991;266(6):3760-3767.
 70. Sun D, Lee G, Lee JH, et al. A metazoan ortholog of SpoT hydrolyzes ppGpp and functions in starvation responses. *Nat Struct Mol Biol.* 2010;17(10):1188-1194. doi:10.1038/nsmb.1906

2

Stochasticity in cellular metabolism and growth: approaches and consequences

Martijn Wehrens¹, Ferhat Buke^{1,2}, Philippe Nghe³, Sander J. Tans^{1,2}

1 AMOLF, Science Park 104, 1098XG Amsterdam, the Netherlands

2 Delft University of Technology, Bionanoscience department, Van der Maasweg 9, 2629HZ Delft, the Netherlands

3 ESPCI, 10 Rue Vauquelin, 75005 Paris, France

Abstract

Advances in our ability to zoom in on single cells has revealed striking heterogeneity within isogenic populations. Attention has so far focussed predominantly on underlying stochastic variability in regulatory pathways and downstream differentiation events. In contrast, the role of stochasticity in metabolic processes and networks has long remained unaddressed. Here we review recent studies that have begun to overcome key technical challenges in addressing this issue. First findings have already demonstrated that metabolic networks are stochastic in nature and highlight the plethora of cellular processes that are critically affected by it.

2.1 Stochasticity and metabolism

Elucidating the role of molecular stochasticity in metabolic processes is a central issue in cellular physiology. It is key to understanding cellular homeostasis, and could help explaining heterogeneous phenotypes ubiquitously observed across all domains of life, ranging from persistence to cancer [1,2]. Stochasticity in metabolism could underlie bet-hedging strategies, in which distinct sub-populations anticipate future environmental change [3,4]. On the other hand, metabolic stochasticity could limit optimal growth and require regulatory mechanisms to ensure homeostasis [5]. More generally, as metabolism ultimately drives all cellular processes, fluctuations and instability could impact a myriad of phenomena ranging from the cell cycle to differentiation events. So far however, stochastic variability is commonly considered to have negligible effects in metabolic networks, as reflected by current theoretical models [6]. Indeed, metabolic fluctuations may be insignificant because of averaging over the many reaction events underlying metabolism in cells, chemical equilibration, metabolite secretion, or a lack of limiting steps within metabolic pathways [6–13].

At the practical level, quantifying any type of metabolic fluctuations comes with its own specific challenges. In contrast to regulatory proteins within signalling networks, which can be tagged fluorescently, metabolites are difficult to visualize at the single-cell level. Metabolites can be quantified by single-cell mass spectrometry [14], but so far not dynamically in time. Spectroscopic methods can follow metabolite abundance in time, but only for specific highly abundant molecules such as lipids [15]. FRET and fluorescent sensors hold a lot of promise, but remain limited to some metabolites and cannot yet quantify stochastic fluctuations [16–20].

Recently, important progress has been made in developing novel approaches that circumvent these limitations. In this review, we will examine these new efforts, their first findings, as well as related theoretical modelling. We will also cover recent work that is addressing the impact metabolic variability has on other cellular phenomena.

2.2 Enzyme expression generates metabolic noise

Early single-cell experiments showed how the expression of transcription factors fluctuate and propagate to downstream genes [21–23]. Similarly, such expression noise in key metabolic enzymes could generate variations in the flux of the reaction they catalyse, even if reaction-event noise averages out [24]. Moreover, if these flux variations propagate down-stream along the pathway, they could produce variations in the rate of cellular growth. A recent study by Kiviet et al [25] was based on this premise. While such an approach presents the challenge of quantifying enzyme expression and cellular growth with high accuracy, it avoids the need to measure fluctuations in metabolite concentrations.

Growth was quantified by following the size of individual cells by time-lapse microscopy. Specifically, using the known overall shape of *E. coli* - a rod capped with half-domes - its length could be determined to below the diffraction limit, which may be compared to how fluorophores are positioned in super-resolution microscopy [25]. Currently, a range of different single-cell image analysis approaches are available [26–33], including ones utilizing machine learning [34–36]. Cellular growth has also been quantified by measuring cellular dry mass [37], and by using AFM-like cantilevers [38], as will be discussed more exhaustively below.

The data on the instantaneous cellular growth rate appeared correlated with the expression of metabolic enzymes [25]. However, such correlations could signal that growth fluctuations perturb expression, rather than the other way around. Time dependent correlation analysis can be used to address this issue [21,22] (Fig. 2.1). This approach showed that the correlations were on average stronger after a certain delay, consistent with enzyme production fluctuations happening first, and growth fluctuations happening some time later (Fig 2.1a). In line with the idea that enzyme (expression) fluctuations affect the flux of the reaction they catalyze, this delay was observed only for genes that were considered limiting, such as *gltA* and *icd* in acetate media, and *pfkA* and *icd* in lactose media.

Interestingly, even when considering non-limiting genes, the expression rate was still strongly correlated with growth – however the correlations were now instantaneous and did not show a delay (Fig. 2.1b). It suggested that more generally, proteins are expressed significantly faster in cells that transiently grow faster, which is actually not unreasonable given that some cells grow twice as fast others for almost a full generation, and expression needs diverse metabolites. Put differently, fluctuations in growth-controlling factors, which may be anything from ribosomes to ATP, are also a source of gene expression noise [39]. In turn, metabolic fluctuations may thus affect processes that are controlled by gene expression, such as differentiation events [40,41]. Metabolic noise can be compared to other noise sources such as transcription factors [42] and the cell cycle [43], which can also affect more than one gene or process and hence may be considered as extrinsic noise sources. A picture thus emerges of a system as a cycle of reciprocally interacting sources of extrinsic noise: metabolic fluctuations simultaneously affecting the expression of multiple genes, including transcription factors, polymerases, and metabolic enzymes, and conversely, noise in the latter resulting in fluctuations in metabolic fluxes. At the same time, the precise relations between noisy signals, and hence their ultimate mechanistic origin remains largely unresolved. For instance, it is unclear whether different pathways fluctuate independently, or alternatively, whether observed fluctuations result from a continuous dynamic interplay between them. Overall, the data so far shows that expression and growth are tightly intertwined, not only in terms of their mean levels when comparing different media [44], but also dynamically within constant external conditions.

2.3 (Mis)matching pathways

The notion that metabolic pathways are stochastic raises questions about the dynamic interaction between them. For instance, it is thought that cells co-regulate functionally related genes to balance their overall input and output fluxes [24,45]. In yeast, genes related to either stress response, mitochondria or amino acid biosynthesis were found to fluctuate jointly in response to general regulators [46]. Mismatches between (parts) of the cellular pathways can have large effects. Specifically, it was observed that metabolic imbalance within glycolysis can amplify non-genetic variability within the population [47]. When the upper and lower parts of this central pathway are not well matched, glycolytic intermediates can accumulate while ATP levels are reduced, thus strongly affecting cellular physiology. Expression variability has also been suggested to drive changes in flux partitioning [48]. These studies underscore the importance of further dissecting how cells coordinate different cellular processes in the face of the random fluctuations of its components, and which regulatory mechanisms they employ.

2.4 Metabolism at the center

Metabolism and growth ultimately power all cellular activity. A fluctuating or unstable metabolism thus could have wide-ranging effects. For instance, perturbations of metabolic homeostasis may cause fluxes to collapse and metabolite pools to deplete, which in turn can induce persistence [2]. Metabolic heterogeneity has been suggested to affect the synchronization of metabolic oscillations observed in dense yeast populations, and hence the communication between cells [49], while a recent study revealed a coupling between metabolic oscillations and the cell cycle in yeast [50]. Strikingly, it has recently been reported that slow-growing yeast sub populations display downregulated ribosomal activity and upregulated stress response genes, increased RNA polymerase error rates and indications of DNA damage, which may be explained by oxidative stress [51].

One may also expect that metabolic and growth fluctuations impact cell size. Bacteria grow in exponential fashion - increases in growth rate could thus produce large increases in cell size, which could be further amplified and diverge in subsequent cycles because larger cells effectively grow faster. Some answers to how cells deal with this issue are already emerging. First, the timescale of growth fluctuations in *E. coli* was found to be just below that of the cell cycle for a range of growth media [25]. Cells thus inherit faster growth for just one or two generations, which limits amplifying effects. Second, while the molecular mechanism is unclear, it has been found that cells compensate for growth variability [52–58]. Cells that grow faster on average have a smaller interdivision time, thus yielding similar sizes at division as slow-growing cells (Fig. 2.2a). Moreover, faster-growing cells were also found to initiate DNA replication earlier, providing a further indication of underlying regulatory compensations [52,56]. These findings support the suggestion that the cells compensate for growth variability by measuring size rather than time.

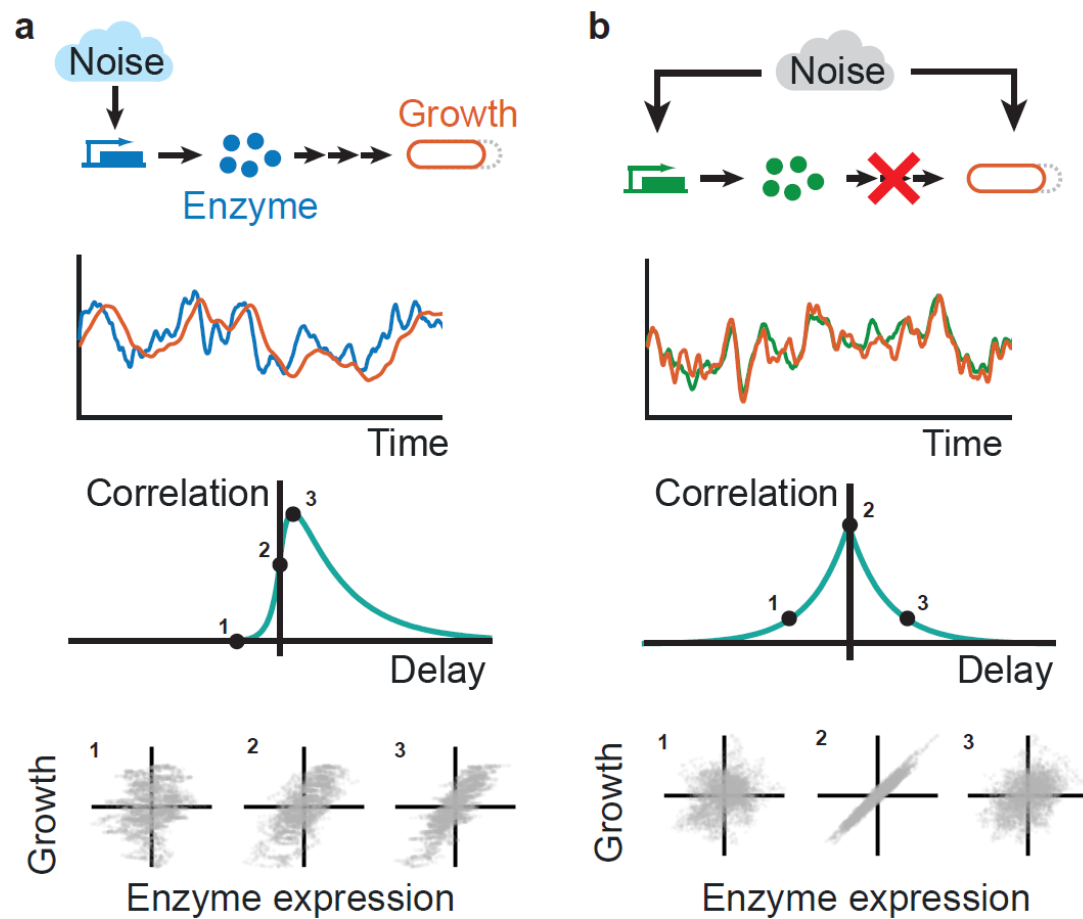


Figure 2.1: Fluctuations from enzyme expression to metabolism, and from metabolism to enzyme expression. Expression measurements of a single metabolic enzyme and growth rates in individual cells can be used to reveal metabolic stochasticity. Two key modes of noise transmission have been observed, which can act both individually and jointly, and may interact. (a) Noise in the expression of a single enzyme (blue trace), result in fluctuations in metabolic flux that are transmitted through the metabolic network and affect growth with some time delay (orange trace). The delay can be quantified by cross-correlation analysis. The cross-correlation curve illustrates that on average, current enzyme expression correlates better with growth sometime later, as illustrated by the expression-growth scatter plots. Note that the sources of expression noise here are not only intrinsic or caused by molecular processes specific to one gene. They also include extrinsic or transmitted noise from other processes, such as transcription factor, polymerase, or metabolic factors such as amino acid abundance, which may affect expression but not growth. Noise sources that affect both expression and growth are discussed in panel b. (b) Noise sources within the metabolic network that perturb both expression (green trace) and growth (orange trace). Fluctuations in components that affect both expression and growth, such as ATP and other central metabolites, could define such sources of noise. In contrast to panel a, the cross-correlation here is symmetric because expression and growth respond approximately equally fast to the fluctuations. Note that the resulting expression noise may affect growth (panel a) or may not (this panel) - for instance because the expressed enzyme is not metabolically active or because it is abundant and hence does not limit growth.

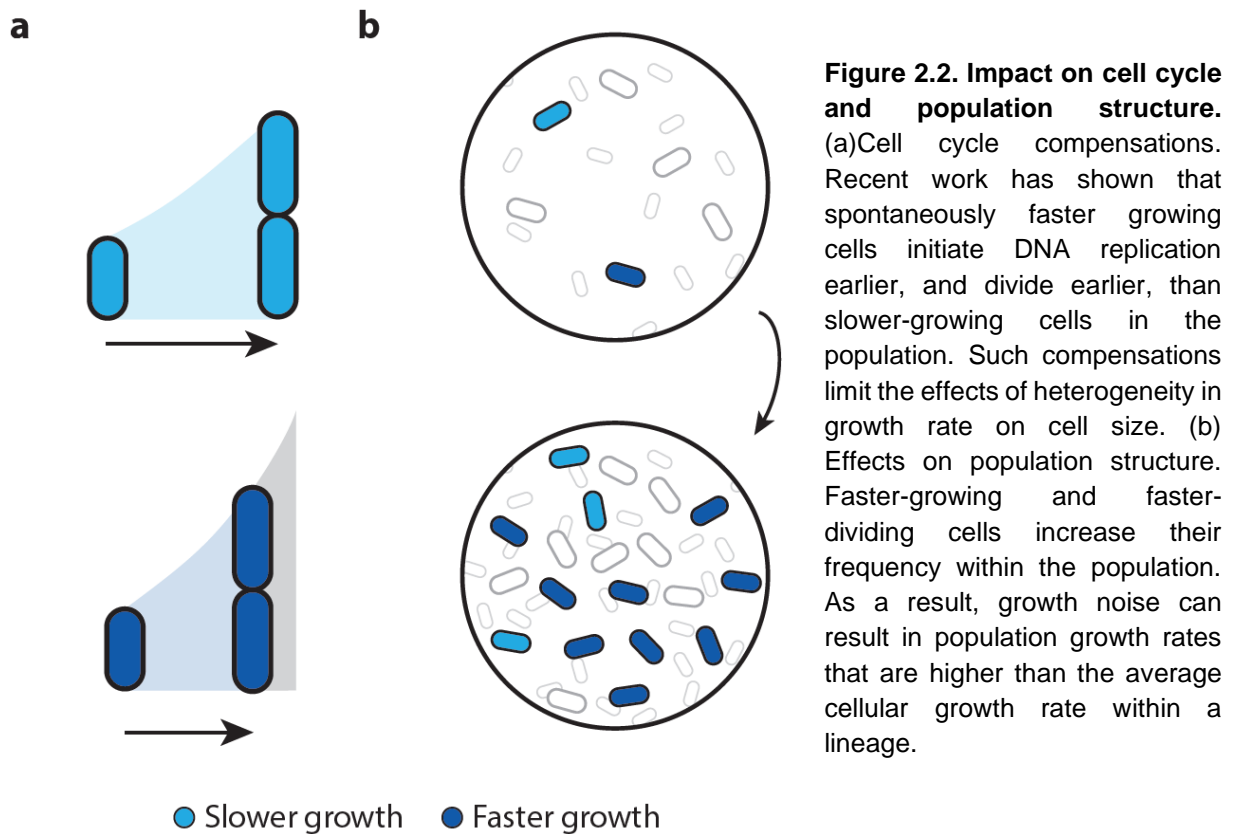


Figure 2.2. Impact on cell cycle and population structure. (a) Cell cycle compensations. Recent work has shown that spontaneously faster growing cells initiate DNA replication earlier, and divide earlier, than slower-growing cells in the population. Such compensations limit the effects of heterogeneity in growth rate on cell size. (b) Effects on population structure. Faster-growing and faster-dividing cells increase their frequency within the population. As a result, growth noise can result in population growth rates that are higher than the average cellular growth rate within a lineage.

2.5 Benefits of metabolic fluctuations

Stochasticity of growth and expression is directly observed within individual cells, but it can also affect the composition of the population in non-trivial ways. This issue has been studied theoretically and in experiments [59–61]. Counter-intuitively, analysis showed that growth rate distribution along a single lineage is not necessarily equal to the distribution within the population at a single time point [61]. The cause however is actually quite simple: faster growing phenotypes produce more offspring, and hence become overrepresented within the population (Fig. 2.2b). The effects are most striking when the mean concentration of a growth-controlling enzyme is suboptimal, as gene expression noise and resulting growth noise can then increase the growth rate of the population as a whole [59]. Such sub-optimal regulation of enzyme expression has been observed experimentally (e.g. [62]), and in one direct study, population growth rates were found to be almost 10% faster than the average single-cell growth rate [61]. A similar study in yeast showed a 4-7% increase in growth rate for the population as a whole [60]. Additionally, an artificial reduction of gene expression noise in catabolic networks decreased heterogeneity in cellular division times [60], consistent with noise in metabolic enzymes controlling growth [25].

The advantage of fluctuating gene expression in variable environments was studied earlier in a synthetic system, in which bistable switching allowed cells to be prepared for environmental change [63]. The idea of "stochastic sensing" has been addressed theoretically [3] and observed in metabolic networks [64–66]. It has been proposed that the regulatory control of metabolic genes constrains the space of possible random

metabolic phenotypes, and hence come with entropic energy costs [67]. Overall, noise in metabolic systems thus may not exclusively limit optimal growth but can also be beneficial. This point is further illustrated by observed evolutionary adaptation towards more heterogeneous phenotypes [51,68–71].

2.6 An expanding array of experimental approaches

Tracking cell size and fluorescence has already led to surprising insights to the dynamics of cellular physiology. Novel approaches will open up additional possibilities. Fluorescence methods have been used to detect the synthesis of single proteins in eukaryotic cells [72]. The growth rates of eukaryotic cells are difficult to measure using time-lapse microscopy, given their complex three-dimensional shapes. A recent technique overcomes this problem, by quantifying how the cell volume reduces the abundance of fluophores in the surrounding medium [73]. The accuracy of gene expression measurements is also improving. Single proteins could be visualized in *E. coli* cells by slowing down their diffusion [74]. Measuring metabolite concentrations would allow direct access to fluxes. Concentrations of FAD and NADH can be measured using auto fluorescence [49,75], while FRET sensors have already been developed for calcium [16,17], ATP [18,19] and cAMP [20]. Additionally, it is possible to obtain single cell Raman spectra, which allow for determination of concentrations of certain abundant metabolites [15]. Together, these novel and existing approaches will be central to arrive at a dynamic view of physiology at the single-cell level.

2.7 Concluding remarks

In this review, we have discussed recent studies that have revealed the stochastic nature of metabolism and its interplay with gene expression and other cellular processes. The results press the notion of cells as autocatalytic and stochastic systems engaged in a dynamic equilibrium, with metabolism and enzyme expression as two fluctuating and interdependent processes. One may expect other processes to be in similar dynamic equilibria, and it will be intriguing to decipher how the result can be stable and robust. In recent decades, growth has not been considered as an important piece of the cellular puzzle. This new wave of experiments is revising this view and re-affirms metabolism and growth at the centre of cellular activity and dynamics.

2.8 Acknowledgements

Work in the group of S.J.T. is supported by the Netherlands Organization for Scientific Research (NWO).

Author contributions

FB and MW conducted literature review. FB, MW and SJT wrote the manuscript.

References

1. Walsh AJ, Skala MC: Optical metabolic imaging quantifies heterogeneous cell populations. *Biomed Opt Express* 2015, 6:559–573.
2. Radzikowski JL, Vedelaar S, Siegel D, Ortega AD, Schmidt A, Heinemann M: Bacterial persistence is an active σ S stress response to metabolic flux limitation. *Mol Syst Biol* 2016, 12:882.
3. Kussell E: Information in Fluctuating Environments Phenotypic Diversity , Population Growth , and Information in Fluctuating Environments. *Methods* 2005, 309:2075–2078.
4. Acar M, Mettetal JT, van Oudenaarden A: Stochastic switching as a survival strategy in fluctuating environments. *Nat Genet* 2008, 40:471–475.
5. Wang Z, Zhang J: Impact of gene expression noise on organismal fitness and the efficacy of natural selection. *Proc Natl Acad Sci U S A* 2011, 108:E67-76.
6. Herrgård MJ, Covert MW, Palsson BØ: Reconstruction of microbial transcriptional regulatory networks. *Curr Opin Biotechnol* 2004, 15:70–77.
7. Neidhardt FC, Ingraham JL, Schaechter M: *Physiology of the Bacterial Cell: A Molecular Approach*. Sinauer Associates Inc; 1990.
8. Rodríguez M, Good TA, Wales ME, Hua JP, Wild JR: Modeling allosteric regulation of de novo pyrimidine biosynthesis in Escherichia coli. *J Theor Biol* 2005, 234:299–310.
9. Hart Y, Madar D, Yuan J, Bren A, Mayo AE, Rabinowitz JD, Alon U: Robust control of nitrogen assimilation by a bifunctional enzyme in E. coli. *Mol Cell* 2011, 41:117–27.
10. Klumpp S, Zhang Z, Hwa T: Growth rate-dependent global effects on gene expression in bacteria. *Cell* 2009, 139:1366–75.
11. Yun HS, Hong J, Lim HC: Regulation of ribosome synthesis in Escherichia coli: Effects of temperature and dilution rate changes. *Biotechnol Bioeng* 1996, 52:615–624.
12. El-Mansi EMT, Holms WH: Control of Carbon Flux to Acetate Excretion During Growth of Escherichia coli in Batch and Continuous Cultures. *J Gen Microbiol* 1989, 135.
13. Wilson WA, Roach PJ, Montero M, Baroja-Fernández E, Muñoz FJ, Eydallin G, Viale AM, Pozueta-Romero J: Regulation of glycogen metabolism in yeast and bacteria. *FEMS Microbiol Rev* 2010, 34:952–985.
14. Esaki T, Masujima T: Fluorescence Probing Live Single-cell Mass Spectrometry for Direct Analysis of Organelle Metabolism. *Anal Sci* 2015, 31:1211–3.
15. Yue S, Cheng J-X: Deciphering single cell metabolism by coherent Raman scattering microscopy. *Curr Opin Chem Biol* 2016, 33:46–57.
16. Nakai J, Ohkura M, Imoto K: A high signal-to-noise Ca(2+) probe composed of a single green fluorescent protein. *Nat Biotechnol* 2001, 19:137–41.
17. Nagai T, Sawano A, Park ES, Miyawaki A: Circularly permuted green fluorescent proteins engineered to sense Ca2+. *Proc Natl Acad Sci* 2001, 98:3197–3202.
18. Yaginuma H, Kawai S, Tabata K V, Tomiyama K, Kakizuka A, Komatsuzaki T, Noji H, Imamura H: Diversity in ATP concentrations in a single bacterial cell population revealed by quantitative single-cell imaging. *Sci Rep* 2014, 4:6522.

19. Imamura H, Huynh Nhat KP, Togawa H, Saito K, Iino R, Kato-Yamada Y, Nagai T, Noji H: Visualization of ATP levels inside single living cells with fluorescence resonance energy transfer-based genetically encoded indicators. *Proc Natl Acad Sci* 2009, 106:15651–15656.
20. Klarenbeek J, Goedhart J, van Batenburg A, Groenewald D, Jalink K: Fourth-Generation Epac-Based FRET Sensors for cAMP Feature Exceptional Brightness, Photostability and Dynamic Range: Characterization of Dedicated Sensors for FLIM, for Ratiometry and with High Affinity. *PLoS One* 2015, 10:e0122513.
21. Dunlop MJ, Cox RS, Levine JH, Murray RM, Elowitz MB: Regulatory activity revealed by dynamic correlations in gene expression noise. *Nat Genet* 2008, 40:1493–8.
22. Munsky B, Khammash M: Transient analysis of stochastic switches and trajectories with applications to gene regulatory networks. *IET Syst Biol* 2008, doi:10.1049/iet-syb.
23. Pedraza JM, van Oudenaarden A: Noise propagation in gene networks. *Science* 2005, 307:1965–9.
24. Chubukov V, Gerosa L, Kochanowski K, Sauer U: Coordination of microbial metabolism. *Nat Rev Microbiol* 2014, doi:10.1038/nrmicro3238.
25. Kiviet DJ, Nghe P, Walker N, Boulineau S, Sunderlikova V, Tans SJ: Stochasticity of metabolism and growth at the single-cell level. *Nature* 2014, doi:10.1038/nature13582.
26. Stylianidou S, Brennan C, Nissen SB, Kuwada NJ, Wiggins PA: Robust image segmentation, analysis and lineage tracking of bacterial cells. 2016,
27. Paintdakhi A, Parry B, Campos M, Irnov I, Elf J, Surovtsev I, Jacobs-Wagner C: Oufiti: An integrated software package for high-accuracy, high-throughput quantitative microscopy analysis. *Mol Microbiol* 2016, 99:767–777.
28. Kaiser M, Jug F, Silander O, Deshpande S, Julou T, Myers G, Nimwegen E Van: Tracking single-cell gene regulation in dynamically controlled environments using an integrated microfluidic and computational setup. *bioRxiv* 2016, doi:10.1101/076224.
29. Sachs CC, Grünberger A, Helfrich S, Probst C, Wiechert W, Kohlheyer D, Nöh K: Image-based single cell profiling: High-throughput processing of mother machine experiments. *PLoS One* 2016, 11:1–15.
30. Nobs J-B, Maerkl SJ: Long-term single cell analysis of *S. pombe* on a microfluidic microchemostat array. *PLoS One* 2014, 9:e93466.
31. Sliusarenko O, Heinritz J, Emonet T, Jacobs-Wagner C: High-throughput, subpixel precision analysis of bacterial morphogenesis and intracellular spatio-temporal dynamics. *Mol Microbiol* 2011, 80:612–627.
32. Sadanandan SK, Baltekin O, Magnusson KEG, Boucharin A, Ranefall P, Jalden J, Elf J, Wahlby C: Segmentation and Track-Analysis in Time-Lapse Imaging of Bacteria. *IEEE J Sel Top Signal Process* 2016, 10:174–184.
33. Chowdhury S, Kandhavelu M, Yli-Harja O, Ribeiro AS: Cell segmentation by multi-resolution analysis and maximum likelihood estimation (MAMLE). *BMC Bioinformatics* 2013, 14:S8.
34. Van Valen DA, Kudo T, Lane KM, Macklin DN, Quach NT, DeFelice MM, Maayan I, Tanouchi Y, Ashley EA, Covert MW: Deep Learning Automates the Quantitative Analysis of Individual Cells in Live-Cell Imaging Experiments. *PLoS Comput Biol* 2016, 12:1–24.

35. Van Heerden JH, Kempe H, Doerr A, Maarleveld T, Nordholt N, Bruggeman FJ: Statistics and simulation of growth of single bacterial cells: Illustrations with *B. subtilis* and *E. coli*. *Sci Rep* 2017, 7:1–11.
36. Arganda-Carreras I, Kaynig V, Rueden C, Eliceiri KW, Schindelin J, Cardona A, Seung HS: Trainable Weka Segmentation: A machine learning tool for microscopy pixel classification. *Bioinformatics* 2017, 33:2424–2426.
37. Mir M, Wang Z, Shen Z, Bednarz M, Bashir R, Golding I, Prasanth SG, Popescu G: Optical measurement of cycle-dependent cell growth. *Proc Natl Acad Sci* 2011, 108:13124–13129.
38. Son S, Tzur A, Weng Y, Jorgensen P, Kim J, Kirschner MW, Manalis SR: Direct observation of mammalian cell growth and size regulation. *Nat Methods* 2012, 9:910–912.
39. Tsuru S, Ichinose J, Kashiwagi A, Ying B-W, Kaneko K, Yomo T: Noisy cell growth rate leads to fluctuating protein concentration in bacteria. *Phys Biol* 2009, 6:36015.
40. Balázsi G, Van Oudenaarden A, Collins JJ: Cellular decision making and biological noise: From microbes to mammals. *Cell* 2011, 144:910–925.
41. Maamar H, Raj A, Dubnau D: Noise in gene expression determines cell fate in *Bacillus subtilis*. *Science (80-)* 2005, 317:526–529.
42. Elowitz MB, Levine AJ, Siggia ED, Swain PS: Stochastic gene expression in a single cell. *Science* 2002, 297:1183–6.
43. Walker N, Nghe P, Tans SJ: Generation and filtering of gene expression noise by the bacterial cell cycle. *BMC Biol* 2016, 14:11.
44. Scott M, Gunderson CW, Mateescu EM, Zhang Z, Hwa T: Interdependence of Cell Growth and Gene Expression: Origins and Consequences. *Science (80-)* 2010, 330.
45. Hui S, Silverman JM, Chen SS, Erickson DW, Basan M, Wang J, Hwa T, Williamson JR: Quantitative proteomic analysis reveals a simple strategy of global resource allocation in bacteria. *Mol Syst Biol* 2015,
46. Stewart-Ornstein J, Weissman JS, El-Samad H: Cellular Noise Regulons Underlie Fluctuations in *Saccharomyces cerevisiae*. *Mol Cell* 2012, 45:483–493.
47. van Heerden JH, Wortel MT, Bruggeman FJ, Heijnen JJ, Bollen YJM, Planqué R, Hulshof J, O'Toole TG, Wahl SA, Teusink B: Lost in Transition: Startup of Glycolysis Yields Subpopulations of Nongrowing Cells. *Science* 2014, doi:10.1126/science.1245114.
48. Murima P, Zimmermann M, Chopra T, Pojer F, Fonti G, Dal Peraro M, Alonso S, Sauer U, Pethe K, McKinney JD: A rheostat mechanism governs the bifurcation of carbon flux in mycobacteria. *Nat Commun* 2016, 7:12527.
49. Gustavsson A-K, Adiels CB, Mehlig B, Goksör M: Entrainment of heterogeneous glycolytic oscillations in single cells. *Sci Rep* 2015, 5:9404.
50. Papagiannakis A, Niebel B, Wit EC, Heinemann M: Autonomous Metabolic Oscillations Robustly Gate the Early and Late Cell Cycle. *Mol Cell* 2017, 65:285–295.
51. Van Dijk D, Dhar R, Missarova A, Espinar L, Blevins W, Lehner B, Carey L: Slow growing subpopulations have increased DNA damage and RNA polymerase error rates. *Nat Commun* 2015, doi:10.1038/ncomms8972.
52. Adiciptaningrum A, Osella M, Moolman MC, Cosentino Lagomarsino M, Tans SJ: Stochasticity and homeostasis in the *E. coli* replication and division cycle. *Sci Rep* 2015, 5:18261.

53. Iyer-Biswas S, Wright CS, Henry JT, Lo K, Burov S, Lin Y, Crooks GE, Crosson S, Dinner a. R, Scherer NF: Scaling laws governing stochastic growth and division of single bacterial cells. *Proc Natl Acad Sci* 2014, doi:10.1073/pnas.1403232111.
54. Kennard AS, Osella M, Javer A, Grilli J, Nghe P, Tans SJ, Cicuta P, Cosentino Lagomarsino M: Individuality and universality in the growth-division laws of single *E. Coli* cells. *Phys Rev E* 2016, 93:1–18.
55. Osella M, Tans SJ, Cosentino Lagomarsino M: Step by Step, Cell by Cell: Quantification of the Bacterial Cell Cycle. *Trends Microbiol* 2017, 25:250–256.
56. Wallden M, Fange D, Gregorsson Lundius E, Baltekin Ö, Elf J: The synchronization of replication and division cycles in individual *E. coli* cells. *Cell* 2016, 166:729–739.
57. Taheri-Araghi S, Bradde S, Sauls JT, Hill NS, Levin PA, Paulsson J, Vergassola M, Jun S: Cell-Size Control and Homeostasis in Bacteria. *Curr Biol* 2014, 25:1–7.
58. Campos M, Surovtsev I V., Kato S, Paintdakhi A, Beltran B, Ebmeier SE, Jacobs-Wagner C: A constant size extension drives bacterial cell size homeostasis. *Cell* 2014, 159:1433–1446.
59. Tănase-Nicola S, ten Wolde PR: Regulatory control and the costs and benefits of biochemical noise. *PLoS Comput Biol* 2008, 4:e1000125.
60. Cerulus B, New AM, Pougach K, Verstrepen KJ: Noise and Epigenetic Inheritance of Single-Cell Division Times Influence Population Fitness. *Curr Biol* 2016, 26:1138–1147.
61. Hashimoto M, Nozoe T, Nakaoka H, Okura R, Akiyoshi S, Kaneko K, Kussell E, Wakamoto Y: Noise-driven growth rate gain in clonal cellular populations. *Proc Natl Acad Sci U S A* 2016, 113:3251–3256.
62. Towbin BD, Korem Y, Bren A, Doron S, Sorek R, Alon U: Optimality and sub-optimality in a bacterial growth law. *Nat Commun* 2017, 8:14123.
63. Kashiwagi A, Urabe I, Kaneko K, Yomo T: Adaptive response of a gene network to environmental changes by fitness-induced attractor selection. *PLoS One* 2006, 1.
64. New AM, Cerulus B, Govers SK, Perez-Samper G, Zhu B, Boogmans S, Xavier JB, Verstrepen KJ: Different Levels of Catabolite Repression Optimize Growth in Stable and Variable Environments. *PLoS Biol* 2014, 12:17–20.
65. Boulineau S, Tostevin F, Kiviet DJ, ten Wolde PR, Nghe P, Tans SJ: Single-cell dynamics reveals sustained growth during diauxic shifts. *PLoS One* 2013, 8:e61686.
66. Miot J, Remusat L, Duprat E, Gonzalez A, Pont S, Poinso M: Fe biomineralization mirrors individual metabolic activity in a nitrate-dependent Fe(II)-oxidizer. *Front Microbiol* 2015, 6:1–13.
67. Martino D De, Capuani F, Martino A De: Growth against entropy in bacterial metabolism: the phenotypic trade-off behind empirical growth rate distributions in *E. coli*. *Phys Biol* 2016, 13:36005.
68. Schreiber F, Littmann S, Lavik G, Escrig S, Meibom A, Kuypers MMM, Ackermann M: Phenotypic heterogeneity driven by nutrient limitation promotes growth in fluctuating environments. *Nat Microbiol* 2016, in press:1–7.
69. Metzger BPH, Yuan DC, Gruber JD, Duveau FD, Wittkopp PJ: Selection on noise constrains variation in a eukaryotic promoter. *Nature* 2015, 521:344–347.

70. Mars RAT, Nicolas P, Ciccolini M, Reilman E, Reder A, Schaffer M, Mäder U, Völker U, van Dijl JM, Denham EL: Small Regulatory RNA-Induced Growth Rate Heterogeneity of *Bacillus subtilis*. *PLoS Genet* 2015, 11:1–27.
71. Beaumont HJE, Gallie J, Kost C, Ferguson GC, Rainey PB: Experimental evolution of bet hedging. *Nature* 2009, 462:90–93.
72. Morisaki T, Lyon K, DeLuca KF, DeLuca JG, English BP, Zhang Z, Lavis LD, Grimm JB, Viswanathan S, Looger LL, et al.: Real-time quantification of single RNA translation dynamics in living cells. *Science (80-)* 2016, 352:1425–1429.
73. Cadart C, Monnier S, Grilli J, Attia R, Terriac E, Baum B, Cosentino-Lagomarsino M, Piel M: Size control in mammalian cells involves modulation of both growth rate and cell cycle duration. *bioRxiv* 2017, 152728.
74. Okumus B, Landgraf D, Lai GC, Bakhsi S, Arias-Castro JC, Yildiz S, Huh D, Fernandez-Lopez R, Peterson CN, Toprak E, et al.: Mechanical slowing-down of cytoplasmic diffusion allows in vivo counting of proteins in individual cells. *Nat Commun* 2016, 7:11641.
75. Georgakoudi I, Quinn KP: Optical Imaging Using Endogenous Contrast to Assess Metabolic State. *Annu Rev Biomed Eng* 2012, 14:351–367.

3

ppGpp is a bacterial cell size regulator

Ferhat Büke^{1,2}, Jacopo Grilli³, Marco Cosentino Lagomarsino^{4,5}, Gregory Bokinsky^{1*}, Sander Tans^{1,2*}

(1) Department of Bionanoscience, Kavli Institute of Nanoscience, Delft University of Technology, Delft, The Netherlands

(2) AMOLF, Amsterdam, The Netherlands.

(3) The Abdus Salam International Centre for Theoretical Physics (ICTP), Strada Costiera 11, 34014 Trieste, Italy

(4) IFOM, FIRC Institute of Molecular Oncology, Via Adamello 16, 20143, Milan, Italy

(5) Physics Department, University of Milan, and I.N.F.N., Via Celoria 16, 20133, Milan, Italy

*Corresponding authors. These authors contributed equally to the manuscript.

Email: s.tans@amolf.nl; g.e.bokinsky@tudelft.nl

3.1 Summary

Growth and division are central to cell size. Bacteria achieve size homeostasis by dividing when growth has added a constant size since birth, termed the “adder” principle, by unknown mechanisms^{1–4}. Growth is well known to be regulated by ppGpp, which controls anything from ribosome production to metabolic enzyme activity and replication initiation, and whose absence or excess can induce the stress response, filamentation, and yield growth-arrested miniature cells^{5–8}. These observations raise unresolved questions about the relation between ppGpp and size homeostasis mechanisms during normal growth. Here, to untangle effects of ppGpp and nutrients on growth and cell size, we gained control of cellular ppGpp by inducing the synthesis and hydrolysis enzymes RelA and Mesh1. We found that ppGpp not only exerts control over the growth rate, but also over cell division and hence the steady state cell size. The added size responds rapidly to changes in the ppGpp level, aided by transiently accelerated or delayed divisions, and establishes its new constant value while the growth rate still changes. Importantly, the magnitude of the added size and resulting steady-state birth size correlate with the ppGpp level, rather than with the growth rate. The resulting differences in overall size yet identical growth rates underscoring the size control exerted by ppGpp. Our results suggest that ppGpp serves as a critical regulator that coordinates cell size with growth.

3.2 Results

3.2.1 Ectopic control of ppGpp synthesis and hydrolysis

To study the relation between ppGpp and cell growth and division, two enzymes were used: the catalytic domain of the *E. coli* ppGpp synthesis enzyme RelA (RelA*)^{9,10}, and the ppGpp hydrolysis enzyme Mesh1 from *Drosophila melanogaster*^{11,12}, which were fused to YFP and CFP respectively (Fig. 3.1A). The former was inducible by doxycycline (dox) and the latter by isopropyl- β -D-thiogalactopyranoside (IPTG). We characterized this co-expression system in a ppGpp⁰ strain ($\Delta relA$, $\Delta spoT$) that cannot produce ppGpp. In minimal medium lacking amino acids, growth was undetectably low in absence of RelA* induction, consistent with previous reports^{8,12}, as ppGpp is then required to activate amino acid biosynthesis operons^{13,14}. However, growth became exponential if both RelA* and Mesh1 we co-expressed (S. Fig. 3.2A). These findings confirm that balanced synthesis and hydrolysis can achieve the constant ppGpp levels that are critical to normal exponential growth. If RelA* and Mesh1 indeed counteract in ppGpp production, then the same growth rates should be achievable by increasing both in parallel, as the additional synthesis by RelA* can then be cancelled by the additional hydrolysis by Mesh1. The data indeed showed similar growth profiles for different combinations of RelA* and Mesh1 expression; with both either at lower levels, or both at higher levels (S. Fig. 3.2A).

3.2.2 ppGpp exerts cell size control

We studied the effects of ppGpp at the single-cell level using a microfluidic chip that allowed media exchange, phase contrast and fluorescence microscopy, and cell-tracking algorithms¹⁵. We determined the length at birth (LB) and division (LD), the

cycle duration (T_{cyc}) and exponential growth or elongation rate (μ) for each cell cycle, and RelA* and Mesh1 enzyme concentrations, as quantified by the mean fluorescence per pixel (Fig. 3.1B, Supp. Fig. 3.1A-D). Here, we expressed either RelA*-YFP or Mesh1-CFP at moderate levels in the WT background (*relA+* and *spoT+*), in order to produce minor deviations in the ppGpp concentration, from above to below basal levels, while maintaining balanced exponential growth (Fig. 3.1C, D). As a control, we showed that expression of a fluorescent protein alone did not significantly affect cell size or growth rate (S. Fig. 3.1E-F).

The (population-mean) trend in the growth rate μ showed an optimum while the birth size LB went up monotonically, as ppGpp decreased from above to below basal levels (Fig. 3.1C, D). The relation between LB and μ (Fig. 3.1E) contained a number of intriguing features. First, as ppGpp decreased, both LB and μ increased initially (Fig. 3.1E), in agreement with the well-known finding that faster growing cells are larger. However, decreasing ppGpp further led to an inverted trend, in which slower growing cells are larger (Fig. 3.1E). This deviation began at near-endogenous ppGpp levels (Fig. 3.1C-E). A counter-intuitive consequence of this inversion is that excursions above and below this endogenous ppGpp level leads to cells that differ in size but grow equally fast (Fig. 3.1E). The same trends were observed for the ppGpp0 strain with RelA* and Mesh1 (S. Fig 3.2B-C).

The data are thus inconsistent with models in which ppGpp is a regulator of growth, and in turn, growth sets cell size, as described by the general growth law^{16,17}. In such hierarchical models, LB would follow the increase-optimum-decrease trend observed for μ (Fig. 3.1C). Instead, the monotonic increase of LB with increasing ppGpp (Fig. 3.1D) suggested that ppGpp affects size in a way that is not mediated by μ . In recent years, it has become clear that the bacterial cell size is set by adding a constant size each cell cycle. Hence, we surmised that if ppGpp plays a μ -independent role in setting LB, as our data suggests, it should also play a role in this adder mechanism.

3.2.3 ppGpp dynamically controls added cell size

In order to investigate the effect of ppGpp on the added size, we quantified the added length (ΔL) each cell cycle. First, we found that the adder principle was obeyed at all ppGpp concentrations: for the different levels of dox and IPTG induction, ΔL was birth-size independent (Fig. 3.2A). In line with previous adder principle observations, we find that T_{cyc} rather than μ is modulated to achieve a constant ΔL , as larger-born cells divide sooner (Fig. 3.2B). Indeed, ΔL increased monotonically with decreasing ppGpp (S. Fig. 3.2D), and thus did not follow the trend observed for μ (Fig. 3.1C). These data indicated that the added size correlated with population-average ppGpp concentration rather than the rate of growth.

Next, we considered how shifts in ppGpp concentration affect cell size and its control dynamically. Within the microfluidic flow-cell, we followed individual cells as they were exposed to a shift from basal ppGpp concentrations (-dox) to different levels of RelA* induction (+dox), in various growth media. First, the growth response underscored the important differences between the moderate induction that we focus on here (1 and 2

ng/ml) and the strong induction that mimics the stringent response (10 ng/ml dox), with strong induction yielding a rapid growth arrest while moderate induction led to an approximately two-fold slower decrease in growth rate and allowed exponential growth to continue (Fig. 3.2C).

Notably however, the added size did respond rapidly even to low RelA* induction levels. Added size ΔL decreased halfway at about 25 min., and subsequently reached its final value at about 55 min (Fig. 3.2D, red trace). In contrast, μ responded substantially slower, and required about 100 min. to decrease halfway and over 300 min. to stabilize (Fig. 3.2C, blue trace). A similar pattern of rapid ΔL and slow μ responses were observed for different media and dox induction levels (Fig. 3.2E), as well as for Mesh1 induction (Fig. 3.2F). Consistently, ΔL increased more rapidly than μ decreased upon Mesh1 induction (Fig. 3.2F).

The data show a temporal order in which ΔL responds to ppGpp deviations prior to μ . Indeed, ΔL typically has already stabilized to its post-shift level when μ has decreased only half-way from pre-induction to post-induction level (Fig. 3.2D-F). These data support the idea that μ and ΔL are decoupled, and further extend the notion that ppGpp affects cell size independently from its role in growth rate control. We hypothesize that a change in ppGpp concentration sets a new added size by affecting the division rate, which in turn results in a new steady-state birth size.

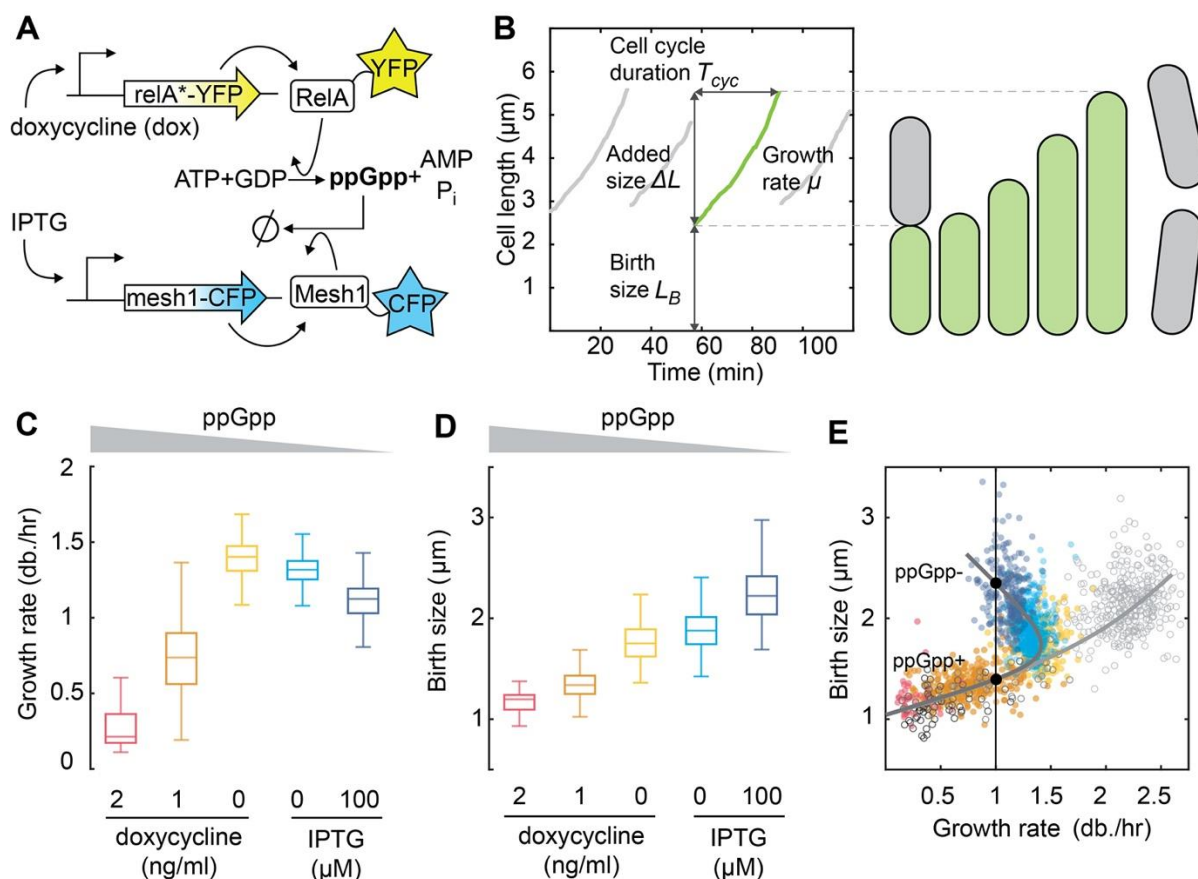


Figure 3.1. ppGpp exerts control over bacterial cell size. **A** Scheme to control the cellular ppGpp concentration. A RelA truncate from *E. coli* (*relA**), which synthesizes ppGpp, is fused to YFP and induced by doxycycline (dox). The ppGpp hydrolysis enzyme Mesh1 is fused to CFP and induced by IPTG. See S. Fig. 3.1 and 3.2 for characterization of these constructs. **B** Measured length of single cells grown in a microfluidic device. For each cell cycle we quantify; size (length) at birth (L_B), cell cycle duration (T_{cyc}), added size (ΔL), and the growth rate (μ) by exponential fitting. **C** Growth rate for decreasing ppGpp levels. ppGpp increases above basal levels when inducing *relA** with dox, and decreases below when inducing *mesh1* by IPTG, in *WT* (*relA+*, *spot+*) cells. Left to right: $N = 42, 316, 257, 403, 241$ cell cycles. μ peaks at basal (endogenous) ppGpp levels, and then decreases. **D** Birth size for decreasing ppGpp levels. Conditions as in panel C. L_B increases continuously while μ decreases for below-basal ppGpp levels. The L_B thus follows the ppGpp trend rather than that of μ . **E** Birth length against growth rate. Closed circles: single cell cycles in minimal media, colors and conditions as panels C and D. Drawn lines are guides to the eye. For below-basal ppGpp, slower growing cells are larger, owing to an inversion of the growth law. Cells of different size can thus have the same growth rate (black dots). Open circles: single cell cycles in rich media, with 2 ng/ml, 1 ng/ml, or 0 ng/ml dox, and $N = 66, 35, 336$ cell cycles (dark to light gray).

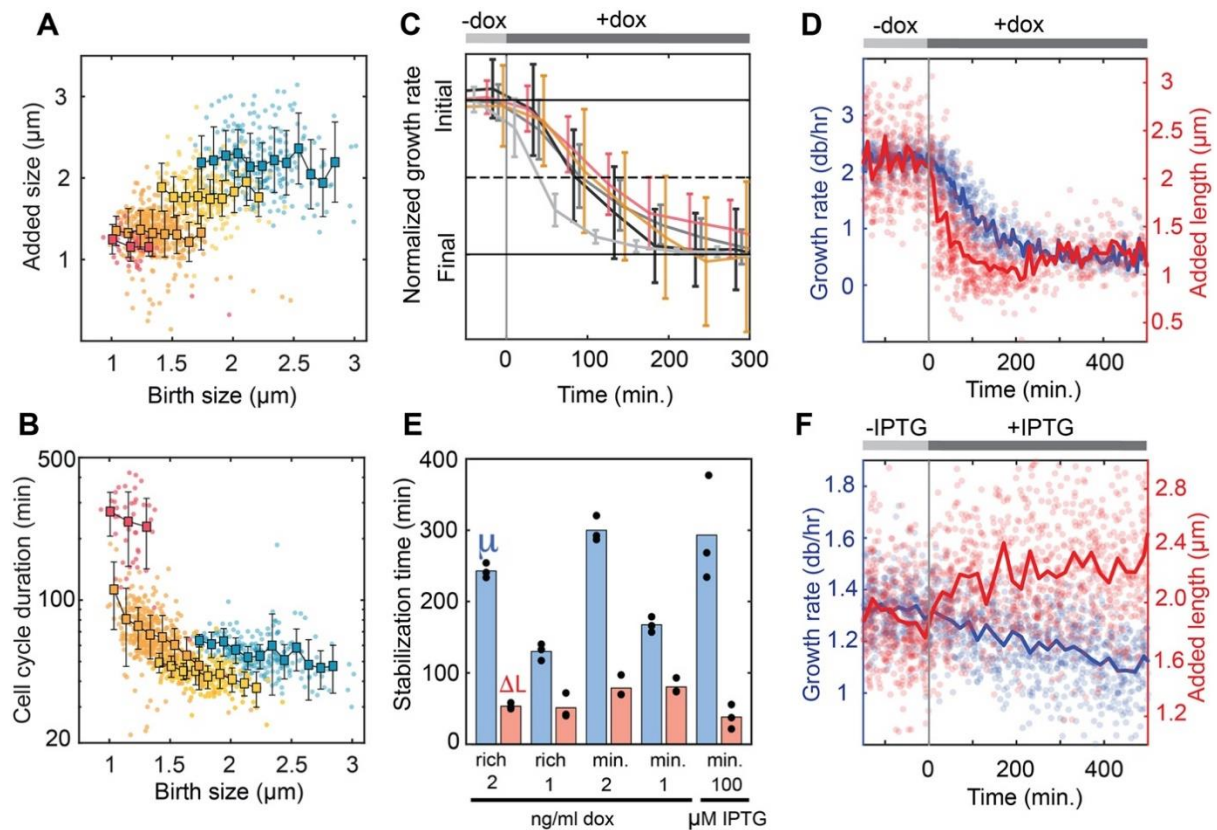


Figure 3.2. ppGpp dynamically controls added cell size. **(A)** Cell length added (ΔL) per cell cycle against birth length (L_B) of that cycle, for different constant ppGpp levels. Dots are single cell cycles, squares are means for L_B bin, bars are s.e. Left to right: clouds for decreasing ppGpp levels of ppGpp, starting with dox in ng/ml: 2 (red), 1 (orange), 0 (yellow), and then 100 μM IPTG (blue). $N = 42, 316, 257, 241$ cell cycles. For each cloud, ΔL is constant for different L_B , consistent with “adder” principle. **(B)** Cell cycle duration (T_{cyc}) against birth length (L_B) of that cycle. When L_B is smaller, T_{cyc} is larger, indicating it is modulated as cells compensate for stochastic variations in L_B , which is consistent with the adder principle. Colours and conditions as in panel A. **(C – F)** Cells during ppGpp shift, from basal to above and below basal levels. **(C)** Growth rate (μ) during ppGpp increases, by RelA* induction with dox, in rich and minimal media. μ response timescale for these various conditions is assessed by normalizing rate to initial (pre-shift) and final (post-shift) value. Top bar indicates dox induction. In minimal media, shift from 0 ng/ml dox to: 2 (pink), and 1 (orange). In rich media, shift from 0 ng/ml to: 1 (dark grey), 2 (intermediate grey), and 10 (light grey). Bars are s.e., averaged over multiple cell cycles. Curves show similar adaptation time for moderate shifts, in contrast to the large 10 ng/ml shift, which is significantly faster, and serves as a control: growth indeed arrests at high ppGpp levels, as studied before, in line with the stringent response. **(D)** Growth (μ) and added size (ΔL) during ppGpp increase. Circles are single cell cycles, lines are moving averages, for shift from 0 to 2 ng/ml dox, in rich medium. ΔL responds faster than μ and stabilizes to post-shift value while μ still varies. **(E)** Stabilization time for μ (blue) and ΔL (red). See methods for quantification approach. Each black dot shows the results of the analysis from 1/3rd of the available data points. ΔL responds faster than μ under all moderate shifts. **(F)** Growth (μ) and added size (ΔL) during ppGpp decrease. Circles are single cell cycles, lines are moving averages, for shift from 0 to 100 μM IPTG dox, in minimal medium.

3.2.4 Division accelerates transiently to achieve constant added size after induced ppGpp synthesis

We used mathematical modelling to understand the interplay between growth, division, and size, and compare different possible scenarios. Current size homeostasis models consider constant growth conditions, as well as a strict coupling between μ and ΔL ^{2,3,18,19}. We first tested a *hierarchical* model (Fig. 3.3A), which thus preserves the μ - ΔL coupling as growth conditions change. This model takes the observed initial and final values of μ and ΔL as input, lets μ decrease exponentially with the observed rate, and averages over multiple resulting simulated stochastic trajectories in ΔL and division rate $1/T_{cyc}$. The results of the hierarchical model (Fig. 3.3A) appeared inconsistent with the experimental observations (Fig. 3.3B). In particular, ΔL and μ decrease at similar rates in this model, while L_B decreases slower than μ (Fig. 3.3A), while the experiments show that both ΔL and L_B decrease faster than μ (Fig. 3.3B). Notably, the experimental data also indicate a transient increase in $1/T_{cyc}$ before it decreases (Fig. 3.3B), unlike the hierarchical control model (Fig. 3.3A).

Next, we considered a model of *direct* ppGpp control (Fig. 3.3C), which allows μ and ΔL to respond to ppGpp changes via independent routes and timescales. In this model, as also observed in the data (Fig. 3.2D), the mean ΔL responds directly by decreasing linearly to its post-shift value in about two pre-shift cell-cycles (note that division events in the averaged lineages are not synchronized), while μ decreases in the same way as in the previous model (Supp. Fig. 3.3A). The direct control model reproduces many features of the experimental data. Specifically, L_B responds slower than ΔL but faster than μ , and surprisingly, $1/T_{cyc}$ showed a transient increase (Fig. 3.3B and C).

This increase in $1/T_{cyc}$ may appear paradoxical, as it must decrease ultimately to match the lower μ . However, as illustrated by the model, it is a logical consequence of the μ and ΔL speed differences: ΔL reaches the lower post-shift value rapidly, while μ is still close to its high pre-shift value. With a comparatively high μ , the post-shift ΔL is achieved early, and hence divisions are early as well. Yet, it is indeed notable that the division rate appears readily modulated upwards and downwards. Together with the observation that ΔL is already stable at its new value while μ and $1/T_{cyc}$ are still varying towards theirs (Fig. 3.3B), these findings support a picture in which the cells act to realize their target ΔL (set in part by the concentration of ppGpp), and consequently L_B , regardless of the rate of growth, and thus yielding a corresponding division rate.

Further observations are consistent with this picture. First, $1/T_{cyc}$ changes on a timescale (within 25 minutes of the shift) that is shorter than the cell cycle duration, or even the C+D period (~65-75 minutes)²⁰. Scenarios in which division occurs a fixed time after the moment of replication initiation²¹⁻²³, with ppGpp affecting the added size by modulating the initiation rate, are inconsistent with these observations. These

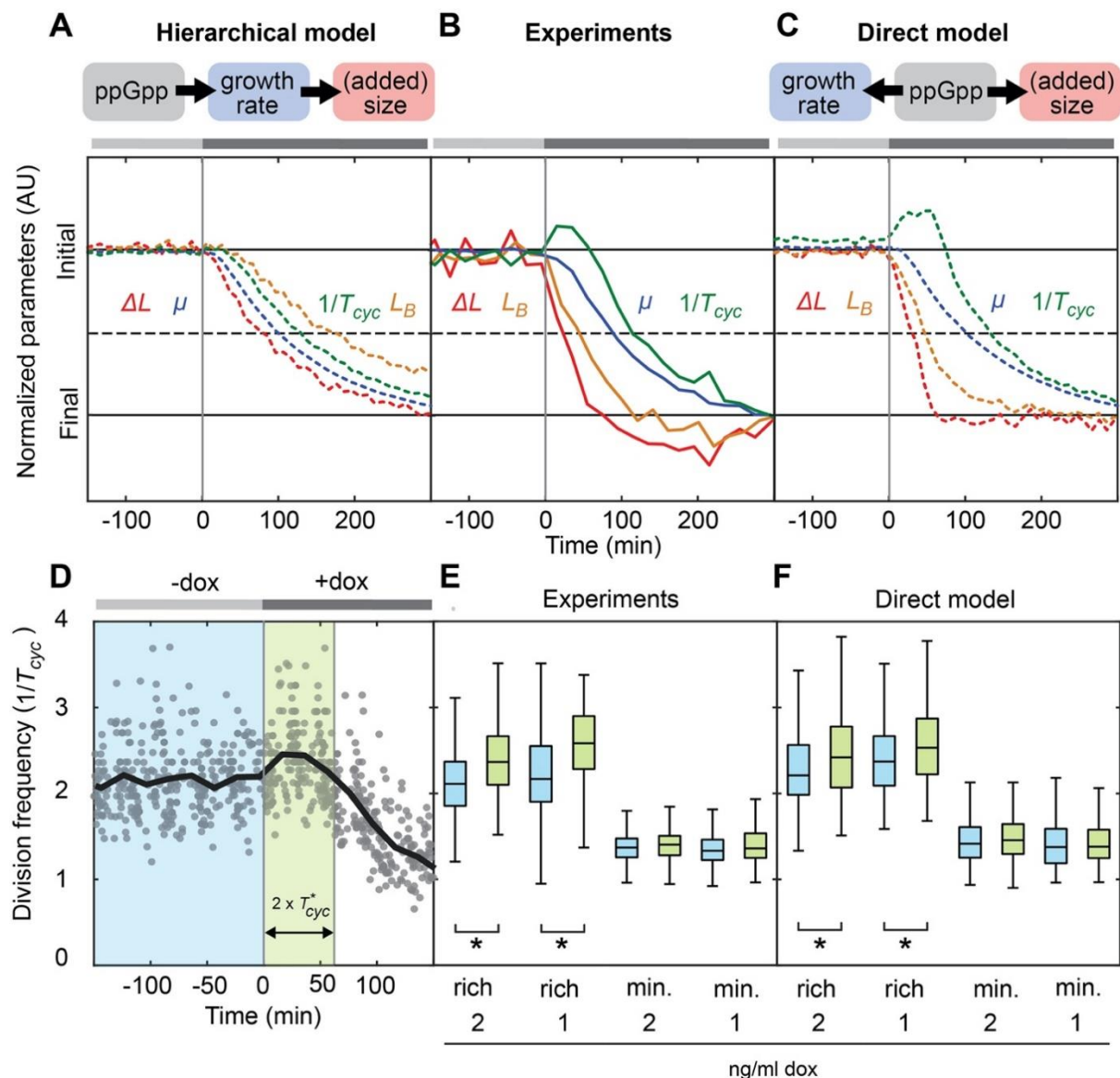


Figure 3.3 Division accelerates transiently to achieve constant added size. (A) Predictions of hierarchical model, in which ppGpp affects the growth rate (μ), and size in turn adjusts to the growth rate. To compare response speeds, indicated quantities are normalized to initial (pre-shift) and final (post-shift) values. Top bar indicates ppGpp increase. **(B)** Experimental data. Conditions and display as in panel A. **(C)** Predictions of direct model, in which ppGpp exerts control over division and hence (added) size independently of μ . Conditions and display as in panel A. Experiments agree with direct model in terms of the temporal order of the responses and the transient acceleration of divisions. **(D)** Quantification of transient effects in the division frequency ($1/T_{cyc}$). Data is averaged in purple and green zones to obtain data in panels E and F. Circles are single cell cycles for shift from 0 to 2 ng/ml dox, in minimal medium. Drawn line is moving average. **(E)** Pre- and post-shift division frequency ($1/T_{cyc}$), as defined in panel D. In rich media, a ~15% increase is observed between the purple and green zones. Star: $p < 0.01$. **(F)** Direct model reproduces transient acceleration in rich media but not in minimal media, as seen in the experiments (panel E).

scenarios require completion of ongoing cell cycles before registering ppGpp effects. The $1/T_{cyc}$ response would then exceed the C+D period and decrease exclusively, to match the new μ . Second, the growth rate independent model predicts the $1/T_{cyc}$ increase is too small to detect in minimal media (Fig. 3.3D and E), owing to the lower μ , which is indeed observed in the experiments (Fig. 3.3F). Third, upon Mesh1 induction, T_{cyc} increases within 20 minutes and then stays constant (S. Fig. 3.3B). These results indicate that ppGpp can exert control over division, and hence over cell size, in a way that is not mediated hierarchically through its effects on initiation and the rate of growth.

3.3 Conclusions

Elucidating the coordination between cell growth and cell cycle progression is a foundational challenge of microbial physiology. The adder mechanism has emerged as a key principle in recent years: it is observed across diverse domains of life and experimental conditions, and elegantly explains how size remains constant despite (division) stochasticity and exponential volume growth[2–4,15,22–26]. By *adding* a constant size every cycle, stochastic size variations are averaged out without needing a specific response to size deviations. How the adder mechanism relates to ppGpp is central, given the inherently intertwined nature of size and growth, yet remains poorly understood. ppGpp is implicated in diverse cellular metabolism and growth processes, including regulating ribosome production[27–29], modulating membrane synthesis[30,31] DNA replication initiation[5,32–34], and triggering the stringent response[35–37], a stress reaction that arrests growth until conditions improve.

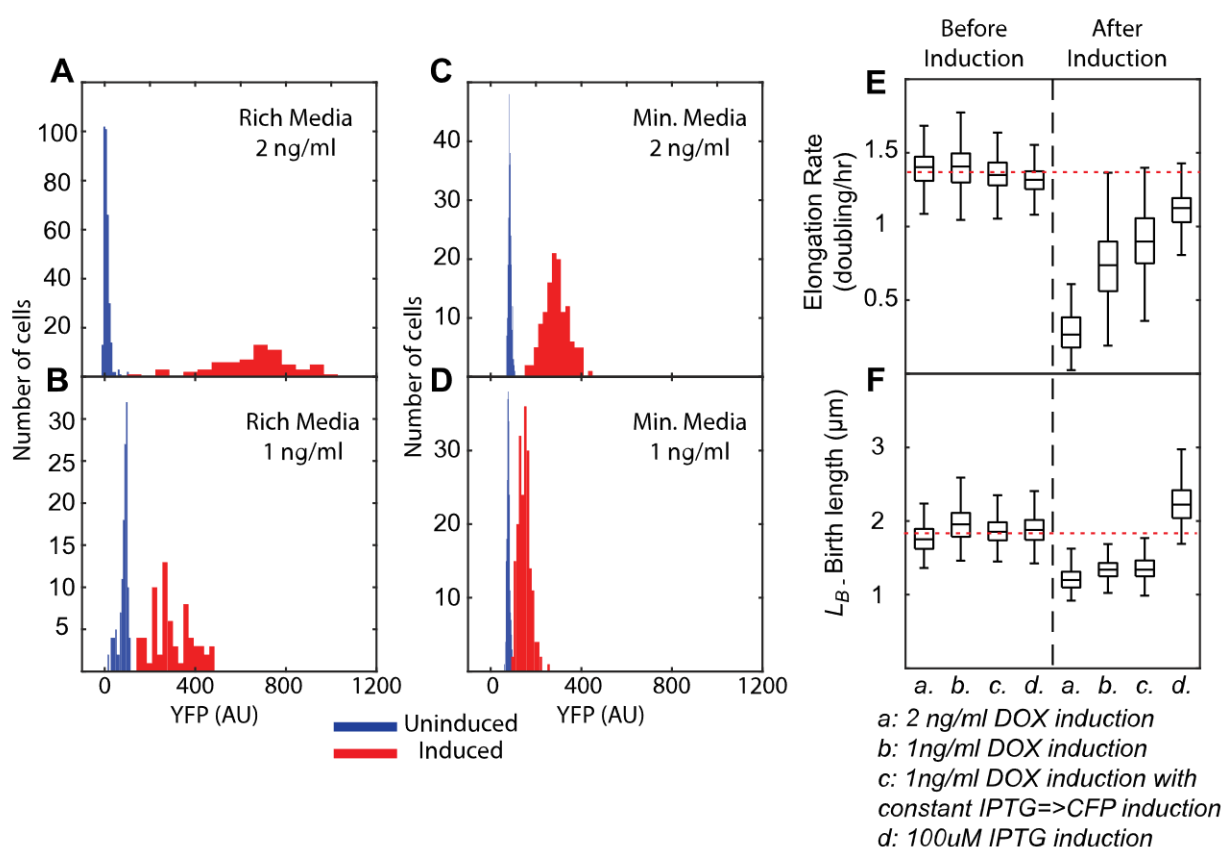
Here we found that ppGpp is a cell size regulator, and hence serves as a link between growth and size control mechanisms. More specifically, we showed that *E. coli* cells do not follow a hierarchical model, in which cell size adjusts to the growth rate (as described in the general growth law[1,16–18]), and ppGpp controls growth (by tuning ribosome production depending on amino acid availability, for instance). Rather, the (added) size correlates with the level of ppGpp (instead of the growth rate), and adjusts rapidly to ppGpp deviations, prior to the growth rate response, indicating that ppGpp exerts independent control over cell division and growth.

The findings give rise to a number of speculations. ppGpp-mediated cell cycle control could help accommodate different physiological limitations. For instance, the metabolic burden caused by ribosome excess may favour larger cells, rather than the smaller cell size resulting from a strictly positive size-growth correlation in hierarchical models. Consistently, overexpression of a non-functional protein was shown to yield larger cells[38]. The growth adjustments caused by the minor ppGpp changes studied here were also notably slowed than those that characterize the stringent response and large ppGpp changes. The former could be caused by ppGpp inhibition of ribosome production, and the resulting dilution of ribosomes by volume growth.

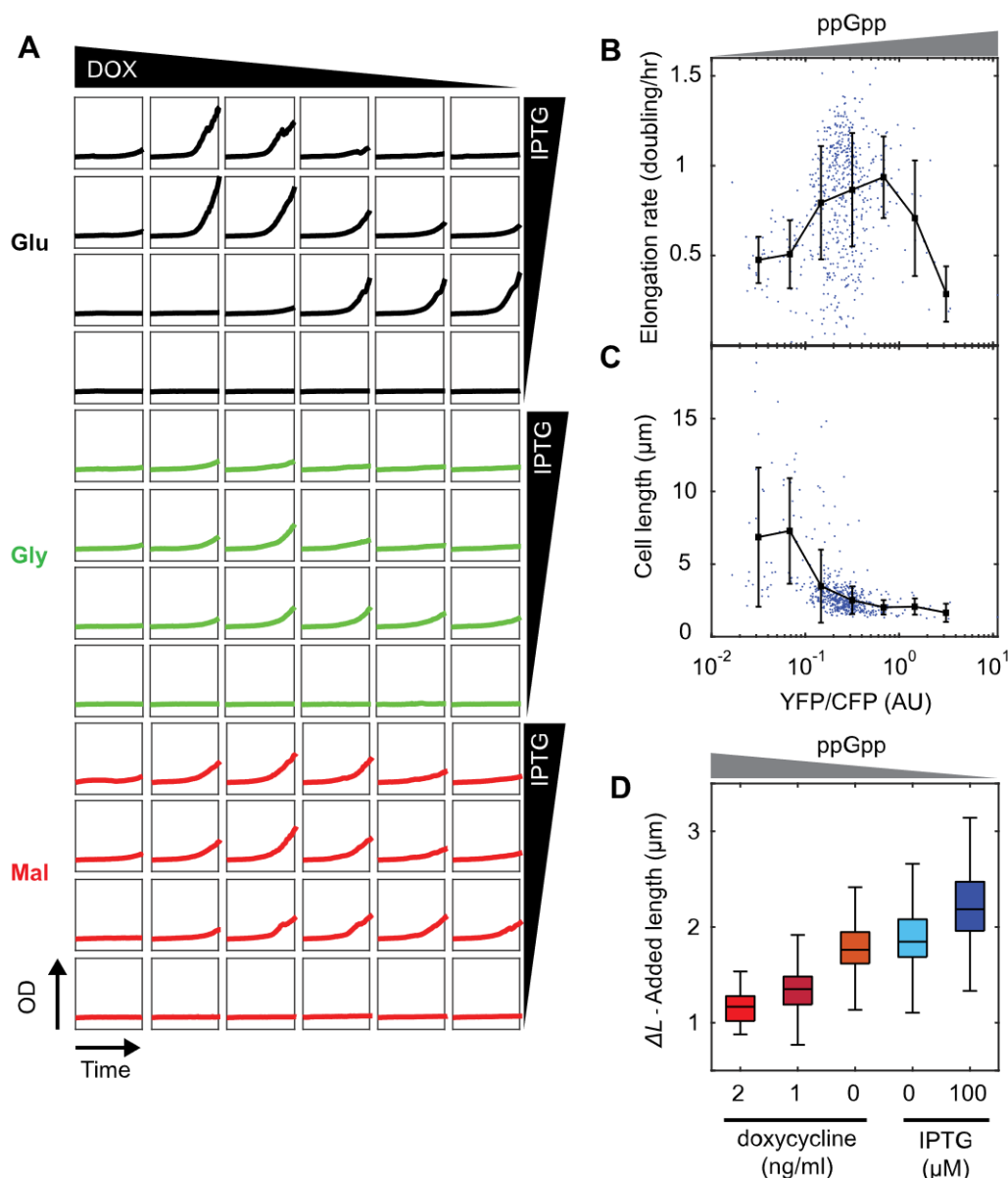
In recent years, diverse mechanisms have been proposed to explain cell size homeostasis and its dependence on growth[2–4,15,22–26]. Our findings suggest these mechanisms are under control of ppGpp. For instance, the constant added size is proposed to result from the accumulation of a signalling molecule throughout the cell cycle, which triggers division when a threshold is exceeded[23,39]. One may speculate that ppGpp alters the production of this molecule and its threshold. Owing to the central role of ppGpp in metabolism and its many

regulatory targets (hundreds of genes[40] and dozens of proteins[41]), ppGpp could control size in many possible ways. It was found that OpgH can suppress FtsZ ring formation depending on the growth rate. One may consider whether OpgH mediates the ppGpp division effects, though it is not a known ppGpp interactor[42]. Nucleoid occlusion mechanisms have also been proposed to explain variations in added size[2]. Nucleoid volume could be modulated by ppGpp-induced decreases in the overall DNA replication initiation[43–45] or transcription rates[46,47].

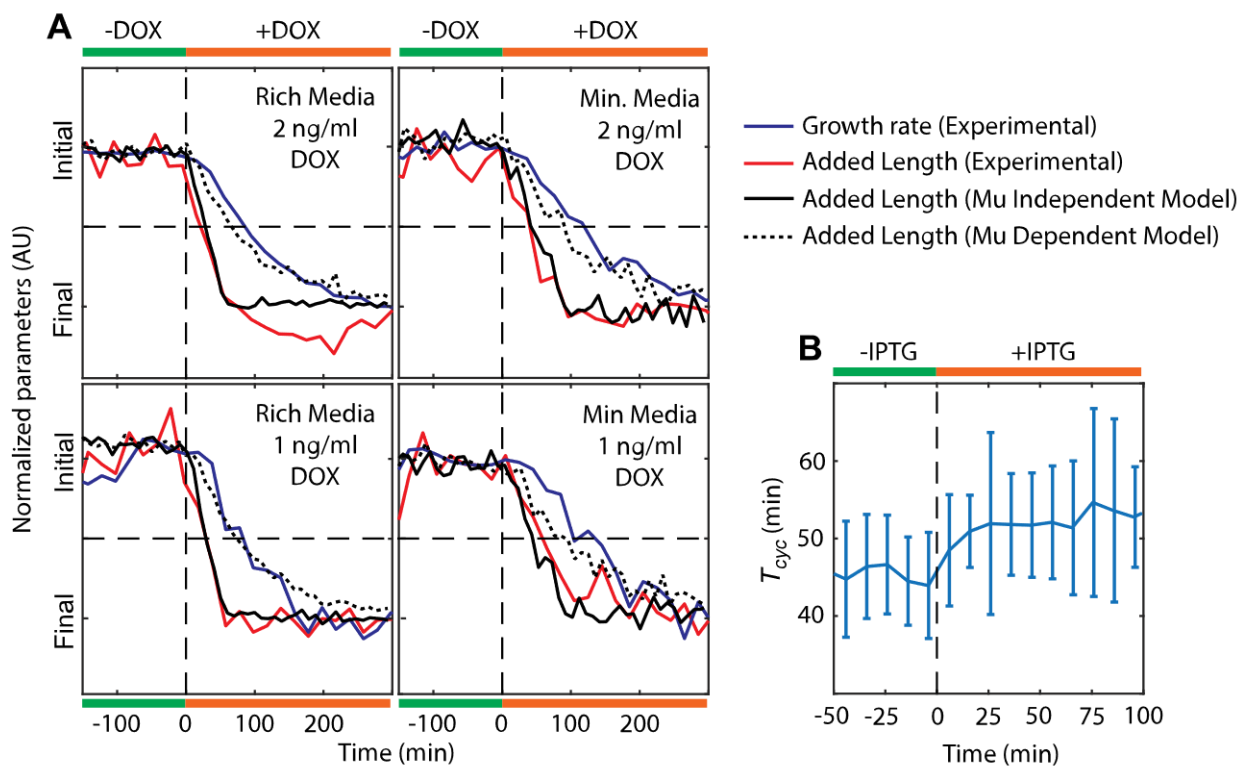
3.4 Supplementary Information



Supplementary Figure 3.1: Mild induction produces homogeneous populations and excess functionless protein synthesis (CFP) does not lead to changes in size and growth rate at our induction levels. A, B, C, D, For all the induction and initial growth conditions, fluorescence reporter distributions confirm that all the observed cells are getting induced homogeneously. **E-F** Strains carrying RelA* (**a-b**), RelA*+CFP(**c**) or Mesh1(**d**) plasmids were grown in the same nutritional media and RelA* or Mesh1 was induced (vertical dotted line left-right, before-after induction). For strain **c** CFP was constantly induced. Growth rates of constant CFP induction and Mesh1 plasmid carrying strains(**c,d**) are slightly lower than RelA* plasmid carrying strains (**a,b**) before induction of RelA* or Mesh1. After induction all the strains grow slower. Induction of Mesh1 leads to a significant increase cell size which is not observed under constant CFP induction indicating that the effect from Mesh1 induction is not related to cost of the peptide. 2 ng DOX induction (**a**) decreases growth rate to ~ 0.25 doubling/hr while 1ng induction in **b** or **c** leads to a similar final growth rate 0.75 and 0.89 doubling/hr respectively. Red dotted line shows the average of 4 experiments before spike.



Supplementary Figure 3.2: Varying induction of RelA* and Mesh1 leads to changes in cell size correlating with ppGpp concentration while growth rate shows optimum behavior. **A** OD data (range 0-0.5(AU)) through time (range 0-900(min)) from a ppGpp0 (Δ RelA, Δ SpoT) strain that is co-transformed with both RelA* and Mesh1 plasmids in minimal media with different carbon sources (black-glucose, green-glycerol, red-malate). With no IPTG (bottom row) there is no growth as presumably leakage from RelA plasmid is lethal due to accumulation of ppGpp. Similarly, if Mesh1 is induced at maximum rate while RelA is not induced (top right plots) growth is minimal since lack of ppGpp is detrimental to growth in minimal media. Growth defects caused by increase or decrease of Mesh1 or RelA induction can be compensated by balancing the induction of the other enzyme. This is shown by diagonal boxes (top-left to bottom-right) showing the fastest growth. **B** As in (A) when a ppGpp0 strain is transformed with both enzymes, stochastic differences between individual cells reveal similar result. Too high or too low YFP/CFP level (which indicates unbalanced Mesh1 and RelA production) leads to slower growth. **D** Even though the cells are slower growing with low ppGpp (low YFP/CFP level) they are larger. High YFP/CFP cells are slower and smaller due to higher than optimum ppGpp. **C** Altered ppGpp levels reversely correlate with ΔL similar to (Fig 3.1D) independent of growth.



Supplemental Figure 3.3. A Green bars above the plots represent no induction and orange bars shows induction, vertical line shows induction and horizontal lines show half-way between initial and final normalized values. μ -dependent adder simulation fails to represent the experimentally observed ΔL trajectory, while the μ -independent adder simulation shows close match. Same plots for 4 different experimental conditions are shown. **B** Induction of Mesh1 leads to rapid increase in T_{cyc} suggesting inhibition of division by decreased ppGpp levels.

3.5 Materials and Methods

Strains and plasmids

E. coli K-12 strain NCM3722 (CGSC# 12355) and ppGpp0 (CF10237) which were transformed with the RelA_YFP and/or Mesh1_CFP induction plasmids were used in all the experiments. A negative control of Mesh1 expressing plasmid where instead of Mesh1_CFP, only CFP is present was also used to test protein cost effects. Plasmid pRelA* was constructed by replacing mCherry on a pBbS2k-RFP plasmid (KAN Resistance, Tet promoter, sc101** origin) with a DNA sequence encoding the first 455 amino acids of the native RelA gene. YFP fluorophore mVenus was fused to RelA* via a glycine-serine linker using restriction cloning. Similarly, a codon optimized sequence of Mesh1 or CFP replaced mCherry in the plasmid pBbA5a-RFP (AMP Resistance, lacUV5 promoter, p15A origin). CFP was later fused to Mesh1 with a GS linker using restriction cloning.

Chemocompetent NCM3722 cells were transformed with the pRelA* plasmids and spread on LB Agar plates with 25ug/ml KAN. pMesh1_CFP and pCFP plasmids were transformed and plated on LB Agar plates with 50ug/ml AMP. Plates older than 3 weeks were discarded and fresh transformations were prepared to prevent mutants.

Chemocompetent ppGpp0 cells were co-transformed with pRelA* and pMesh1_CFP and plated on LB Agar plates with 50ug/ml AMP, 25ug/ml KAN and 100uM IPTG to allow growth. Without 100uM IPTG, leakage from pRelA* inhibits growth enough to prevent visible colonies next day morning (data not shown). Plates with colonies were only used on the day where the colonies first appear (next morning after transformation) as older plates lose viability rapidly due to lack of ppGpp.

Culture Conditions

Cells for bulk and microscopy experiments were grown using defined MOPS medium containing 0.2% (with volume) carbon source⁴⁷ with 100uM MnCl₂ (minimal media). Rich medium is the same as minimal media except for the supplementation of 0.2% Casamino Acids, 400µg/ml Serine and 40µg/ml Tryptophan. AMP 50ug/ml and KAN 25ug/ml were added to the media along with appropriate plasmid bearing strains.

For the microscopy experiments, cells were initially inoculated in 10mL tubes with 5ml MOPS rich medium from a single colony in the morning. The tube was placed in a 37°C room on an orbital shaker until the growth becomes visible (OD₆₀₀~0.1). Cells were then spun down at 4000G for 5 minutes and re-inoculated in 10µL top media. 2µL of the concentrated cells were injected into the microfluidic chip by hand via a p2.5 pipette and appropriate pipette tip.

ppGpp0 strain requires different handling due to its inability to respond to stress. For the 96 well plate experiments a single colony was inoculated in 5ml Glucose rich media with 100uM IPTG and placed on a shaker for up to 4 hours until OD reaches 0.4. After

that 40ng/ml DOX is added to prime the culture with high ppGpp production which allows it to handle stress and initiate growth in minimal media. This culture is then diluted in fresh media (MOPS minimal with different carbon sources) without any inducers. Immediately after the dilution 98uL of the culture is pipetted into wells of 96 well plates with 1+1uL (DOX + IPTG with 100x final concentration) inducers present, reaching a final volume of 100uL. 96 well plates which were prepared as above were placed in a Biotek Synergy HTX plate reader @370C with constant orbital shaking. OD was measured every 10 minutes. A similar method is applied for the microscopy experiment with the ppGpp0 strain. A single colony is grown in rich media with proper antibiotics from the morning and when OD reached 0.1, 40ng/ml DOX is added to induce ppGpp production. This allows cells to survive the stressful process of being concentrated and loaded into the chip by forcing them to produce ppGpp beforehand.

The chip is then placed under the objective in a warm chamber set to 370C for all the experiments. After cells populate the growth chamber input and output tubes are connected to the chip and appropriate media is pushed through the chip at 0.5ml/hr. This corresponds to 250-500x dilution per hour since the chip's inner volume is between 1-2uL.

Microfluidic Chip

The microfluidic chip's Epoxy mould which was kindly sent by Daan J. Kiviet from Ackermann Lab is a variant of the mothermachine from Jun lab. Each flow line consists of an input which splits up into 2 arms, in each arm there are a number of extruding growth chambers varying in depth and width (80, 60, 40, 20, 10, 5 μm width, 60, 30, 50, 40 μm depth) and a single output after the 2 arms reconnect into a single line.

Chip is built by first preparing the PDMS mix using the protocol from ¹⁵. Polymer and curing agent (Sylgard 184 elastomer, Dow Corning) were prepared by mixing 7.7 g of polymer with 1mL of curing agent. The slight deviation from the suggested 10g/1mL were implemented to create a more rigid chip allowing low height growth chambers to not collapse. Mixture was then thoroughly mixed using a vortexer and plastic mixer. The mixture is then poured into the Epoxy mould (provided by Ackermann lab) and placed in a desiccator for 30 minutes to remove air bubbles formed during mixing. Then the mould is baked at 800C for 1hr. After the baking period, the PDMS chip is removed from the mould using scalpels and rough edges were cut to allow for better binding to glass. Inlet and outlet holes were punched using a hole puncher. The PDMS chip is then covalently attached to a glass slide by using a hand-help corona treatment device (model BD-20ACV, Electro-Technic Products). Application was done by passing the corona treatment device 6-7 times, each pass lasting ~5seconds, 5-10mm away from the surface of both the PDMS chip and glass cover slip. After the corona application, PDMS chip is placed on the treated glass surface and tapped by a gloved finger to assure full bonding. Prepared chips could be used couple weeks after preparation however after more than a month, chambers start to collapse, so chips older than 1 month were not often used.

Imaging and Image Analysis

Cells growing in the microfluidic chambers were imaged using an inverted Nikon TE2000. Using 100x and a 1.5x zoom lenses in tandem a pixel size of 0.041 μm was achieved. Imaging was done using a CMOS camera (Hamamatsu Orca Flash 4.0) via illumination from an LED light source (ImSpec, HPX-L5) with a liquid light guide. The microscope stance was equipped with computer-controlled stage (Marzhauser, SCAN IM 120 3 100) allowing to move between several chambers for imaging. A phase contrast image was taken every minute and a YFP image every 5min using Chroma filter set 49003 and a computer-controlled shutter (Sutter, Lambda 10-3 with SamrShutter). Control of the automated microscopy systems was achieved through MetaMorph software. Each experiment lasts between 24-36 hours, images were initially visually analysed to check for major issues such as cells washing away from the wells or halting of growth due to clogs.

After the initial checks, a MatLab based software customized by Tans Lab was used to quantify growth rates and cell sizes. Individual cells are identified and tracked from phase contrast images. Cell's lengths and volumes were estimated assuming the shape of cylinders with semi-circular caps and fitting a polynomial to skeleton data. Estimated length data through time is used to calculate either instantaneous growth rate or average growth rate using exponential fits. Fluorescence values are calculated from a small strip inside the cells to decrease errors caused by fluorescence falloff that occurs at the edges of the cell. Added length is calculated by simply subtracting size at division (end of cycle) from size at birth (beginning of cycle). Duration of the cycles are calculated from timestamps of the initial and final image a cell has been seen. Any cell that does not divide within the growth chamber is ignored along with cells that approach the exit of the wells due to increase speed and possible tracking issues that arise.

Calculation of stabilization time

Data points enclosed by a sliding window with width ($\sim 1 \times T_{\text{cyc}}$) starting from the beginning of the experiment is compared against all the data points where growth rate is stable after induction. As the sliding window moves through time, both growth rate and added length change and start to approach the final stable value. When the t-test between the sliding window and final stable growth regime results in a p-value greater than 0.05, 3 times in a row, the centre of the window is taken as "Stabilization Time". For each experiment the data is split into 3 by maintaining relative data density through time and each 1/3rd batch is analysed using the same method to estimate technical repeatability (black dots, Fig. 3.2D).

Division frequency analysis

All the data points representing $60/T_{\text{cyc}}$ from before induction ($-150 < t < 0$ min) are compared against the data points from immediately after ($0 < t < 2 * T_{\text{cyc}}$ minutes). A simple t-test is applied, and boxplots represent the tested data points (Fig. 3.3E-F).

Models

We considered two alternative models describing size control during the transient. In both models a cell divides with a hazard rate¹⁹ that depends on the added size and a target added size ΔL (which in stationary conditions corresponds to the average added size). Both the target added size $\Delta L(t)$ and the growth rate $\mu(t)$ are functions of time during the transient. In both the models the growth rate $\mu(t)$ is exponentially relaxing to the stationary value observed in each of the experiments.

The two models differ for the relation between growth rate and size scale during transient. In the growth dependent model, the typical size is a deterministic function of the growth rate $\Delta L(t) = D \exp(\mu(t) T)$. Parameters were as follows: $T = \log(\text{size}_{\text{Final}} / \text{size}_{\text{Initial}}) / (\mu_{\text{Final}} - \mu_{\text{Initial}})$ and $D = \text{size}_{\text{Initial}} * \exp(-\mu_{\text{Initial}} * T)$. In the growth independent model, $\Delta L(t)$ is relaxing to the stationary value linearly in two pre shift cycle duration time.

Author contributions

G.B., S.J.T., and F. B. conceived the experiments, F.B. performed the experiments, F. B., M.C.L, J.G. performed the modelling, all authors contributed to the writing of the manuscript.

References

1. Schaechter, M., MaalOe, O., and Kjeldgaard, N.O. (1958). Dependency on Medium and Temperature of Cell Size and Chemical Composition during Balanced Growth of *Salmonella typhimurium*. *J. Gen. Microbiol.* *19*, 592–606.
2. Campos, M., Surovtsev, I. V., Kato, S., Paintdakhi, A., Beltran, B., Ebmeier, S.E., and Jacobs-Wagner, C. (2014). A constant size extension drives bacterial cell size homeostasis. *Cell* *159*, 1433–1446. Available at: <http://dx.doi.org/10.1016/j.cell.2014.11.022>.
3. Taheri-Araghi, S., Bradde, S., Sauls, J.T., Hill, N.S., Levin, P.A., Paulsson, J., Vergassola, M., and Jun, S. (2015). Cell-size control and homeostasis in bacteria. *Curr. Biol.* *25*, 385–391. Available at: <http://dx.doi.org/10.1016/j.cub.2014.12.009>.
4. Sauls, J.T., Li, D., and Jun, S. (2016). Adder and a coarse-grained approach to cell size homeostasis in bacteria. *Curr. Opin. Cell Biol.* *38*, 38–44. Available at: <http://dx.doi.org/10.1016/j.ceb.2016.02.004>.
5. Schreiber, G., Ron, E.Z., and Glaser, G. (1995). ppGpp-Mediated Regulation of DNA Replication and Cell Division in. *Curr. Microbiol.* *30*, 27–32.
6. Vadia, S., Tse, J.L., Lucena, R., Yang, Z., Kellogg, D.R., Wang, J.D., and Levin, P.A. (2017). Fatty Acid Availability Sets Cell Envelope Capacity and Dictates Microbial Cell Size. *Curr. Biol.* *27*, 1757–1767.
7. Magnusson, L.U., Gummesson, B., Joksimović, P., Farewell, A., and Nyström, T. (2007). Identical, independent, and opposing roles of ppGpp and DksA in *Escherichia coli*. *J. Bacteriol.* *189*, 5193–5202.

8. Xiao, H., Kalman, M., Ikehara, K., Zemel, S., Glaser, G., and Cashel, M. (1991). Residual guanosine 3',5'-bispyrophosphate synthetic activity of *relA* null mutants can be eliminated by *spoT* null mutations. *J. Biol. Chem.* *266*, 5980–5990.
9. Gropp, M., Strausz, Y., Gross, M., and Glaser, G. (2001). Regulation of *Escherichia coli* *RelA* requires oligomerization of the C-terminal domain. *J. Bacteriol.* *183*, 570–579.
10. Schreiber, G., Metzger, S., Aizenman, E., Roza, S., Cashel, M., and Glaser, G. (1991). Overexpression of the *relA* gene in *Escherichia coli*. *J. Biol. Chem.* *266*, 3760–3767.
11. Sun, D., Lee, G., Lee, J.H., Kim, H.-Y., Rhee, H.-W., Park, S.-Y., Kim, K.-J., Kim, Y., Kim, B.Y., Hong, J.-I., *et al.* (2010). A metazoan ortholog of *SpoT* hydrolyzes ppGpp and functions in starvation responses. *Nat. Struct. Mol. Biol.* *17*, 1188–94. Available at: <http://dx.doi.org/10.1038/nsmb.1906>.
12. Zhu, M., and Dai, X. (2019). Growth suppression by altered (p)ppGpp levels results from non-optimal resource allocation in *Escherichia coli*. *Nucleic Acids Res.* *47*, 4684–4693.
13. Paul, B.J., Barker, M.M., Ross, W., Schneider, D.A., Webb, C., Foster, J.W., and Gourse, R.L. (2004). *DksA*: A Critical Component of the Transcription Initiation Machinery that Potentiates the Regulation of rRNA Promoters by ppGpp and the Initiating NTP. *Cell* *118*, 311–322.
14. Paul, B.J., Berkmen, M.B., and Gourse, R.L. (2005). *DksA* potentiates direct activation of amino acid promoters by ppGpp. *Proc. Natl. Acad. Sci. U. S. A.* *102*, 7823–7828.
15. Wehrens, M., Ershov, D., Rozendaal, R., Walker, N., Schultz, D., Kishony, R., Levin, P.A., and Tans, S.J. (2018). Size Laws and Division Ring Dynamics in Filamentous *Escherichia coli* cells. *Curr. Biol.* *28*, 972-979.e5. Available at: <https://doi.org/10.1016/j.cub.2018.02.006>.
16. Pierucci, O. (1978). Dimensions of *Escherichia coli* at various growth rates: model for envelope growth. *J. Bacteriol.* *135*, 559–574.
17. Si, F., Li, D., Cox, S.E., Jun, Y., Si, F., Li, D., Cox, S.E., Sauls, J.T., Azizi, O., Sou, C., *et al.* (2017). Invariance of Initiation Mass and Predictability of Cell Size in *Escherichia coli*. *Curr Biol.* *27*, 1278–1287.
18. Vadia, S., and Levin, P.A. (2015). Growth rate and cell size: A re-examination of the growth law. *Curr. Opin. Microbiol.* *24*, 96–103. Available at: <http://dx.doi.org/10.1016/j.mib.2015.01.011>.
19. Amir, A. (2014). Cell size regulation in bacteria. *Phys. Rev. Lett.* *112*, 1–5.
20. Osella, M., Nugent, E., and Lagomarsino, M.C. (2014). Concerted control of *Escherichia coli* cell division. *Proc. Natl. Acad. Sci. U. S. A.* *111*, 3431–3435.
21. Bremer, H., and Dennis, P.P. (2008). Modulation of Chemical Composition and Other Parameters of the Cell at Different Exponential Growth Rates. *EcoSal Plus* *3*.
22. Witz, G., van Nimwegen, E., and Julou, T. (2019). Initiation of chromosome replication controls both division and replication cycles in *E. coli* through a double-adder mechanism. *bioRxiv*, 593590.
23. Si, F., Le Treut, G., Sauls, J.T., Vadia, S., Levin, P.A., and Jun, S. (2019). Mechanistic Origin of Cell-Size Control and Homeostasis in Bacteria. *Curr. Biol.* *29*, 1760-1770.e7.

24. Wallden, M., Fange, D., Lundius, E.G., Baltekin, O., and Elf, J. (2016). The Synchronization of Replication and Division Cycles in Individual *E. coli* Cells. *Cell* *166*, 729–739.
25. Barber, F., Ho, P.Y., Murray, A.W., and Amir, A. (2017). Details matter: Noise and model structure set the relationship between cell size and cell cycle timing. *Front. Cell Dev. Biol.* *5*, 1–16.
26. Cadart, C., Monnier, S., Grilli, J., Sáez, P.J., Srivastava, N., Attia, R., Terriac, E., Baum, B., Cosentino-Lagomarsino, M., and Piel, M. (2018). Size control in mammalian cells involves modulation of both growth rate and cell cycle duration. *Nat. Commun.* *9*. Available at: <http://dx.doi.org/10.1038/s41467-018-05393-0>.
27. Molodtsov, V., Sineva, E., Zhang, L., Huang, X., Cashel, M., Ades, S.E., and Murakami, K.S. (2018). Allosteric Effector ppGpp Potentiates the Inhibition of Transcript Initiation by DksA. *Mol. Cell* *69*, 828–839.e5.
28. Giordano, N., Mairet, F., Gouzé, J.-L., Geiselmann, J., and de Jong, H. (2016). Dynamical Allocation of Cellular Resources as an Optimal Control Problem: Novel Insights into Microbial Growth Strategies. *PLoS Comput. Biol.* *12*, e1004802. Available at: <http://journals.plos.org/ploscompbiol/article?id=10.1371/journal.pcbi.1004802>.
29. Burgos, H.L., O'Connor, K., Sanchez-Vazquez, P., and Gourse, R.L. (2017). Roles of transcriptional and translational control mechanisms in regulation of ribosomal protein synthesis in *Escherichia coli*. *J. Bacteriol.* *199*, 1–14.
30. Noga, M.J., Büke, F., van den Broek, N.J., Imholz, N., Scherer, N., Bokinsky, G., Broek, N.J. van den, Imholz, N., Scherer, N., and Bokinsky, G. (2019). Post-translational control is sufficient to coordinate membrane synthesis with growth in *Escherichia coli*. *bioRxiv*, 728451. Available at: <https://www.biorxiv.org/content/10.1101/728451v2.abstract?%3Fcollection=>.
31. Merlie, J.P., and Pizer, L.I. (1973). Regulation of phospholipid synthesis in *Escherichia coli* by guanosine tetraphosphate. *J. Bacteriol.* *116*, 355–366.
32. McAuley, S., Vadia, S., Jani, C., Huynh, A., Yang, Z., Levin, P.A., and Nodwell, J.R. (2019). A Chemical Inhibitor of Cell Growth Reduces Cell Size in *Bacillus subtilis*. *ACS Chem. Biol.* *14*, 688–695.
33. Traxler, M.F., Summers, S.M., Nguyen, H.T., Zacharia, V.M., Hightower, G.A., Smith, J.T., and Conway, T. (2008). The global, ppGpp-mediated stringent response to amino acid starvation in *Escherichia coli*. *Mol. Microbiol.* *68*, 1128–1148.
34. Liang, S.-T., Bipatnath, M., Xu, Y., Chen, S., Dennis, P., Ehrenberg, M., and Bremer, H. (1999). Activities of constitutive promoters in *Escherichia coli*. *J. Mol. Biol.* *292*, 19–37.
35. Jishage, M., Kvint, K., Shingler, V., and Nyström, T. (2002). Regulation of σ factor competition by the alarmone ppGpp. *Genes Dev.* *16*, 1260–1270.
36. Ferullo, D.J., and Lovett, S.T. (2008). The stringent response and cell cycle arrest in *Escherichia coli*. *PLoS Genet.* *4*, 21–23.
37. Traxler, M.F., Summers, S.M., Nguyen, H.T., Zacharia, V.M., Hightower, G.A., Smith, J.T., and Conway, T. (2008). The global, ppGpp-mediated stringent response to amino acid starvation in *Escherichia coli*. *Mol. Microbiol.* *68*, 1128–1148.
38. Basan, M., Zhu, M., Dai, X., Warren, M., Sévin, D., Wang, Y., and Hwa, T. (2015). Inflating bacterial cells by increased protein synthesis. *Mol. Syst. Biol.* *11*, 836.

39. Harris, L.K., and Theriot, J.A. (2016). Relative rates of surface and volume synthesis set bacterial cell size. *Cell* 165, 1479–1492. Available at: <http://dx.doi.org/10.1016/j.cell.2016.05.045>.
40. Liu, K., Bittner, A.N., and Wang, J.D. (2015). Diversity in (p)ppGpp metabolism and effectors. *Curr. Opin. Microbiol.* 24, 72–79. Available at: <http://dx.doi.org/10.1016/j.mib.2015.01.012>.
41. Zhang, Y., Zborníková, E., Rejman, D., and Gerdes, K. (2018). Novel (p)ppGpp binding and metabolizing proteins of *Escherichia coli*. *MBio* 9, 1–20.
42. Hill, N.S., Buske, P.J., Shi, Y., and Levin, P.A. (2013). A Moonlighting Enzyme Links *Escherichia coli* Cell Size with Central Metabolism. *PLoS Genet.* 9.
43. Cooper, S., and Helmstetter, C.E. (1968). Chromosome replication and the division cycle of *Escherichia coli* B r. *J. Mol. Biol.*
44. Kraemer, J.A., Sanderlin, A.G., and Laub, M.T. (2019). The Stringent Response Inhibits DNA Replication Initiation in *E. coli* by Modulating Supercoiling of *oriC*. *MBio* 10, 1–18.
45. Fernández-Coll, L., Maciag-Dorszynska, M., Taylor, K., Vadia, S., Levin, P.A., Szalewska-Palasz, A., and Cashel, M. (2020). The Absence of (p)ppGpp Renders Initiation of *Escherichia coli* Chromosomal DNA Synthesis Independent of Growth Rates. *MBio* 11, 1–14. Available at: <http://mbio.asm.org/lookup/doi/10.1128/mBio.03223-19>.
46. Nastaran H. Yazdi, Calin C. Guet, Reid C. Johnson, and J.F.M. (2013). Variation of the folding and dynamics of the *Escherichia coli* chromosome with growth conditions. *Mol Microbiol.* 86, 1318–1333.
47. Jin, D.J., and Cabrera, J.E. (2006). Coupling the distribution of RNA polymerase to global gene regulation and the dynamic structure of the bacterial nucleoid in *Escherichia coli*. *J. Struct. Biol.* 156, 284–291.
48. Neidhardt, F.C., Bloch, P.L., and Smith, D.F. (1974). Culture Medium for Enterobacteria. *J. Bacteriol.* 119, 736–747.

4

Engineering a light activatable ppGpp hydrolysis enzyme

4.1 Introduction

E. coli metabolism responds rapidly to changes to the nutrient conditions [1-6]. This is beneficial since slower response would lead to decreased growth and fitness amongst faster responding competitors. For example, *E. coli*'s transcription rate was shown to increase within 1 minute of a nutritional upshift where amino acids are added to a minimal growth media. It was shown that the decrease in the intracellular concentration of the signalling molecule Guanosine-tetraphosphate (ppGpp) which occur after an amino acid upshift, is the main cause of the rapidly increased transcription rate [6]. ppGpp is a signalling molecule whose concentration reversely correlates with steady state growth rate and adjusts overall translation and transcription rate [7]. This achieves optimum translation capacity under various media conditions. However, it takes several hundred minutes to reach a new steady state concentration of a protein after a change in production rate, such as induction. [8]. On the other hand, some enzymes' activity can be directly controlled by ppGpp concentration allosterically [9,10,11]. For example, we have recently shown that membrane synthesis can be regulated by ppGpp via allosteric regulation of PlsB whose activity controls flux into phospholipid synthesis pathways[12-Preprint]. This was shown by modulating ppGpp concentrations using chloramphenicol, rifampicin and ectopic ppGpp synthesis and measuring flux through phospholipid synthesis pathway. Results matched well with simulations where ppGpp modulated PlsB activity allosterically. Activity of PlsB responded to changes in the ppGpp concentration within 2 minutes.

Currently it is still not fully understood whether basal concentrations of ppGpp observed during steady state growth (>0.5/hr) affect other processes such as DNA replication initiation, division and translation post-translationally [13-14]. Unfortunately, methods applied to identify PlsB as a ppGpp target, cannot be used to test other machinery as they interfere with translation and replication initiation itself. Other methods such as amino acid upshifts to decrease ppGpp levels [5] are also limiting because it becomes impossible to decouple the effects of the nutritional change itself from the effects of decreased ppGpp. For example, in order to test whether ppGpp can inhibit translation allosterically, one can add amino acids to the minimal growth media and rapidly decrease ppGpp levels in growing cells. If ppGpp is inhibiting translation rate allosterically, when ppGpp concentrations decrease translation rate should increase. However, a possible increase in translation rate after the upshift, could be caused by the increased amino acids concentration itself simply by increasing the substrates of translation. In order to answer the above question, one needs to develop a method to decrease ppGpp levels rapidly without changing the nutrient condition.

A way to decrease ppGpp levels in an exponentially growing *E. coli* is to induce translation of a ppGpp hydrolysis enzyme such as Mesh1[15-16]. It was shown that induction of Mesh1 leads to a lower ppGpp concentrations in-vivo [16]. However, the

limitation with this approach is the speed with which ppGpp would decrease and this was only shown for steady-state growth. Induction of an enzyme is on the same timescale as transcriptional regulation since most induction systems rely on triggering transcription of a gene via addition of specific inducers. This could lead to a gradual decrease in ppGpp levels as the enzyme concentration slowly stabilizes. In order to probe possible direct allosteric regulation of ppGpp on various metabolic pathways one possibility is to engineer a ppGpp decreasing mechanism which is faster than transcription->translation timescale. Because otherwise by the time ppGpp change happens, proteome can be altered by the slowly changing ppGpp. This would make it impossible to decouple the effects of ppGpp from the effects of changing proteome itself.

A light activated Mesh1 construct would allow rapid changes to ppGpp levels without needing nutrient change. The enzymes production could be induced under dark conditions and allowed to stabilize. Later when desired the light can be applied to induce a sudden burst of ppGpp hydrolysis by activating the enzyme. There are several ways to engineer a light activated version of a target enzyme (reviewed in [17]). In general, these methods utilize conformational changes that occur on various known light-sensitive domains. Two main strategies were followed in these studies. (1) A genetic construct was created to fuse a target enzyme with a light-sensitive domain which changes conformation under light. This change is then relayed to the fused enzyme and leads to variable activity under dark and light conditions [18,19,20,21]. (2) Protein-protein interactions were used to localize or sequester the target enzyme which is fused to a light-sensitive domain [22,23,24]. For our purposes a method under the first category using light sensitive LOV2 domain from *Avena sativa* is the most appropriate. LOV2 domain has a C-terminal alpha-helix which under blue light (470nm) is free to move. However, under dark conditions the helix is attracted to the rest of the domain [25]. This conformational change can be used to alter the activity of a fused enzyme using light. If fused enzyme has an N-terminal alpha-helix, the two helices can be fused to create a continuous helix link between LOV2 and target enzyme. This link can be used to trigger changes to the conformation and decreased activity of the target enzyme by attracting the shared helix to the LOV2 domain in dark. Later when light is turned on and the shared helix is released from the LOV2 domain, the target enzyme can assume its correct conformation and gain increased activity.

Here we describe how we engineered and tested a LOV2_Mesh1 fusion (LOVEsh-m14) using a simple growth assay as a way to measure enzyme activity. As described before, ppGpp levels need to be balanced to allow for optimum growth. Too much or too little ppGpp is detrimental to *E. coli* growth under various conditions [Chapter 2 This Thesis, 16, 26]. We tested our constructs with two complimentary experiments where ppGpp hydrolysis would either promote or inhibit growth and showed that a final construct (LOVEsh-m14) shows higher hydrolysis activity in light compared to dark. Preliminary measurements of in-vivo ppGpp concentrations also show ~20% decreased ppGpp levels 3 minutes after light activation of LOVEsh-m14. While the

observed change in ppGpp concentration after light induction is not large this construct can be used to probe various allosteric effects of ppGpp. Further, our results support that LOV2 domain is a viable modular light-sensitive domain for enzymes with N-terminal alpha helices.

4.2 Results

4.2.1 Methodology of engineering and testing a light activatable ppGpp hydrolysis enzyme

We have designed two experiments where light would promote or inhibit growth if the tested variant is light responsive. (1) In a strain where excess RelA production can be induced growth arrest occurs due to overproduction of ppGpp. Later when a ppGpp hydrolysis enzyme such as Mesh1 is induced growth can resume since excess ppGpp is hydrolysed. If a light activated Mesh1 variant can be constructed it is expected to recover growth under RelA overexpression with blue light but not in dark (Fig 4.1A). (2) If the growth medium is lacking amino acids, an optimum concentration of ppGpp is required for fastest growth [16,27]. If the ppGpp concentrations are decreased in minimal media, growth is slower. Therefore, another experiment is designed where growth is expected to be limited in minimal media in light but not in dark with possible light activated variants (Fig 4.1B). This allows us to identify possible effects of light itself on growth and removes the possibility of identifying false positive constructs.

In the first cycle of variant generation we tested different locations for where to fuse the two alpha helices of LOV2 and Mesh1 peptides. We initially created several “indents (-1 to -10 amino acids)” in Mesh1 while using all of the LOV2 domain. A positive control was also constructed where LOV2 domain and Mesh1 were connected with a GS-Linker. Because glycine-serine is a helix-breaking linker, such a construct is expected to prevent light-driven conformational changes in the LOV2 domain from affecting Mesh1 activity. This thus served as a control which allowed us to have a variant which should always have light independent high activity. A metabolically non-active protein (Cerulean) was used as a negative control which should never show ppGpp hydrolysis activity (Fig 4.1C).

Once a variant was identified to be light activated (v-3), the activity difference between dark and light was then improved by using targeted mutagenesis. Two amino acids at the fusion point (Tyr4, Pro5) were identified as alpha-helix breakers and semi-random primers were used to rapidly generate a mutant library with several alpha helix joining amino acids replacing the two.

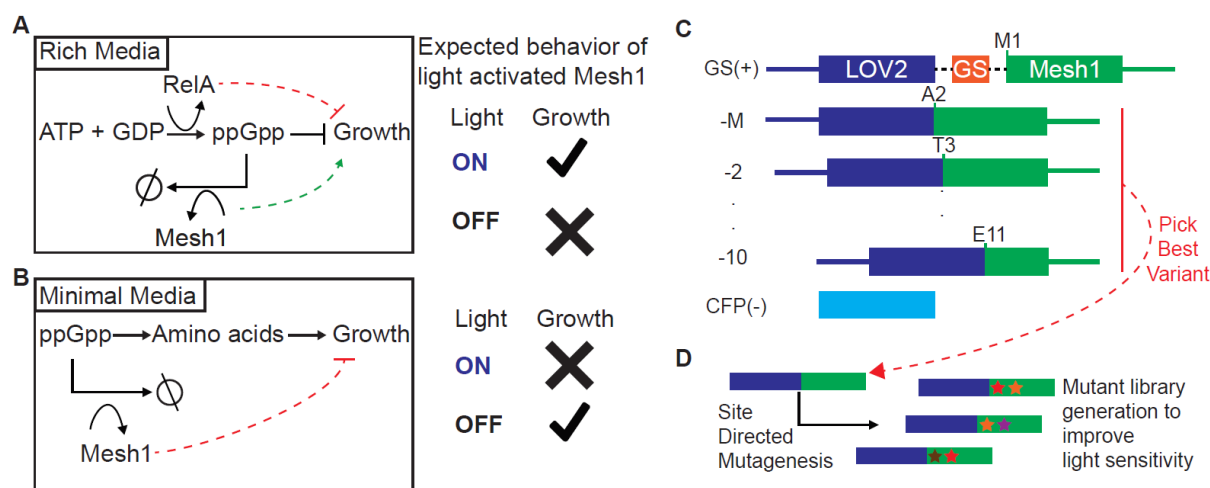


Figure 4.1. Engineering a new variant with less activity in dark by increasing the shared helix's stability using site directed semi-random mutagenesis. (A) Two amino acids at the interface between LOV2 and Mesh1 (4Tyr-Y and 5Pro-P) are known to disrupt alpha helix formation. Forward and reverse primers with 5 prime phosphorylation allow for easy ligation and transformation. Using a degenerate forward primer which limits the possible amino acids at Mesh1 positions 4 and 5 in 1 cloning step we generate numerous possible mutants. (B) Testing of the mutants reveals that in competition against RelA the original -3 variant can grow in the dark when enough time is allowed, however some of the new mutants(14, 18, 32) show no growth in dark indicating less activity due to presumably increased shared alpha helix stability

4.2.2 Variant (-3) rescues growth from ectopic ppGpp synthesis in response to light

In order to test the light responsiveness of the assorted variants, we designed a simple light box (S. Fig 4.1A) which can house a standard petri dish. All the variants created, along with controls were transformed in MG1655 carrying an inducible RelA plasmid. Each transformant was then grown to mid exponential phase in LB media without any induction. Next the cultures were diluted to the same OD (0.01) and 5 μ l spots were placed on two agar dishes containing the inducers for RelA and LOV2_Mesh1 variants. Another plate where no inducer was present was also used to test the viability of the cells under no induction. The plates were grown under dark or light conditions for 18 hours. Results showed that positive control was able to grow both in dark and light. Since activity of Mesh1, flexibly fused to LOV2 domain via a GS linker, should be light insensitive (Fig. 4.2A). Similarly, negative control where a protein with no ppGpp hydrolysis activity (Cerulean) was produced, did not grow under light nor dark, however it did grow with no inducer. This shows that our controls were working properly. When different variants were tested -M (-1) and -2 were shown to behave like the positive control. Indicating that the alpha helix link has not formed in these variants and Mesh1 is free from LOV2 -like the GS linker-. This was expected as the first 5-6 amino acids of the Mesh1 peptide is thought to not join the N terminal alpha helix [pdb entry 3NQW]. Variants -3 and -4 showed interesting results. Both of them showed growth in light but very little growth was observed in dark. This was the expected behaviour from a light activated Mesh1(Fig. 4.2A and Fig. 4.1A). Deeper

variants (-5 to -10) showed behaviour similar to either one of the controls indicating light insensitive behaviour.

To test the variants under different light intensities the light box was modified to illuminate 3 plates (S. Fig. 4.1B). The plate closest to the light source (1st) should experience the highest intensity of light and later plates less. Cells were allowed to grow for an overnight (~16hrs) to see small differences in growth rate. If the growth is allowed for long, different growth rates can create similar looking colonies as faster growing colonies reach the maximum size and stop growing (Fig. 4.2B). We observed again that positive control grew, and negative did not regardless of light. However interestingly variant -4 did not show colonies under dark nor light, most likely indicating that the activity of -4 is lower than -3 and thus requires longer growth times to become visible. Variant -3 however showed light dose dependent growth. Colonies closest to the light source created the densest growth on the plate.

In order to allow for proper light dimming an Arduino based light box prototype was built (Supplementary Fig. 4.1C). Arduino is a cheap and small programmable computer which allows hobbyists and scientists to build electronic devices. This prototype was designed to illuminate a 6 well plate and had individually controllable LED's for each well. Similar results were observed where -3 and -4 showed growth in light but not in dark. Furthermore, it was shown that the LED lamps that we used were highly directional and only allowed growth of a colony directly under the LED (Fig. 4.2C). This led to the building of the final light box where 6 LED's were illuminating each well of a 6 well plate (S. Fig. 4.1D). With proper light dimming and a higher throughput testing method we then showed that mutants -3 and -4 were allowing growth in a light and inducer concentration does dependent manner. The variants were placed under IPTG inducible promoters which allowed us to show that at higher inducer concentrations, growth starts to be visible even in the dark, indicating background activity from the variants even in dark. Furthermore, when little inducer was used for variants, growth could be recovered by increasing light intensity (Fig. 4.2D). Again, supporting a light responding enzyme behaviour.

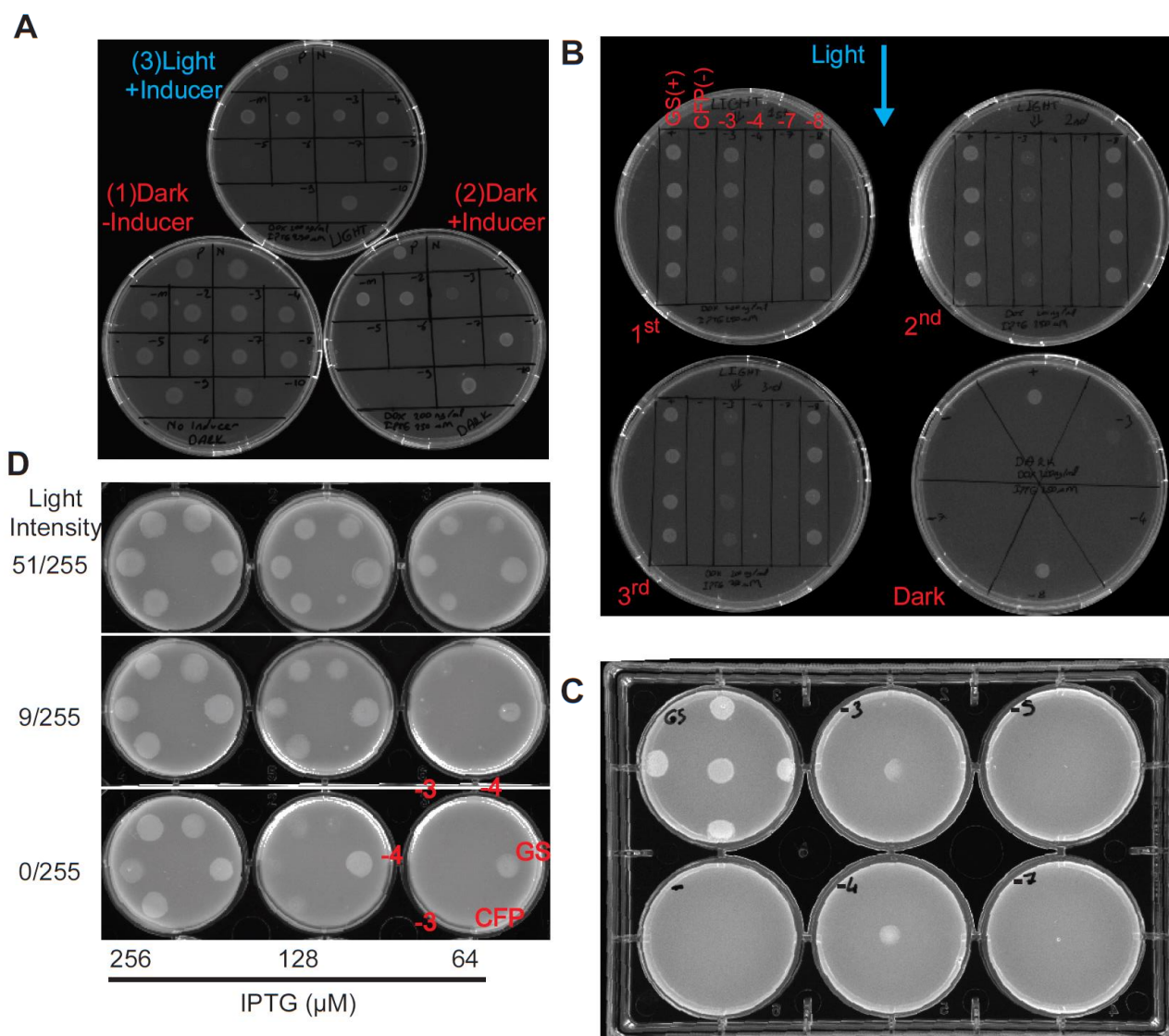


Figure 4.2. Variants (-3 and -4) rescues growth from ectopic ppGpp synthesis in response to light (A) 10 variants were tested against ectopic ppGpp synthesis on 3 plates with the same strains grown under different conditions (1) In dark with no inducers, all the strains manage to grow as expected (Bottom left). (2) In dark where RelA and LOV2_Mesh1 variants are induced, negative control does not grow and positive does while variants behave differently (Bottom right). (3) Finally, with inducers in the light, variants except -3 and -4 behave as they do in dark, indicating no light sensitive behaviour. However, -3 and -4 show higher growth in light plate (Top). (B) When the light is applied from one side (cyan arrow), the colonies closest to the source grow the most for variant -3. 1st plate is closest to the light source while 3rd is farthest (C) A new Arduino light box prototype shows that LED's are quite directional and only allow growth directly under each lamp. (D) A new light box allows testing of 36 spots under 6 different condition. -3 and -4 show light and LOV2_Mesh1 induction dose dependent growth as expected from a light activated enzyme.

4.2.3 Engineering an improved variant with less activity in dark by increasing the shared helix's stability

The variant which showed the greatest difference was further improved using the 36 LED Arduino controlled light box which allowed us to test 33 possible new variants with 3 controls (GS(+), CFP(-), best fusion(-3)) and targeted mutagenesis at the fusion location. We have identified 2 amino acids in the merging position of two alpha helices which are known to not-participate or indeed disrupt the formation of alpha helices (Tyr4, Pro5) (S. Table 4.2) [28,30]. This suggested that the required continuous alpha helix link between the LOV2 domain and Mesh1 in variant -3 could be unstable. This would explain the present activity in dark. Since we did not know which specific amino acids would be best suited to replace the two (Tyr4, Pro5) we designed a degenerate primer (Fig. 4.3A) which replaces each 4th and 5th position with 12 possible amino acids and 2 stop codons (S. Table 4.2). By using degenerate primers one can exclude specific nucleotides from occurring in a location. However, this does not allow picking any amino acid. We picked a degenerate primer with ...NWNWN... corresponding to Tyr4 and Pro5 sequence. W allows an A or a T and excludes C and G nucleotides. The possible codons from this degenerate primer are marked with red stars in supplementary table 4.2 and shows a possible amino acid pool with on average higher alpha helix joining propensity. This allowed us to create a mutant library which has high chance of replacing 4th and 5th position with high alpha helix joining propensity amino acids while still producing numerous different combinations to hopefully find one that is better than -3.

We then tested the new mutants in rich media competing against RelA, where growth was allowed longer before imaging the plates. Longer growth time(24hrs) allows growth to be visible in the variant -3 even in the dark because activity in dark is still present presumably due to weak alpha helix link. If one of our mutants has less activity in dark, we should see a difference in growth between -3 and the mutant in dark where an improved mutant's growth is expected to be slower.

Indeed, the results show several promising candidates. At growth times where -3 starts to grow in dark, several mutants such as 14, 18 and 32 don't show any growth in dark. Supporting that the mutations helped stabilize the alpha helix and decreased activity in dark. Furthermore, in light these mutants show comparable growth to -3 variant which suggests that the decreased activity in dark was not accompanied by a decreased activity in light (Fig. 4.3B). Sequencing confirmed that mutant 14 had replaced Tyr4 and Pro5 with Val4 and Lys5. Both Val and Lys have higher propensity to join an alpha helix (S. Table 4.2).

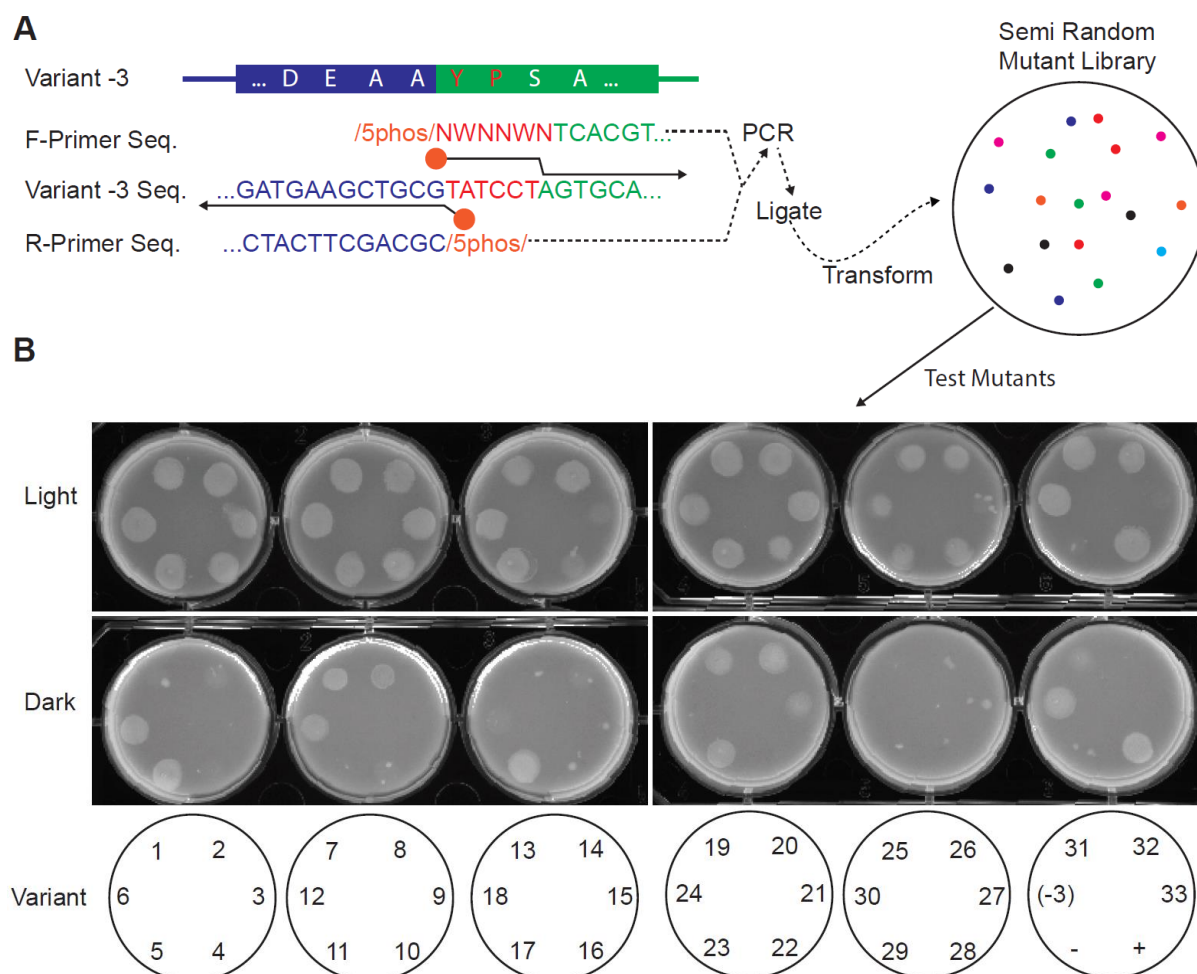


Figure 4.3. Engineering a new variant with less activity in dark by increasing the shared helix's stability using site directed semi-random mutagenesis. (A) Two amino acids at the interface between LOV2 and Mesh1 (4Tyr-Y and 5Pro-P) are known to disrupt alpha helix formation. Forward and reverse primers with 5 prime phosphorylation allow for easy ligation and transformation. Using a degenerate forward primer which limits the possible amino acids at Mesh1 positions 4 and 5 in 1 cloning step we generate numerous possible mutants. (B) Testing of the mutants reveals that in competition against RelA the original -3 variant can grow in the dark when enough time is allowed, however some of the new mutants(14, 18, 32) show no growth in dark indicating less activity due to presumably increased shared alpha helix stability.

4.2.4 Testing the new mutants in minimal media to observe growth arrest with light on agar plates and in liquid culture.

In the previous experiments the variants were competing against RelA's ppGpp synthesis so the increase in variant activity led to permission of growth under light, by increased hydrolysis activity. In order to have a more rigorous confirmation we performed another test where the activity of variants would lead to slower growth, removing doubt that light itself could be allowing growth not the constructs. This can be done as explained before (Fig. 4.1B).

8 mutants were selected from the results in Fig. 4.3B (mutants 6, 11, 14, 17, 18, 27, 32, 33). These 8 were then spotted on minimal agar plates and allowed to grow under light or in dark overnight. Results showed that for the positive control where Mesh1's activity is light independent; growth is not possible in dark nor light. Conversely the negative control which does not hydrolyse ppGpp grow occurs both in light and dark. As described (Fig. 4.1B and Chapter 3) ppGpp is needed in minimal media conditions for growth. Of the 8 tested mutants 3 show behaviour expected from an improved enzyme (mutants 14, 18, 32). All these 3 manage to grow in the dark where Mesh1 was evidently inactive/less active. However, under light, growth is not permitted as presumably activity of Mesh1 is restored and ppGpp is hydrolysed (Fig. 4.4A).

After identifying 3 mutants that appeared better than the original -3 variant, we conducted several liquid media experiments. Initially the mutants were competed against RelA and a measure of $\text{Growth}_{\text{Light}}/\text{Growth}_{\text{Dark}}$ was used to attempt at quantifying the activity difference (Supplementary Table 4.1). These results showed that mutant 14 was consistently faster growing in light compared to dark ($\text{Growth}_{\text{Light}}/\text{Growth}_{\text{Dark}} = 1.27$ and 1.56 unitless, 2 experiments' results). By using mutant 14 we also show that it is possible to inhibit growth in liquid minimal media under light however not in dark. (Fig. 4.4B). Supporting that mutant 14 can be used in liquid media as a light activatable enzyme. Preliminary results from a ppGpp harvesting experiment revealed that 3 minutes after activating the LOVEsh-m14 via blue light, ppGpp levels showed a ~22% decrease (S. Fig. 4.2). While more experiments are needed to confirm the speed and amplitude of the effect, these results show that rapid changes in ppGpp levels can be achieved using our construct LOVEsh-m14.

Furthermore sequencing the 3 mutants which showed least activity in dark (14,18,32) (Fig. 4.4A, bottom left plate) revealed the 2 amino acids replacing the Tyr4 and Pro5 were indeed high alpha helix joining propensity amino acids (mutant14=>Val4-Lys5, mutant18=> Met4-Val5, mutant32=>Val4-Val5). Valine, methionine and lysine all have higher alpha helix joining propensities (S. Table 4.2). This supports the suggested mechanism of LOV2 domain based light activated enzymes. Alpha helix stability appears important to regulate activity in dark.

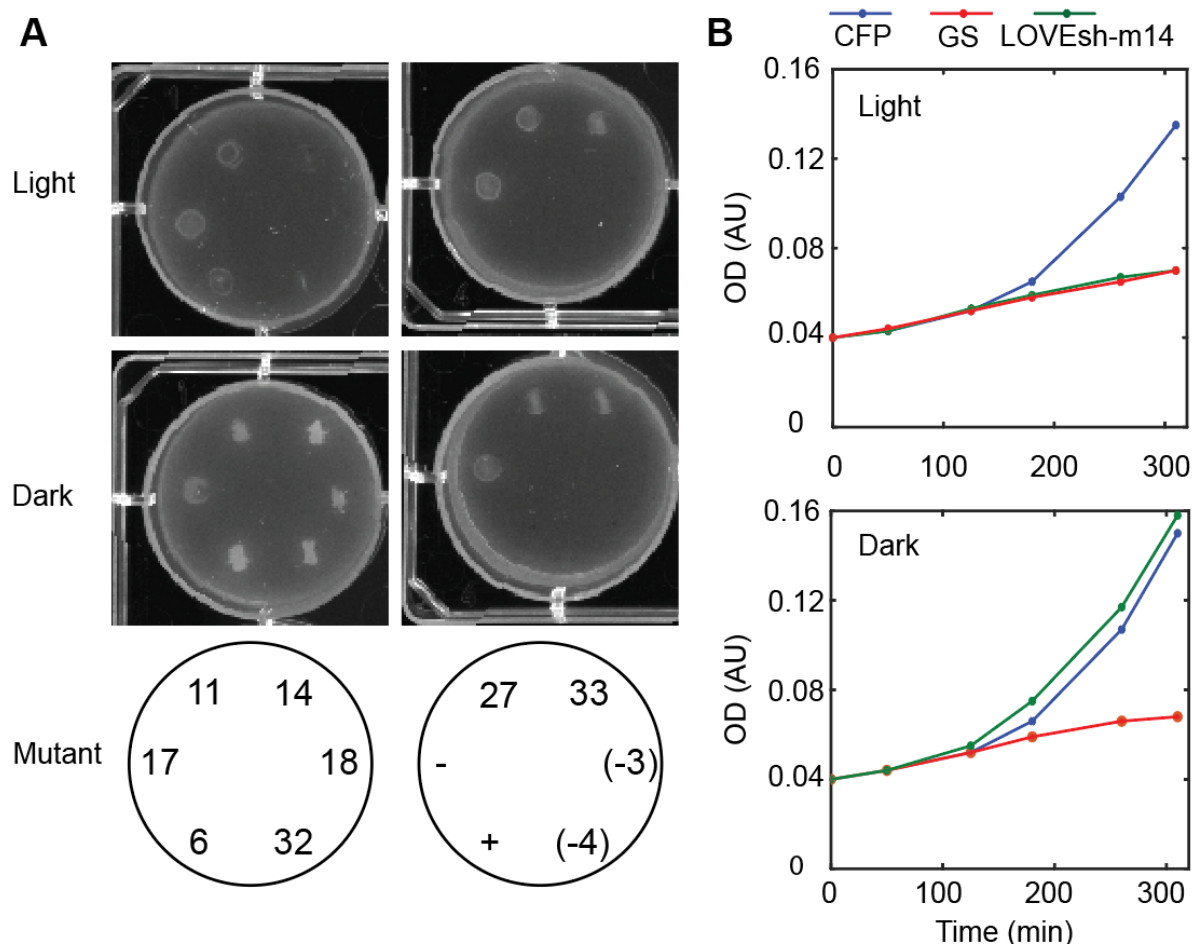


Figure 4.4. Testing the new mutants in minimal media to observe growth arrest with light on agar plates and in liquid culture. (A) Experiments conducted on minimal media reveal that the positive control cannot grow under light or dark due to light independent activity of Mesh1. Conversely negative control can grow under both conditions because it does not have ppGpp hydrolysis activity. Mutants 14, 18 and 32 appear to grow in dark indicating less hydrolysis activity and do not grow in light showing that the activity was regained in light. All 3 of these mutants appear better than -3 which cannot grow in dark nor light indicating high activity in dark, presumably due to less stable shared alpha helix which was improved in the new mutants. (B) The experiment was repeated in liquid media using LOVEsh-m14 and the results are similar to the plate experiment. CFP grows both under dark and light while Mesh1 cannot grow due to constant excess ppGpp hydrolysis. LOVEsh-m14 on the other hand only grows in dark but not in light, indicating light activated ppGpp hydrolysis activity.

4.3 Discussion

There are several questions regarding the function of the signalling molecule ppGpp which remained unanswered. This is in part because currently there are no techniques which can mimic the wild-type behaviour of rapid concentration drops. Existing methods rely on either (1) changes to the nutrient media which itself overshadows the effects of ppGpp drop or (2) induction of a hydrolysis enzyme and allowing ppGpp to decrease as fast as the hydrolyser concentration increases, which happens at the timescale of Transcription->Translation. Both of these methods make it hard to decouple the effects ppGpp decrease from other influencers like changing substrate concentration (1) or changes in the proteome itself (2).

In order to create a tool which can decrease ppGpp rapidly without needing nutrient shifts, we looked to create a light activated Mesh1. We used a simple growth assay to assess activity difference of the created variants in dark and light and further improved one of the variants by site directed mutagenesis. Our results reveal that using a proper fusion location between light sensitive domain LOV2 and Mesh1, we could create a ppGpp hydrolysis enzyme which could compete with RelA's ppGpp synthesis activity under light and permit growth (Fig. 4.2). This was shown using several different versions of the light box. Intensity of the light was also shown to have a dose dependent effect on growth. However, we also observed that there was still ppGpp hydrolysis activity in dark of the best working variant (-3) (Figs. 4.3B and 4.4A). In order to decrease the activity in dark we next sought to improve the -3 variant by using site directed mutagenesis with degenerate primers.

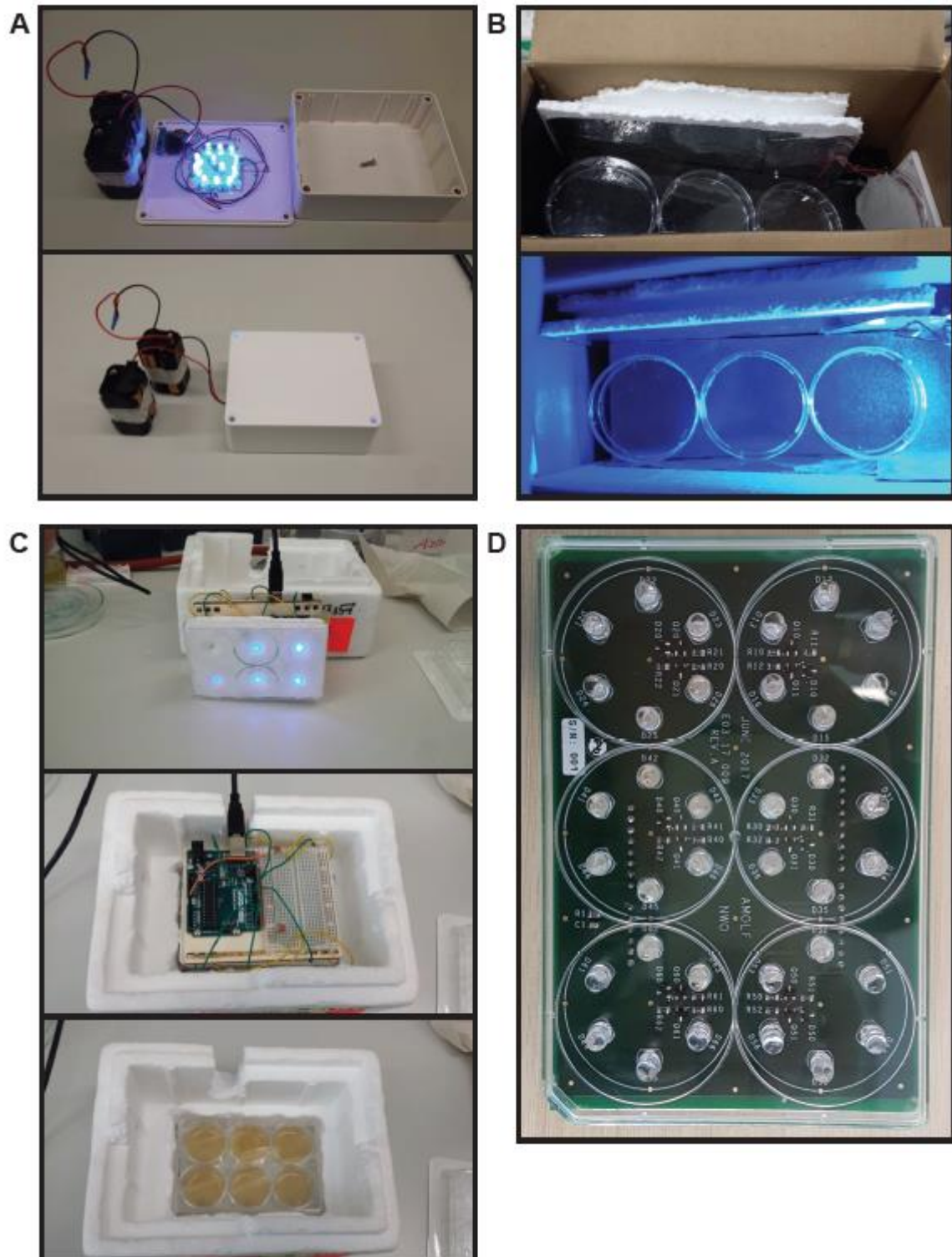
Sequence analysis of the supposed shared alpha helix of the variant -3 revealed two amino acids right at the interface between the LOV2 domain and Mesh1 which have very low propensities to join alpha helices (Tyr4, Pro5) (S. Table 4.2). We designed primers that only allow for 12 possible amino acids to replace the 4th and 5th amino acid location that were biased to be higher alpha helix joining (S. Table 4.2). This makes it so that in 1 round of PCR -> Ligation, we can get create many different combinations. By testing 33 randomly selected strains we were likely to try different combinations of amino acids on 4th and 5th position. Our results where these mutants competed against RelA showed that while -3 allowed growth in the dark at longer growth times due to present activity, some of the mutants did not grow in the dark at all. A subset of these mutants also allowed growth in the light (Fig. 4.3). We picked 8 of these supposedly better mutants and tested them in minimal agar and liquid media using the design explained in Fig. 4.1B.

In minimal media lack of ppGpp is detrimental to growth which allows for an experiment with an opposite expected result under light (lower growth) compared to RelA competition experiments. Indeed 3 of our newly tested mutants showed that they could grow in the dark while -3 couldn't. This supports that the new mutants had less activity in dark and allowed sufficient ppGpp production which permitted growth. However, in light these 3 mutants did not grow again suggesting that they had high enough activity

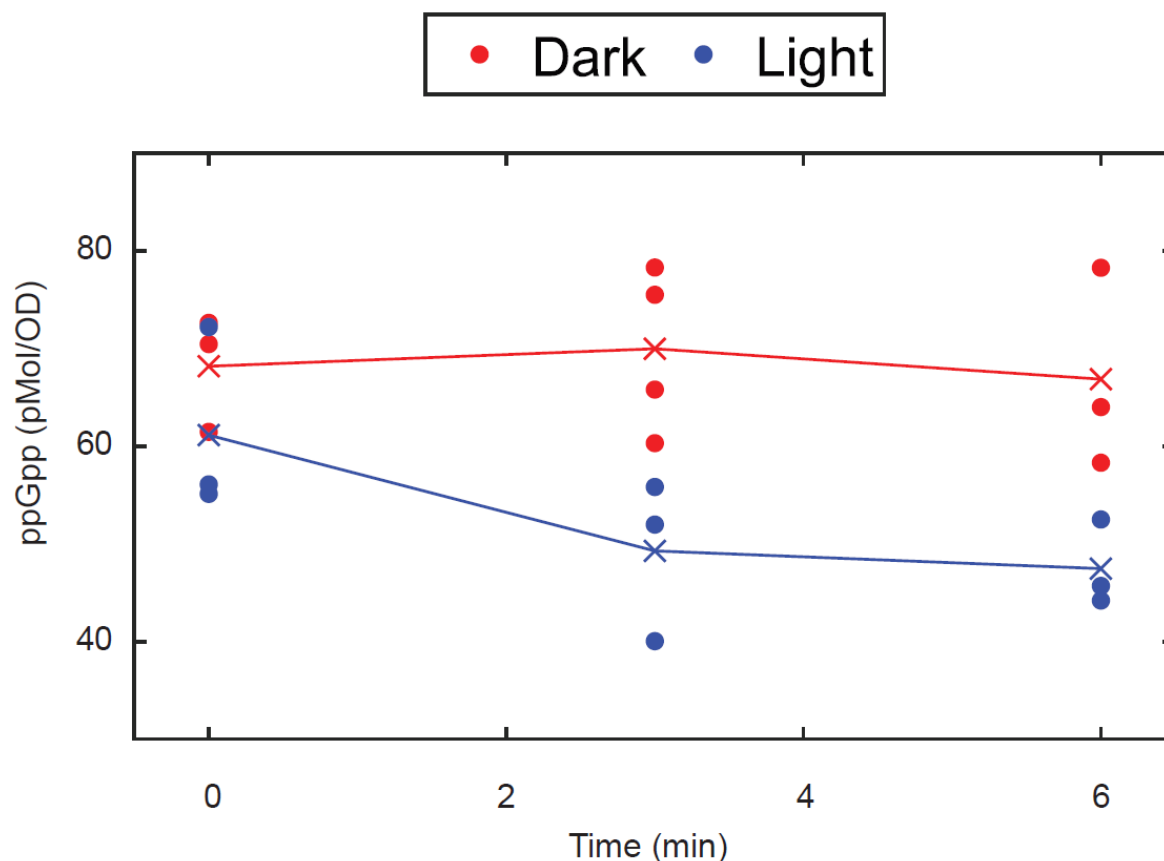
in light to hydrolyse ppGpp and stop growth (Fig. 4.4). Further testing of the mutants revealed that mutant 14 (LOVEsh-m14) was the most consistent version. This mutant replaced the Tyr4 and Pro5 with Val4 and Lys5 both amino acids with high alpha helix joining propensity (S. Table 4.2). In competition against RelA experiments in liquid media this mutant resulted in 25-50% higher growth rates under light compared to dark. Preliminary experiments also revealed that 3 minutes after turning on the Light, LOVEsh-m14 was decreasing the ppGpp concentration by ~22% ($p < 0.05$).

Our results show that LOV2 is indeed a modular light sensitive domain which can be used to create light activatable versions of enzymes with N-Terminal alpha helices. The final mutant (LOVEsh-m14) can possibly be further improved by altering other amino acids, especially Serine-6 is a good target to test as it (while not as bad as Tyr or Pro) also has low alpha helix joining propensity. Initial tests in liquid media revealed the enzyme to be usable in liquid media growth to sample various cellular biochemicals. While more liquid media experiments are needed to confirm the activity difference between dark and light to show that ppGpp levels are indeed rapidly changing, we believe LOVEsh-m14 can be used to rapidly decrease ppGpp levels. Measuring DNA replication and initiation, translation, metabolite levels from various pathways, cell division and other cellular machinery; immediately after light activation of LOVEsh-m14, could reveal allosteric effects of ppGpp on these machineries if a quick response is observed. Furthermore, localized changes to the ppGpp levels that can be applied on a growing biofilm could allow for probing the effects of ppGpp on biofilm formation and maintenance [31]

3.4 Supplementary Information



Supplementary Figure 4.1. Different light box designs used throughout the project. (A) Initial light box (v1) which allowed a single petri dish to be tested in light with binary light intensity (ON/OFF). (B) Using the box v1, different light intensities were created by placing petri dishes at a different distance from the light source. (C) An Arduino based prototype box (v2) was made to test proper light dimming possibilities. (D) Final light box design with a total of 36 LED's (6 LED's per single 6-wellplate well).



Supplementary Figure 4.2. Sampling of ppGpp after application of light on a LOVEsh-m14 producing strain. (A) a strain carrying RelA and LOVEsh-m14 plasmids were grown and LOVEsh-m14 was induced at -50 minutes, then RelA was induced at -30 minutes, finally at minute 0 light was turned on. We observe that in the light ppGpp concentrations were ~22% lower than that of the dark, supporting the light activatable nature of the LOVEsh-m14 ppGpp hydrolysis activity.

Strain	Rep-1	Rep-2
	$\mu_{\text{light}}/\mu_{\text{dark}}$	$\mu_{\text{light}}/\mu_{\text{dark}}$
Mutant 14	1.27 ± 0.02	1.56 ± 0.01
Mutant 18	0.87 ± 0.02	1.37 ± 0.01
Mutant 32	1.11 ± 0.06	1.08 ± 0.01
-3 fusion	1.16 ± 0.02	1.19 ± 0.01
Positive control	0.91 ± 0.01	0.78 ± 0.00
Negative control	1.07 ± 0.03	0.92 ± 0.01

Supplementary Table 4.1. Ratio of growth rates in dark and light of 3 mutants and controls against ectopic RelA synthesis in liquid media. Mutant 14 consistently grows faster in light when Mesh1 activity is needed to counter RelA activity. 2 repeats are shown in 2 columns.

Amino Acids	Abbreviation	Propensity
Glutamate	Glu	1.53 ★
Alanine	Ala	1.45
Leucine	Leu	1.34 ★
Histidine	His	1.24 ★
Methionine	Met	1.20 ★
Glutamine	Gln	1.17 ★
Tryptophan	Trp	1.14
Valine	Val	1.14 ★
Phenylalanine	Phe	1.12 ★
Lysine	Lys	1.07 ★
Isoleucine	Ile	1.00 ★
Aspartate	Asp	0.98 ★
Threonine	Thr	0.82
Arginine	Arg	0.79
Serine	Ser	0.79
Cysteine	Cys	0.77
Asparagine	Asn	0.73 ★
Tyrosine	Tyr	0.61 ★
Proline	Pro	0.59
Glycine	Gly	0.53

Supplementary Table 4.2. Predicted alpha helix joining propensities of all 20 amino acids. Amino acids which are possible to occur using our degenerate primer have been marked with a gray star. As can be seen possible amino acids are biased towards higher alpha helix joining propensity. Two stop codons are also possible for us (TAG, TAA) which were not shown on this table. Mutants where a stop codon replaces the 4th and 5th position would behave as negative controls.

4.4 Materials and Methods

Strains and plasmids

E. coli K-12 strain MG1655 or its derivatives prepared by transforming chemocompetent cells either with pRelA and/or various mutants and controls of AsLOV_Mesh1 fusions. pRelA* and pMesh1 plasmids were prepared as described in Chapter 2. As a control for various mutants generated, a plasmid with the same backbone where CFP instead of AsOV2_Mesh1 fusions was used similarly in Chapter 2. Inducers doxycycline and IPTG were used to induce pRelA* and pLac based AsLOV2_Mesh1 fusions or CFP respectively.

Initial variants of AsLOV2_Mesh1 fusions were prepared by using primers which create a 20bp overhangs on both sides of the PCR product which also creates homologous regions at the 5' and 3' ends of the PCR product. This allows SLICE to be used to remove amino acid's codons from the sequence and indenting of AsLOV2 domain into the Mesh1. In order generate a mutant library from variant -3, degenerate forward primer with 5' phosphorylation (/5Phos/) along with a fully matching reverse primer which also has 5' phosphorylation (Fig. 4.3) was used. /5Phos/ allows for direct

ligation of the linear DNA produced from PCR and does not require homology. This allowed rapid generation of numerous mutants in 1 cloning step.

Culture Conditions

For all experiments, cells were grown by diluting overnights 1/100 into fresh media. For plate experiments, this new culture was 10ml and was allowed to grow to $0.3 < OD < 0.5$ and diluted down to OD 0.01. 5 μ L of this dilution was later pipetted on agar plates with proper induction and nutrient levels. Experiments in liquid media were conducted similarly where an overnight was diluted 1/100 into fresh media and allowed to growth either in dark or light in 5ml volumes in 6well plate wells. For ppGpp sampling experiments an overnight was diluted in fresh media and allowed to growth until OD0.1 is reached. At this point RelA was induced and 20mins later LOVEsh-m14 was induced. At time 0, light was turned on and samples were taken at times indicated in the plot (Fig. 4.4). LB was used as rich media and MOPS medium containing 0.2% glucose with 100 μ M MnCl₂ was used as minimal media.

Agar plates for LB were prepared by simply pouring LB-Agar 1.5% onto plates. 25ml was used for standard petri dishes and 5ml was used in each 6well plate well. Minimal plates were prepared by adding 2x MOPS minimal media onto 3%Agar and pouring 5m into 6well plate wells. Plates were imaged using BioRad ChemiDoc XRS+.

Light Boxes

All of the light boxes used 5mm Blue AlGaInP LEDs (theledlight.com) with the part number SS5B4SDACY and typical wavelength between 465-470nm. Note the company has since shut down, however similar light bulbs should also work. Spec sheet for our LEDs can be requested from the author of this thesis if needed.

Light box V1 was designed and built by TU Delft Electronic & Mechanical Support Division. This box operated on 8x1.5V batteries and used 12LED's to disperse the light onto the entire plate. Later hand-made diffusers (lab gloves glued to transparent lids) were used to distribute the light equally.

Light box V2 was designed and built by the author, using an Arduino Genuino and the same LED bulbs. This allowed control of light brightness via the Arduino. Light box V3 was designed and built by AMOLF Electronics Assistance Department. This box had 36 LED's of which each block of 6 LEDs was independently controllable. V2 and V3 were attached to a plate cover of a 6 well plate using McGyverian methods to allow them to be placed on plates with bacteria and stay stable under vibrations in the warm room. Both of these plates were powered from a wall plug.

ppGpp Sampling

An LCMS based method was used to measure ppGpp. The details of the sampling and measurement methods are discussed in Chapter 5 Materials and Methods

References

1. Korem Kohanim, Y., Levi, D., Jona, G., Towbin, B. D., Bren, A., & Alon, U. (2018). A Bacterial Growth Law out of Steady State. *Cell Reports*, 23(10), 2891–2900.
2. Gentry, D. R., & Cashel, M. (1996). Mutational analysis of the Escherichia coli spoT gene identifies distinct but overlapping regions involved in ppGpp synthesis and degradation. *Molecular Microbiology*, 19(6), 1373–1384. <https://doi.org/10.1111/j.1365-2958.1996.tb02480.x>
3. Hauryliuk, V., Atkinson, G. C., Murakami, K. S., Tenson, T., & Gerdes, K. (2015). Recent functional insights into the role of (p)ppGpp in bacterial physiology. *Nature Reviews Microbiology*, 13(5), 298–309.
4. Fernández-Coll, L., & Cashel, M. (2018). Contributions of SpoT hydrolase, SpoT synthetase, and RelA synthetase to carbon source diauxic growth transitions in Escherichia coli. *Frontiers in Microbiology*, 9(AUG), 1–13. <https://doi.org/10.3389/fmicb.2018.01802>
5. Murray, H. D., Schneider, D. A., & Gourse, R. L. (2003). Control of rRNA expression by small molecules is dynamic and nonredundant. *Molecular Cell*, 12(1), 125–134.
6. Ehrenberg, M., Bremer, H., & Dennis, P. P. (2013). Medium-dependent control of the bacterial growth rate. *Biochimie*, 95(4), 643–658. <https://doi.org/10.1016/j.biochi.2012.11.01>
7. Potrykus, K., Murphy, H., Philippe, N., & Cashel, M. (2011). ppGpp is the major source of growth rate control in E. coli. *Environmental Microbiology*, 13(3), 563–575.
8. Erickson, D. W., Schink, S. J., Patsalo, V., Williamson, J. R., Gerland, U., & Hwa, T. (2017). A global resource allocation strategy governs growth transition kinetics of Escherichia coli. *Nature*, 551(7678), 119–123.
9. Shyp, V., Tankov, S., Ermakov, A., Kudrin, P., English, B. P., Ehrenberg, M., ... Hauryliuk, V. (2012). Positive allosteric feedback regulation of the stringent response enzyme RelA by its product. *EMBO Reports*, 13(9), 835–839.
10. Liu, K., Bittner, A. N., & Wang, J. D. (2015). Diversity in (p)ppGpp metabolism and effectors. *Current Opinion in Microbiology*, 24, 72–79.
11. Yong Zhang, Eva Zborníková, D. R., & Gerdes, K. (2018). Novel (p)ppGpp Binding and Metabolizing Proteins of Escherichia coli, 9(2), 1–20.
12. Noga, M. J., Büke, F., van den Broek, N. J., Imholz, N., Scherer, N., Bokinsky, G., ... Bokinsky, G. (2019). Post-translational control is sufficient to coordinate membrane synthesis with growth in Escherichia coli. *BioRxiv*, 728451.
13. Schreiber, G., Ron, E. Z., & Glaser, G. (1995). ppGpp-Mediated Regulation of DNA Replication and Cell Division in. *Current Microbiology*, 30, 27–32.
14. Kraemer, J. A., Sanderlin, A. G., & Laub, M. T. (2019). The Stringent Response Inhibits DNA Replication Initiation in E. coli by Modulating Supercoiling of oriC. *MBio*, 10(4), 1–18.
15. Sun, D., Lee, G., Lee, J. H., Kim, H.-Y., Rhee, H.-W., Park, S.-Y., ... Chung, J. (2010). A metazoan ortholog of SpoT hydrolyzes ppGpp and functions in starvation responses. *Nature Structural & Molecular Biology*, 17(10), 1188–1194.

16. Zhu, M., & Dai, X. (2019). Growth suppression by altered (p)ppGpp levels results from non-optimal resource allocation in *Escherichia coli*. *Nucleic Acids Research*, *47*(9), 4684–4693.
17. Fan, L. Z., & Lin, M. Z. (2015). Optical control of biological processes by light-switchable proteins. *Wiley Interdisciplinary Reviews: Developmental Biology*, *4*(5), 545–554
18. Fenno, L., Yizhar, O., & Deisseroth, K. (2011). The Development and Application of Optogenetics. *Annual Review of Neuroscience*, *34*(1), 389–412. <https://doi.org/10.1146/annurev-neuro-061010-113817>
19. Strickland, D., Moffat, K., & Sosnick, T. R. (2008). Light-activated DNA binding in a designed allosteric protein. *Proceedings of the National Academy of Sciences of the United States of America*, *105*(31), 10709–10714.
20. Jeeyeon Lee, Madhusudan Natarajan, Vishal C. Nashine, Michael Socolich, Tina Vo, William P. Russ, Stephen J. Benkovic, R. R. (2008). Surface Sites for Engineering Allosteric Control in Proteins. *Science Reports*, (October), 1–4.
21. Möglich, A., Ayers, R. A., & Moffat, K. (2009). Design and Signaling Mechanism of Light-Regulated Histidine Kinases. *Journal of Molecular Biology*, *385*(5), 1433–1444. <https://doi.org/10.1016/j.jmb.2008.12.017>
22. Ma, Z., Du, Z., Chen, X., Wang, X., & Yang, Y. (2013). Fine tuning the LightOn light-switchable transgene expression system. *Biochemical and Biophysical Research Communications*, *440*(3), 419–423. <https://doi.org/10.1016/j.bbrc.2013.09.092>
23. Shimizu-Sato, S., Huq, E., Tepperman, J. M., & Quail, P. H. (2002). A light-switchable gene promoter system. *Nature Biotechnology*, *20*(10), 1041–1044. <https://doi.org/10.1038/nbt734>
24. Kennedy, M. J., Hughes, R. M., Peteya, L. A., Schwartz, J. W., Ehlers, M. D., & Tucker, C. L. (2010). Rapid blue-light-mediated induction of protein interactions in living cells. *Nature Methods*, *7*(12), 973–975. <https://doi.org/10.1038/nmeth.1524>
25. Harper, S. M., Christie, J. M., & Gardner, K. H. (2004). Disruption of the LOV-J α helix interaction activates phototropin kinase activity. *Biochemistry*, *43*(51), 16184–16192.
26. Towbin, B. D., Korem, Y., Bren, A., Doron, S., Sorek, R., & Alon, U. (2017). Optimality and sub-optimality in a bacterial growth law. *Nature Communications*, *8*, 14123.
27. Paul BJ, Berkmen MB, Gourse RL. 2005. DksA potentiates direct activation of amino acid promoters by ppGpp. *Proc. Natl. Acad. Sci. USA* *102*:7823–28
28. Chou, P. Y., & Pasman, G. D. (1974). Conformational Parameters for Amino Acids in Helical, β -Sheet, and Random Coil Regions Calculated from Proteins. *Biochemistry*, *13*(2), 211–222.
29. Li, S. C., Goto, N. K., Williams, K. A., & Deber, C. M. (1996). α -Helical, but not β -sheet, propensity of proline is determined by peptide environment. *Proceedings of the National Academy of Sciences of the United States of America*, *93*(13), 6676–6681.
30. Towbin, B. D., Korem, Y., Bren, A., Doron, S., Sorek, R., & Alon, U. (2017). Optimality and sub-optimality in a bacterial growth law. *Nature Communications*, *8*, 14123.

31. Boehm, A., Steiner, S., Zaehring, F., Casanova, A., Hamburger, F., Ritz, D., ... Jenal, U. (2009). Second messenger signalling governs *Escherichia coli* biofilm induction upon ribosomal stress. *Molecular Microbiology*, 72(6), 1500–1516. <https://doi.org/10.1111/j.1365-2958.2009.06739.x>

5

Post-translational control is sufficient to coordinate membrane synthesis with growth in *Escherichia coli*

Marek J Noga[†], Ferhat Büke, Niels JF van den Broek[‡], Nicole Imholz, Nicole Scherer, Gregory Bokinsky*
Department of Bionanoscience, Kavli Institute of Nanoscience, Delft University of Technology, Delft, The Netherlands
Materials and correspondence: *e-mail: g.e.bokinsky@tudelft.nl
[†] Current address: Translational Metabolic Laboratory, Department of Laboratory Medicine, Radboud UMC, Nijmegen, The Netherlands
[‡] Current address: Vaccine Process & Analytical Development, Janssen Vaccines & Prevention B.V., Leiden, The Netherlands

Abstract

Every cell must produce enough membrane to contain itself. However, the mechanisms by which cells couple the rate of membrane synthesis with the rate of growth remain unresolved. By measuring precursors, intermediates, and enzymes of the fatty acid and phospholipid synthesis pathways of *Escherichia coli*, we show that while fatty acid and membrane synthesis capacities are maintained at a constant level across a 3-fold range of growth rates, the steady-state rate of phospholipid synthesis is principally mediated by allosteric control of a single enzyme, PlsB. Surprisingly, metabolic modelling indicates that PlsB activity also strongly influences flux into the synthesis pathway of lipopolysaccharide, the second-most abundant membrane component. In contrast to steady-state regulation, we find that responses to environmental perturbations are triggered directly via changes in acetyl-CoA concentrations, enabling rapid adaptation. Adaptations are further modulated by ppGpp, which regulates PlsB activity during slow growth and growth arrest. The strong reliance upon post-translational regulation for flux control ensures both robustness and responsiveness of membrane synthesis.

5.1 Introduction

The viability of growing cells demands that membrane synthesis be tightly orchestrated with biomass production. The asymmetric architecture and composition of the cell envelope in Gram-negative bacteria demands further coordination between multiple pathways that synthesize membrane components: phospholipid (PL) synthesis must be balanced with lipopolysaccharide (LPS) synthesis to ensure membrane stability (1, 2). PL and LPS pathways must also be coordinated with protein synthesis, which supplies the lipoproteins that tether the outer membrane to peptidoglycan (3). Although several targets and mechanisms of regulation have been identified or proposed in the model organism *Escherichia coli*, how cells use these regulation points to control membrane synthesis remains unclear (4).

Reaction rates (metabolic fluxes) may be modulated through either transcriptional regulation, which adjusts enzyme concentrations, or by post-translational mechanisms that adjust the activities of enzymes that are already present. For instance, the steady-state synthesis rate of proteins is widely thought to be controlled in many bacteria by ribosome abundance, which is transcriptionally regulated to balance amino acid supply with consumption (5). In contrast, fluxes through many essential metabolic pathways are determined instead by steady-state concentrations of substrates and inhibitors (post-translational regulation) rather than by transcriptional regulation (6, 7). Although post-translational regulation has long been known to play a significant role in membrane synthesis (8, 9) (10–12), the exact contributions of transcriptional and post-translational control to the coordination of membrane synthesis with growth remain unclear.

In order to understand how the membrane synthesis rate is coordinated with the growth rate (μ), we quantified enzymes, substrates and intermediates of the fatty acid and PL synthesis pathways in steady-state and dynamic conditions. We find that allosteric regulation of the first enzyme in the PL synthesis pathway, PlsB, ensures μ -dependent regulation of PL synthesis and strongly influences flux into the LPS synthesis pathway. We furthermore find that the fatty acid and PL synthesis pathways are highly sensitive to changes in precursor concentrations caused by internal and external metabolic shifts. This sensitivity enables a rapid response to environmental changes that can be further modulated by allosteric inhibitors such as the global regulator guanosine tetraphosphate (ppGpp).

5.2 Results

5.2.1 The PL to biomass ratio varies inversely with μ

Lipid precursors of both LPS and PL are synthesized in the cytosol as fatty acyl thioesters covalently attached to the acyl carrier protein (acyl-ACP). PL are synthesized by membrane-bound enzymes from long-chain acyl-ACP and *sn*-glycerol-3 phosphate (G3P). G3P is produced either from glyceraldehyde-3-phosphate, an

intermediate of central carbon metabolism, or via glycerol catabolism (Fig. 5.1A). We grew cultures of *E. coli* NCM3722 in 6 defined media that support a 3-fold range of μ (MOPS medium containing 0.2% acetate, succinate, malate, glycerol, glucose, or glucose with Cas-amino acids). Quantities of phosphatidylglycerol (PG), phosphatidylethanolamine (PE), and cardiolipin (CL) per unit biomass (as determined by culture optical density (OD) (13)) decreased with increasing μ (Fig. 5.1B), consistent with previous observations in *E. coli* and other bacteria (14, 15). The PG/PE ratio remained constant across all μ . We quantified steady-state PL flux by multiplying total PE LC/MS counts by μ , which closely approximates the overall PL synthesis rate as PE turnover is slow relative to synthesis (16). PL flux decreased by 2-fold over 3-fold range of μ (Fig. 5.1C). The higher PL to biomass ratio of slow-growing cells likely reflects their higher surface-to-volume ratio (17).

5.2.2 Allosteric regulation of PlsB activity is sufficient to couple PL flux with μ

We first sought to evaluate whether steady-state substrate concentrations determine PL flux. If the PL and fatty acid synthesis rates are modulated by substrate concentrations during steady-state growth, concentrations of these species would necessarily correlate positively with μ and PL flux. We quantified nucleotides, G3P, acyl-ACP, and PL synthesis intermediates using LC/MS (18). No correlation was observed between concentrations of the fatty acid precursor acetyl-CoA or with μ (Fig. 5.1D). We also found no significant correlation between PL flux and long-chain acyl-ACP substrates of PL synthesis (Fig. 5.1E, Pearson correlation coefficients $r < 0.4$, $p > 0.4$, S. Table 5.1). Although G3P concentrations correlate strongly with PL flux ($r > 0.99$), growth in glycerol medium increased G3P by 20-fold without affecting PL content or flux. These trends imply that steady-state PL flux is not modulated by fatty acid or PL precursor concentrations.

In contrast to PL synthesis substrates, concentrations of the fatty acid initiation and elongation substrate malonyl-ACP strongly correlate with PL flux (Fig. 5.1E, $r = 0.9$, S. Table 5.1), suggesting that the fatty acid initiation and elongation rates are determined by malonyl-ACP concentrations and thus by the rate of malonyl-ACP synthesis by ACC and FabD. Concentrations of hydroxyl-acyl-ACP intermediates, including C14:0-OH-ACP, the lipid precursor of LPS, also correlate strongly with PL flux ($r > 0.99$), implying a simple flux-sensitive coupling mechanism between the PL and LPS synthesis pathways (Fig. 1E, S. Fig. 5.1). As ACC substrates acetyl-CoA and ATP do not correlate with μ (Fig. 5.1D, S. Fig. 5.2), and as concentrations of ACC protein subunits and FabD also do not correlate significantly with PL flux (S. Fig. 5.3, S. Table 5.1), we infer that ACC activity is primarily modulated during steady-state conditions via allosteric control. Biochemical experiments have identified several regulators of ACC activity, including nitrogen-responsive regulator GlnB (19) and acyl-ACP substrates of PL synthesis (20).

Unlike long-chain acyl-ACP, the concentrations of all PL synthesis intermediates downstream of PlsB correlate tightly with PL flux (Fig. 5.1F, $r > 0.89$ - 0.99 , S. Table

5.1). The contrast between the trends observed in substrates and products of PlsB suggests that the rates of the reactions following PlsB are primarily determined by substrate concentrations, further implying that transcriptional regulation of PlsB concentration or post-translational regulation of PlsB activity is sufficient to regulate flux into the PL pathway. Transcription of *plsB*, and thus PlsB abundance, is controlled by the μ -sensitive regulator guanosine tetraphosphate (ppGpp) (21) and by the membrane stress-activated sigma factor RpoE (22). Concentrations of ppGpp are inversely correlated with μ (Fig. 5.1D), implying that PL flux may be coupled to μ by transcriptional control of the *plsB* gene by ppGpp. We measured fatty acid and PL synthesis pathway enzymes in each culture using LC/MS to determine whether enzyme concentrations are adjusted to couple PL flux with μ . We found no significant correlation between PL synthesis flux and PlsB concentration (Fig. 5.1G, S. Table 5.1, $p > 0.1$). Instead, PlsB concentrations per unit biomass (OD) are nearly constant across the conditions studied, indicating that PlsB can accommodate at least a 2-fold range of PL flux without a corresponding change in concentration. Surprisingly, the concentrations of most fatty acid synthesis pathway enzymes also do not correlate significantly with PL flux (S. Table 5.1, S. Fig. 5.3). The lack of correlation between PL flux and concentrations of PlsB or its acyl-ACP substrates implies that PL flux is regulated via allosteric control of PlsB. μ can also be modulated independently of culture conditions by artificially varying ppGpp (Fig. 5.1D). Titrating ppGpp above basal concentrations, but far below concentrations experienced during starvation, reduces steady-state μ by reducing ribosomal RNA synthesis (23). Furthermore, PlsB activity is inhibited at high ppGpp concentrations encountered during starvation (24).

We titrated μ by expressing the catalytic domain of the ppGpp synthesis enzyme RelA (RelA*) from an inducible promoter (P_{Tet}) in glucose medium. As previously observed (23), RelA*-titrated cultures exhibit ppGpp concentrations that are elevated 2-fold above wild-type cultures growing at similar rates (Fig. 5.1D). Trends in PL abundance, PL flux, acyl-ACP species, PL intermediates, and PL synthesis enzyme concentrations in ppGpp-limited cultures are highly similar to trends observed as μ is varied by carbon source (Fig. 5.1B-C, 5.1E-G, A Figs. 5.1, 5.3). Concentrations of PlsB and fatty acid pathway enzymes do not substantially vary in ppGpp-limited cultures (Fig. 5.1G, S. Fig. 5.3). The trends in substrate, enzyme, and intermediate concentrations observed in ppGpp-limited cultures are consistent with regulation of PL flux occurring via allosteric control of PlsB. Unexpectedly, concentrations of LpxC, which catalyses the committed step in the LPS pathway (25), decrease 2-fold as PE flux increases (S. Fig. 5.3).

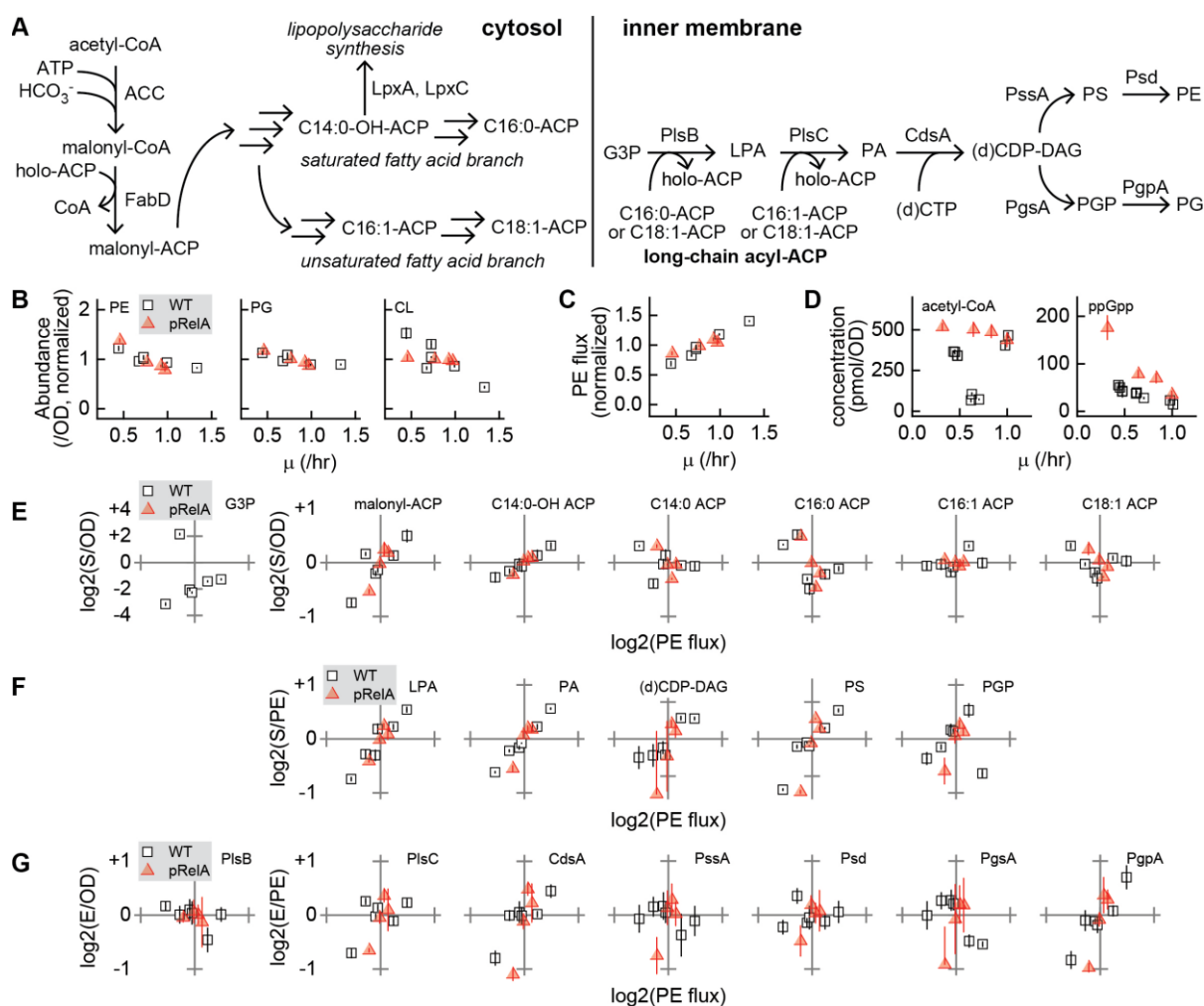


Figure 5.1. Characterization of the *E. coli* fatty acid and PL synthesis pathways during steady-state growth. **A.** *E. coli* fatty acid and PL synthesis pathways highlighting the metabolites and enzymes discussed in the main text. Fatty acid synthesis is initiated by carboxylation of acetyl-CoA by acetyl-CoA carboxylase complex (ACC) to produce malonyl-CoA, from which the malonyl group is transferred to holo-ACP by FabD. Fatty acids are then elongated by iterated cycles of condensation of acyl-ACP with malonyl-ACP, followed by reduction and dehydration. *sn*-glycerol-3-phosphate (G3P) is acylated by PlsB primarily using long-chain acyl-ACP species C16:0-ACP or C18:1-ACP to yield lysophosphatidic acid (LPA), which is acylated by PlsC using C16:1-ACP or C18:1-ACP to yield phosphatidic acid (PA). PA is converted by CdsA to (d)CDP-diacylglycerol ((d)CDP-DAG) using either CTP or dCTP. At the branch point in PL synthesis, PgsA combines G3P with (d)CDP-DAG to produce phosphatidylglycerol phosphate (PGP). Dephosphorylation of PGP by PgpA yields PG, which typically comprises 25% of total PL. Two PG molecules may be further converted to CL, which accounts for ~5% of total PL. (d)CDP-DAG is also converted by PssA to phosphatidylserine (PS), which is decarboxylated by Psd to yield PE (70% of total PL). **B, C.** Growth rate (μ)-dependent abundance of total PG, PE, and CL (**B**) and μ -dependence of PE flux (**C**), normalized to average values across conditions for each strain. **D.** Steady-state concentrations of acetyl-CoA and ppGpp. **E, F, G.** Concentrations of G3P and acyl-ACP species (**E**), PL intermediates (**F**), and PL synthesis pathway enzymes (**G**) as functions of PL flux. Concentrations of soluble substrates and enzymes with exclusively soluble substrates are calculated using cell volume (proportional to OD). For membrane-bound phospholipid intermediates and for enzymes that react with membrane-bound substrates (all enzymes following PlsB in the PL synthesis pathway) we calculate concentration within the membrane volume, proportional to total PE. S/OD , E/OD , S/PE , and E/PE are defined as the concentration of a substrate S or enzyme E (amount per OD or per PE) relative to its average concentration across all conditions measured in that strain (either wild-type (WT) or pRelA). Values are \log_2 -transformed. Error bars represent the standard deviation of measurements from three samples of one culture.

5.2.3 Mathematical modelling supports PlsB control of steady-state PL synthesis

To test whether modulation of PlsB activity alone is sufficient to govern PL synthesis flux, we constructed a simplified differential equation model of fatty acid, LPS initiation, and PL biosynthesis (Fig. 5.2A). The model includes competitive inhibition of ACC by C16:0-ACP as the sole regulatory interaction. The model also includes a branch point at C14:0-OH-ACP into LPS synthesis. This branch point is represented by a single step that combines reactions catalysed by LpxA and LpxC, as LpxC catalyses the first irreversible reaction in the LPS pathway (25). Concentrations of G3P and C16:1-ACP are fixed in the model to reflect experimental observations of enzyme saturation and substrate invariance, respectively (see Supplementary Methods for model details, parameter sets, and sensitivity analysis).

We used the model to predict which enzymes and substrates exert control over PL and LPS flux. Increasing ACC and PlsB V_{\max} parameters by 4-fold each increased PE and LPS synthesis fluxes in parallel by 2-fold, while changes in the V_{\max} parameters of all other enzymes in the model had little or no effect on simulated PE flux. Surprisingly, simulated LPS flux correlates positively with PlsB activity when LpxC V_{\max} is held constant due to the coupling between PE flux and concentrations of the LPS precursor, C14:0-OH-ACP. Changes in the C14:0-OH-ACP dehydration reduction rate and LPS initiation rate (catalysed in the model by FabZ and LpxC, respectively) exerted strong and opposite effects on LPS flux without significantly changing PE flux. Increasing the V_{\max} parameters of PL synthesis enzymes downstream of PlsB also did not change PE synthesis flux, suggesting that the observed variations in PlsC and CdsA concentrations do not affect PE flux. Of the two substrates considered (acetyl-CoA and C16:1-ACP), only variations in acetyl-CoA strongly influences PL and LPS flux (Fig 5.2B).

Simulated variations in acetyl-CoA concentrations and ACC and PlsB enzyme V_{\max} parameters generate changes in intermediate concentrations that closely reproduce most experimentally-observed trends, supporting our model. However, our steady-state measurements strongly contradict simulated C16:0-ACP concentration trends caused by variations in acetyl-CoA and ACC activity. Simulated variations in PlsB V_{\max} closely approximate observed C16:0-ACP trends (Fig. 5.2C). We therefore conclude that PL synthesis flux is primarily regulated during steady-state growth by allosteric control of PlsB activity. However, changes in acetyl-CoA concentration or ACC activity may also influence PL flux during environmental or metabolic perturbations.

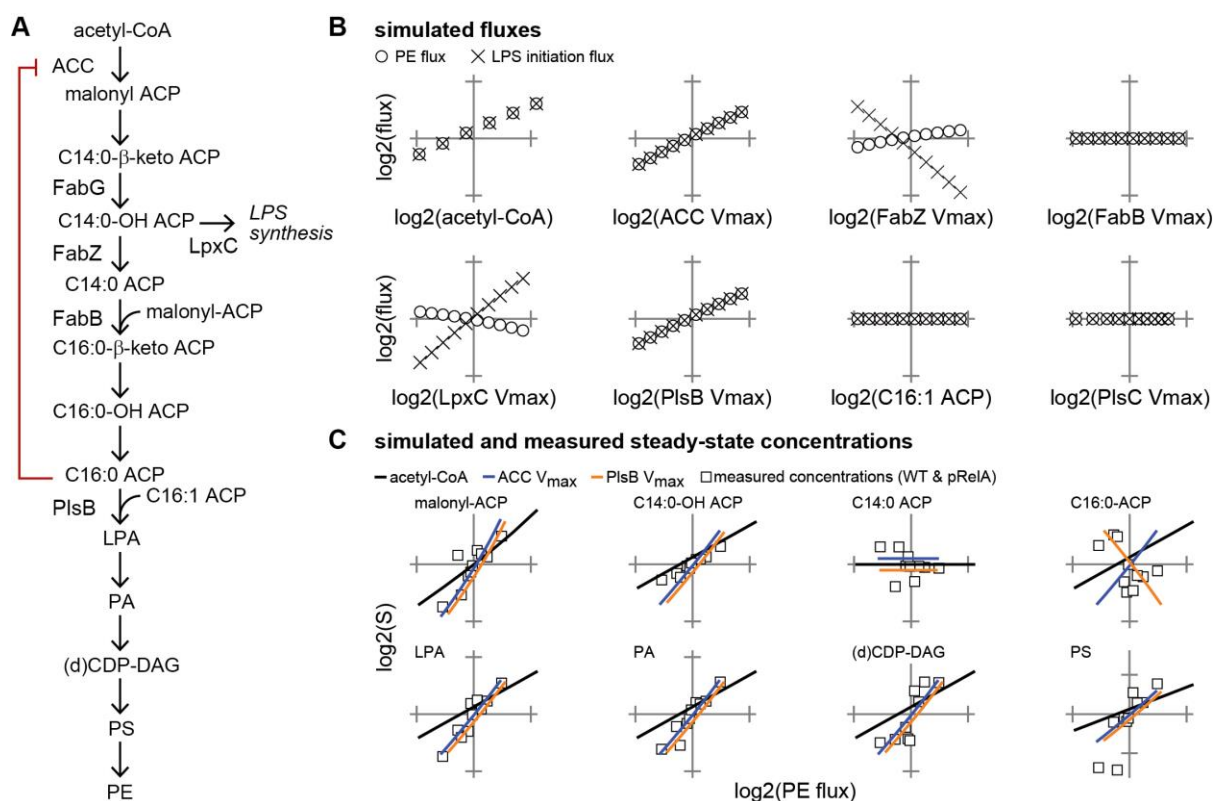


Figure 5.2. Simulated steady-state fluxes and metabolite concentrations of fatty acid and PL pathways identifies PlsB as site of flux control during steady-state growth. **A.** Reactions simulated in the model. For simplicity, only reactions late in the saturated fatty acid pathway are included, and branching of the PL pathway into PE and PG is not included. Each reaction is modelled as an irreversible one- or two-substrate Michaelis-Menten reaction. ACC activity is competitively inhibited by C16:0-ACP. Reactions catalysed by FabI/FabZ and LpxA/LpxC are considered in the model as single reactions represented by “FabZ” and “LpxC”, respectively. **B.** Response of PE and LPS fluxes to varying V_{max} parameters of pathway enzymes and acetyl-CoA and C16:1-ACP concentrations. 4-fold variations in C14:0-β-keto-ACP synthesis, FabG, CdsA, PssA, and Psd V_{max} did not change PE or LPS flux and are therefore not shown. **C.** Simulated changes in metabolite concentrations in response to variations in PlsB and ACC V_{max} and acetyl-CoA overlaid on experimentally-measured concentrations (data from Figure 5.1). Line plots are offset to prevent overlap. Differential equations and parameters are provided in the

5.2.4 Translation inhibition causes carbon overflow into fatty acid synthesis

We set out to evaluate whether a known allosteric regulator of PlsB, ppGpp, is able to directly regulate PlsB activity during steady-state growth. High concentrations of ppGpp are known to inhibit PlsB (24), while low concentrations of ppGpp correlate inversely with μ (Figure 5.1D). The notion that ppGpp concentrations might regulate PL synthesis even at the low basal concentrations present during steady-state growth has been proposed but never tested (26). Although steady-state PlsB activity clearly decreased in response to ppGpp titration, the mode of control by ppGpp (transcriptional regulation of a PlsB-regulating process or protein, or direct post-translational inhibition) cannot be determined from steady-state data alone. We first wished to observe the effects of high concentrations of ppGpp on fatty acid and PL synthesis using our assay. Synthesis of high concentrations of ppGpp by RelA (the

stringent response) is triggered by any stress or starvation conditions that lead to the specific biochemical cue of uncharged tRNA bound to the ribosome. During the stringent response, ppGpp accumulates by more than 10-fold over basal concentrations and PL synthesis rates are reduced by approximately half (24, 26), likely due to PlsB inhibition (27).

We triggered ppGpp accumulation by adding the tRNA aminoacylation inhibitor mupirocin to glucose cultures of wild-type and $\Delta relA$ *E. coli*. Mupirocin inhibits translation in both strains and causes a 10-fold accumulation of ppGpp in the wild-type strain within 1 minute to over 400 pmol/OD, reaching >800 pmol/OD after 3 minutes (S. Fig. 5.4, 5.5). To our surprise, mupirocin treatment also transiently increased malonyl-ACP and hydroxyl-ACP at the expense of holo-ACP in both strains (Fig. 5.3A, S. 5.Fig. 6). The increase in acyl-ACP is matched by a corresponding increase in PL synthesis intermediates, suggesting that mupirocin diverts a pulse of carbon into the fatty acid pathway that is efficiently transmitted into PL synthesis (Fig. 5.3B). In the wild-type strain, the pulse of fatty acid synthesis activity is rapidly followed by C16:0- and C18:0-ACP accumulation, consistent with ppGpp inhibition of PlsB (Fig. 5.3A, S. Fig. 5.6). C16:0-ACP accumulation is followed in turn by an increase in holo-ACP and a decrease in malonyl-ACP, indicating ACC inhibition (Fig. 5.3A). PL intermediates PA, PS, and PGP are rapidly depleted in the wild-type strain after briefly increasing (Fig. 5.3B). The transient carbon influx shifts acyl chains incorporated into PL towards longer-chain fatty acids, likely due to increased malonyl-ACP concentrations favouring fatty acid elongation at the expense of membrane incorporation by PlsB and PlsC (S. Fig. 5.7). While suppression of fatty acid synthesis in the wild-type strain can be attributed to ppGpp, it is unclear what attenuates the carbon influx in the $\Delta relA$ strain; however eventual C14:0-ACP accumulation likely contributes to ACC inhibition. Inhibition of fatty acid elongation also depletes LPS precursor C14:0-OH-ACP, which is expected to decrease LPS synthesis in parallel with PL synthesis (Fig. 5.3A).

As the transient increase in malonyl-ACP after mupirocin treatment occurs in both wild-type and $\Delta relA$ strains, we hypothesized that translation inhibition somehow channels excess carbon into lipid synthesis. We added the ribosome inhibitor chloramphenicol and the transcription initiation inhibitor rifampicin to glycerol cultures of wild-type *E. coli*. Both compounds inhibit translation via mechanisms that suppress ppGpp synthesis. As with mupirocin, chloramphenicol triggered a rapid decrease in holo-ACP and an increase in long-chain unsaturated acyl-ACP species C16:1-ACP and C18:1-ACP (Fig. 5.3C). Both antibiotics triggered an increase in PL synthesis intermediates PA and PS that resembled the increase observed in the $\Delta relA$ strain after mupirocin treatment (Fig. 5.3D). What might cause the transient increase in fatty acid synthesis observed after translation inhibition? Interestingly, both rifampicin and chloramphenicol increased acetyl-CoA concentrations by 3-fold (Fig. 5.3E), suggesting a possible cause. Acetyl-CoA also increased in both the wild-type and the $\Delta relA$ strain after mupirocin addition in glucose medium before decreasing ~30% in the wild-type strain (S. Fig. 5.4, 5.5). While it is unclear why translation inhibition would

increase acetyl-CoA, the observed response of the fatty acid pathway is consistent with our mathematical model, which predicts fatty acid flux to be highly sensitive to acetyl-CoA. We confirmed the sensitivity of the fatty acid and PL synthesis pathways to environmental changes using a fast nutritional upshift. Addition of glucose and amino acids to a glycerol culture also caused a rapid accumulation of PA and PS species that resemble the increases observed following translation inhibition (S. Fig. 5.8).

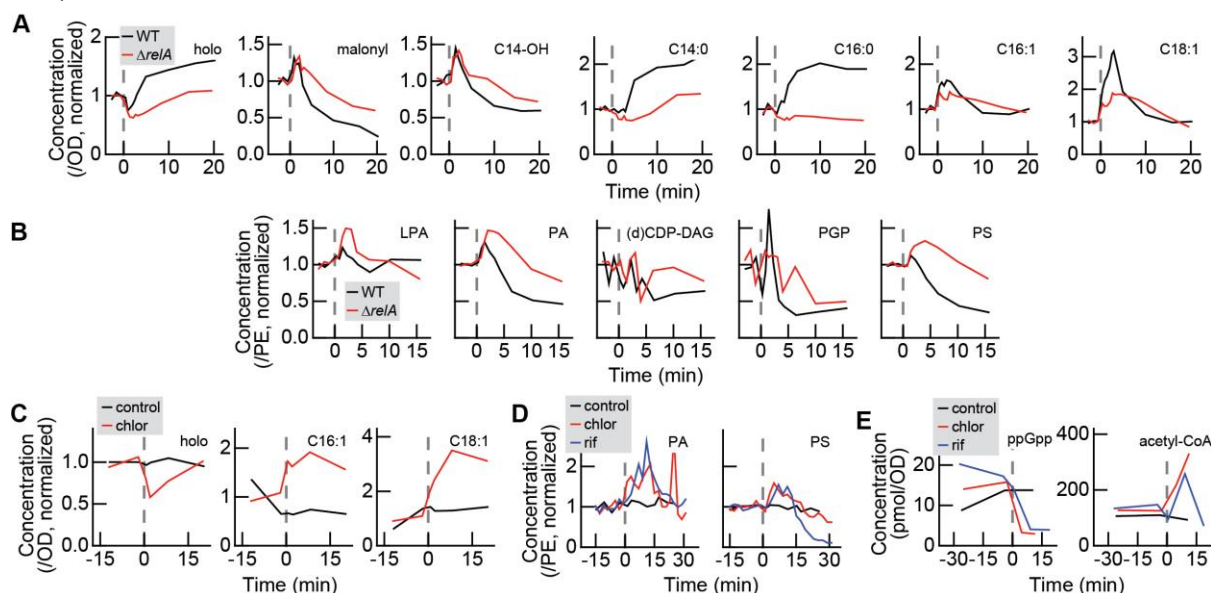


Figure 5.3. Response of the fatty acid and PL synthesis pathways to translational inhibition. A, B. Responses of acyl-ACP (**A**) and PL intermediate pools (**B**) to mupirocin treatment. Mupirocin was added at 0 min (indicated by dashed lines) to glucose cultures of *E. coli* wild-type and $\Delta relA$. **C, D.** Addition of translation inhibitor chloramphenicol or the transcription inhibitor rifampicin to glycerol cultures of wild-type *E. coli* (indicated by dashed lines at 0 min) leads to an influx of carbon into the fatty acid pathway as suggested by a decrease in holo-ACP levels and an increase in unsaturated long-chain acyl-ACP species (**C**). The pulse of carbon continues further into the PL synthesis pathway, as indicated by transient increases in total PA and PS (**D**). Trajectories in **A-D** are each obtained from individual cultures. **E.** Chloramphenicol and rifampicin both trigger a rapid decrease in ppGpp and accumulation of ACC and FabH substrate acetyl-CoA. Values depicted in **E** are averages of triplicates from single cultures.

5.2.5 Moderate ppGpp concentrations regulate PlsB via post-translational control

In order to clearly discern the effects of ppGpp on the fatty acid and PL synthesis pathways without complications introduced by translation inhibition, we monitored fatty acid and PL synthesis pathways after inducing RelA*. The response in the fatty acid and PL synthesis pathways is consistent with PlsB inhibition by ppGpp followed by ACC activity suppression by accumulated long-chain acyl-ACP, depleting malonyl-ACP (Figure 5.4A). PL intermediates also respond in a manner consistent with PlsB inhibition: LPA species steadily decrease, followed by PA, PS, and PG (Figure 4B). Addition of chloramphenicol 10 minutes following RelA* induction causes an increase in unsaturated long-chain acyl-ACP, though the response of the PL pathway is attenuated. We note that the PS pool is depleted more after ppGpp induction than the

LPA and PA pools, suggesting an additional regulatory mechanism downstream of PlsB.

We next sought to evaluate whether basal ppGpp concentrations are also capable of regulating PlsB via post-translational control. As the effects of post-translational control are more rapidly apparent than those that follow transcriptional regulation, we followed the timescale of the response of the PL pathway to ppGpp synthesis. We measured ppGpp and PL synthesis intermediates during RelA* induction to moderate levels. ppGpp increased within 10 minutes of RelA* induction and reached its elevated steady-state concentration (~150 pmol/OD) by 20 minutes. Concentrations of PL intermediates PA and PS began to decrease within 10 minutes (Figure 5.4C). Interestingly, PS decreases further after ~25 minutes, at which point PA increases slightly, suggesting that PS may be back-converted to PA by PssA (28) (Figure 5.4C). The immediate decay of PA and PS pools indicates that ppGpp inhibits PlsB via post-translational regulation at moderate concentrations. To verify that the immediate PA and PS depletion is too fast to be explained by transcriptional regulation, we compared the PA and PS response kinetics with the kinetics of a ppGpp-driven response known to be mediated by transcriptional control. Cyclopropyl PL are produced from unsaturated fatty acids of membrane PL by the enzyme Cfa, expression of which is induced transcriptionally by ppGpp (29). PL cyclopropylation begins 25 minutes after RelA* induction, much slower than the decrease in PA and PS. We conclude that the rapid decrease in PA and PS 5-10 minutes after RelA* induction is mediated via post-translational regulation of PlsB.

We used our model to simulate the observed response of PA and PS concentrations immediately following mild RelA induction (up to 25 minutes post-induction) in order to estimate the concentrations at which ppGpp inhibits PlsB. As the mode of inhibition is unknown (i.e. competitive inhibition, mixed inhibition, or indirect inhibition via a ppGpp-responsive mediator), we used an empirical allosteric inhibition term to obtain an effective K_i parameter (model details provided in Supplemental Methods). We estimate K_i to be approximately 300 pmol/OD, well above the concentrations observed during the slowest steady-state growth condition used here (60 pmol/OD at $\mu \sim 0.5$ /hr). Direct ppGpp inhibition of PlsB may be relevant to PL flux during extremely slow growth when ppGpp concentrations are above 150 pmol/OD, which may occur at μ well below 0.5 hr^{-1} .

5.3 Discussion

Our comprehensive characterization and modelling of the fatty acid and PL biosynthesis pathways establishes the specific regulatory tools used by *E. coli* to couple membrane synthesis with μ . Most importantly, we find that allosteric control of PlsB is sufficient to balance steady-state PL flux with μ . PlsB demand controls flux into the fatty acid pathway through ACC via inhibition by PlsB substrates, consistent with metabolic control theory (30). Membrane synthesis is regulated very differently than

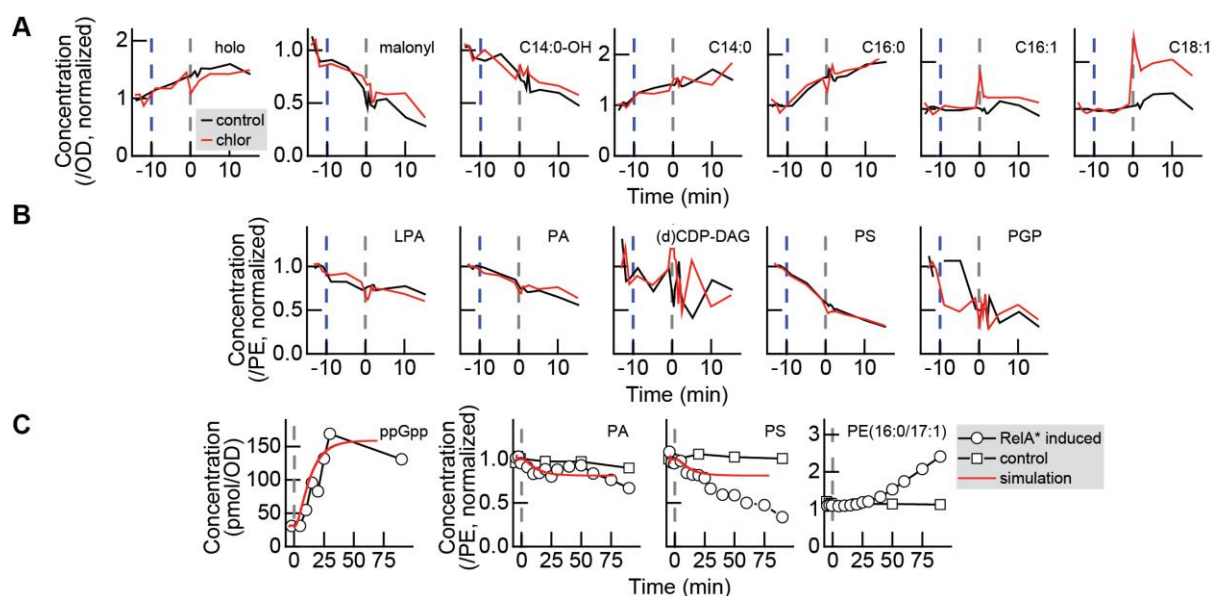


Figure 5.4. PlsB activity is suppressed by moderate to high concentrations of ppGpp via post-translational inhibition. **A**, **B**. Response of acyl-ACP (**A**) and PL intermediate pools (**B**) to maximal induction of RelA*. RelA* expression was induced by addition of 40 ng/mL doxycycline at -10 minutes (dashed blue line), followed 10 minutes later by chloramphenicol addition (dashed grey line at 0 min). **C**. Response of PL intermediates and cyclopropyl-PE to mild induction of RelA* expression by addition of 1 ng/mL doxycycline (dashed grey line at 0 min). Superimposed are simulated kinetic data assuming allosteric inhibition of PlsB by ppGpp with an empirical allosteric inhibition constant $K_i = 300$ pmol/OD. Simulation details are included in the **Supplemental Methods**.

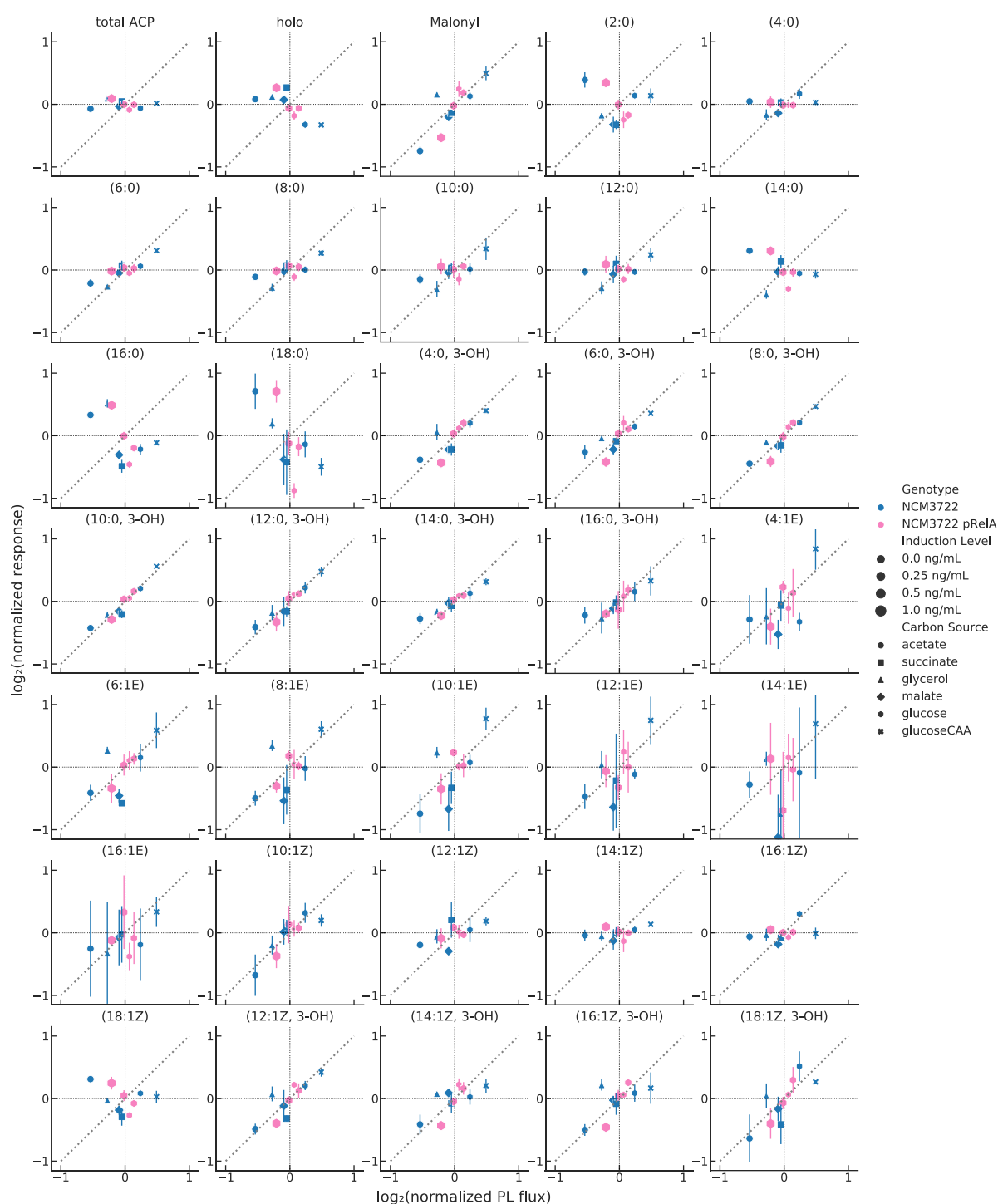
protein synthesis, as membrane synthesis capacity (i.e. concentrations of PlsB and fatty acid synthesis pathway enzymes) is maintained at stable levels across a 3-fold range of μ . Counterintuitively, increased transcription of the fatty acid and PL synthesis pathways reported to occur at higher μ (31) does not increase concentrations of these enzymes, but rather maintains them at a constant concentration. Maintaining a constant capacity for membrane synthesis enables the cell to address any change in membrane synthesis demand at the cost of expressing enzymes that remain inhibited at slow or moderate μ (32).

Both our model and our experimental data indicate that ACC and PlsB activities determine the concentrations of LPS precursor C14:0-OH-ACP, indicating that PL synthesis control also plays a role in coordinating LPS synthesis flux with μ . Perhaps counterintuitively, increasing PL synthesis does not come at the cost of LPS flux, but rather, increases in PL flux directly increase C14:0-OH-ACP by relieving feedback inhibition of ACC. As we observed that LpxC concentrations decrease in response to higher μ , we propose that LpxC concentrations are regulated in response to over-accumulation of LPS that occurs due to increasing concentrations of C14:0-OH-ACP. This regulation may be mediated by increased degradation by the FtsH protease (33), although we cannot exclude that LpxC concentrations are also modulated by transcriptional regulation. Our data will be essential in evaluating existing models of PL-LPS pathway coordination (34).

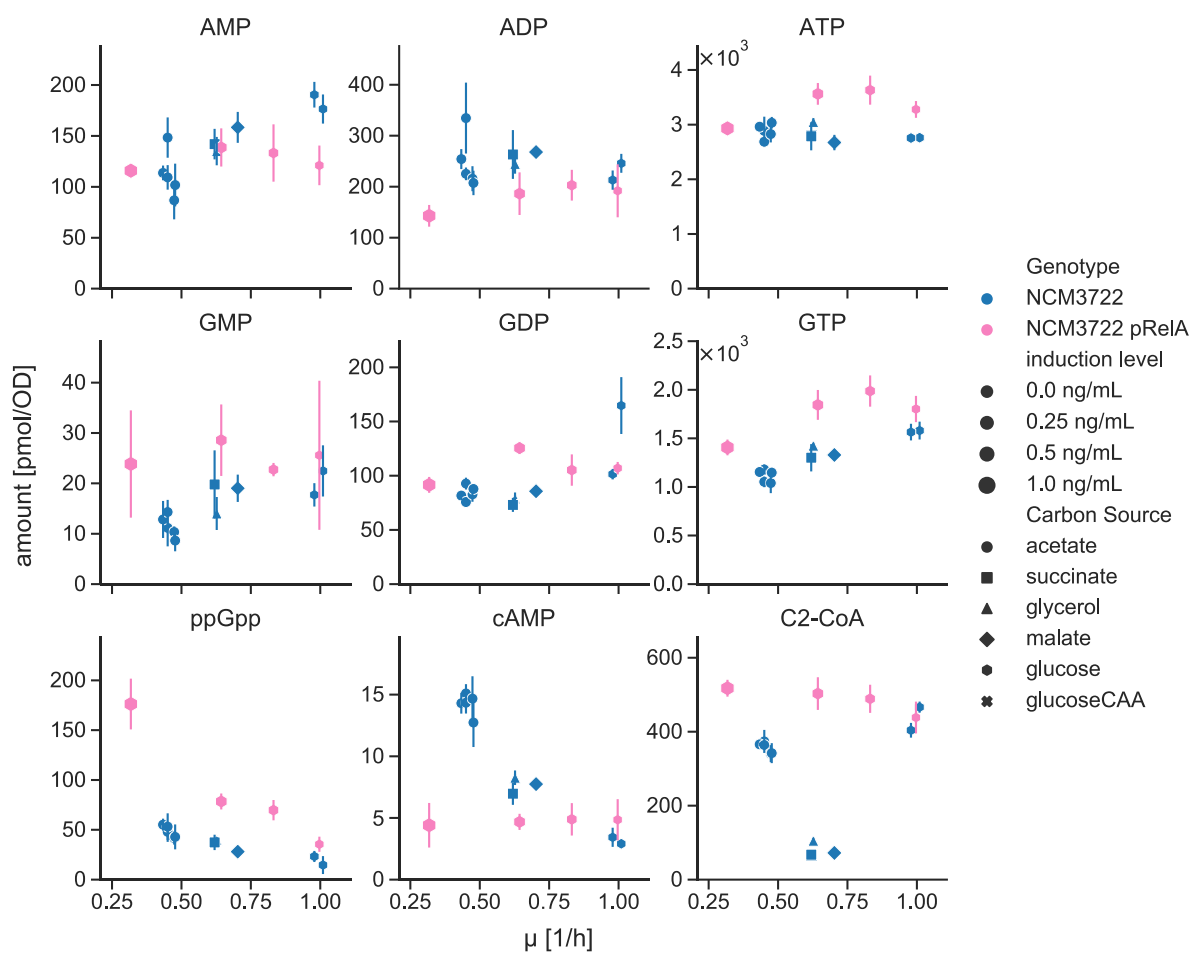
Although PlsB determines PL flux during steady-state growth, this control is not absolute, as the fatty acid and PL pathways (and likely the LPS pathway) are highly sensitive to fluctuations in acetyl-CoA concentrations and ACC activity. The sensitivity of PL flux to central metabolism and even protein synthesis arrest renders membrane synthesis extremely responsive to small environmental changes. While this sensitivity facilitates rapid adaptation of PL flux to changes in μ , the tight connection between protein synthesis, central carbon metabolism, and membrane biogenesis demands additional allosteric control (including inhibition by ppGpp) to re-balance the pathway with μ and prevent PL overflow. If protein synthesis is inhibited in a manner that does not decrease carbon flow into the fatty acid pathway (e.g. by sudden nitrogen starvation), we hypothesize that continued PL and LPS synthesis would outpace synthesis of the lipoproteins that tether the outer membrane to the peptidoglycan layer. Inhibition of PL and LPS pathways by ppGpp would thus prevent production of excess membrane, enforcing the coupling of PL and lipoprotein synthesis. Consistent with this notion, strains lacking the ppGpp response (known as relaxed strains) have been observed to generate higher quantities of extracellular PL and LPS, likely as outer membrane vesicles (35).

We estimate that post-translational control of PlsB by ppGpp, reflected by a relatively high effective K_i (~300 pmol/OD), suggests that ppGpp contributes to steady-state membrane synthesis regulation during growth in conditions that support $\mu > 0.5 \text{ hr}^{-1}$. Although it is generally believed that ppGpp directly inhibits PlsB, multiple groups have been unable to observe ppGpp inhibition of PlsB *in vitro* when acyl-ACP are used as substrates (36, 37). ppGpp may therefore control PlsB indirectly by modulating activity of a regulator or a cellular process that interacts with PlsB. Several candidates for the allosteric regulator of PlsB activity have been discovered. In immunoprecipitation experiments, PlsB has been found to interact with proteins including ACP and PssA, as well as several whose roles are unclear (PlsX and YbgC) (38), suggesting that PlsB forms part of a PL synthesis complex that may couple PlsB activity with μ . As PL synthesis flux has been observed to oscillate with the cell division cycle in *E. coli* and other bacteria (39), PlsB may also be regulated by the divisome or by septum formation. Degradation of PL by phospholipases may also play an important role in membrane homeostasis during steady-state growth (40), as is known to occur during growth and division in eukaryotes (41). In addition to identifying the allosteric regulators of PlsB, studies that integrate connections between PL catabolism and transport with PL synthesis are needed for a comprehensive understanding of membrane homeostasis.

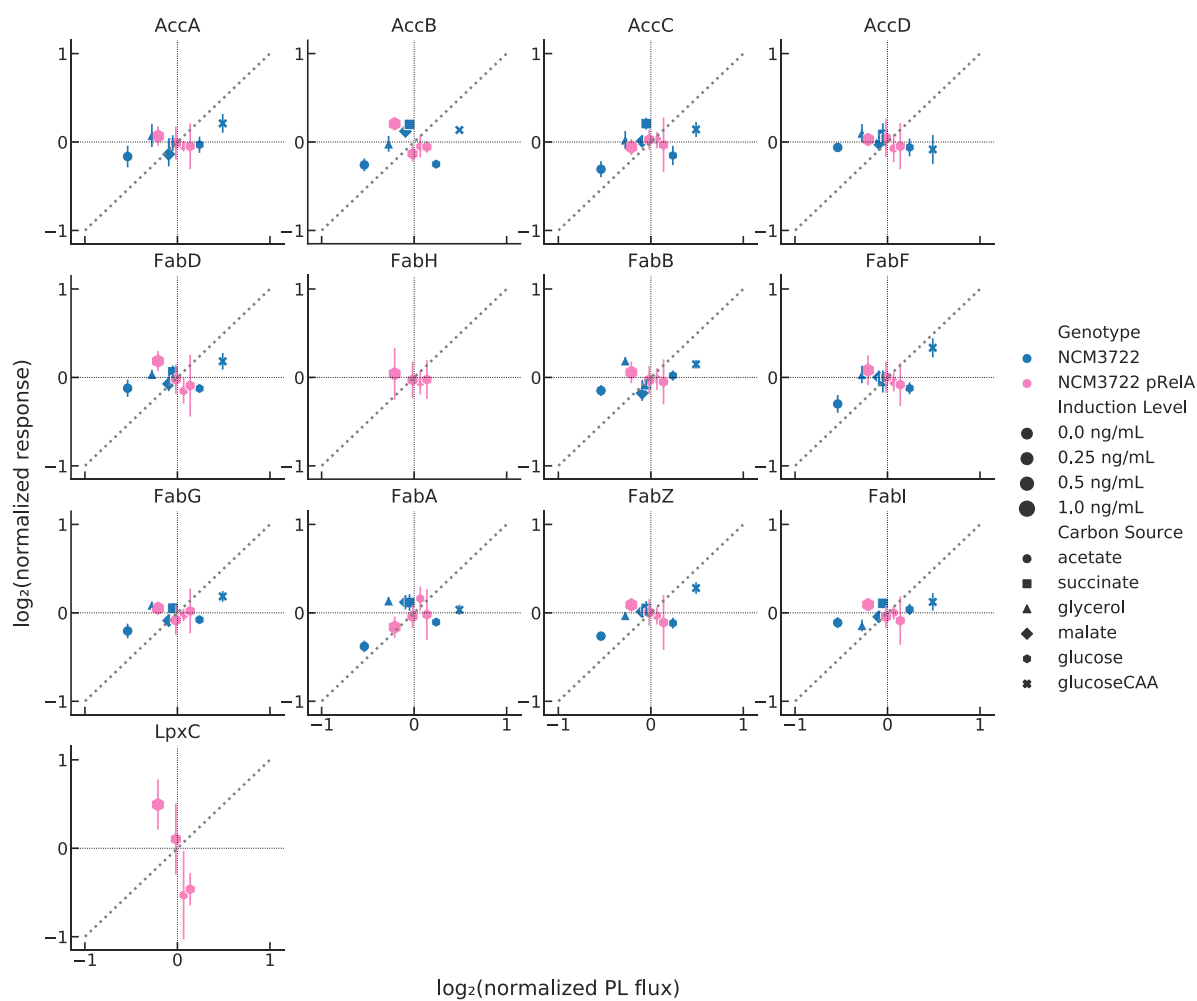
5.4 Supplementary Information



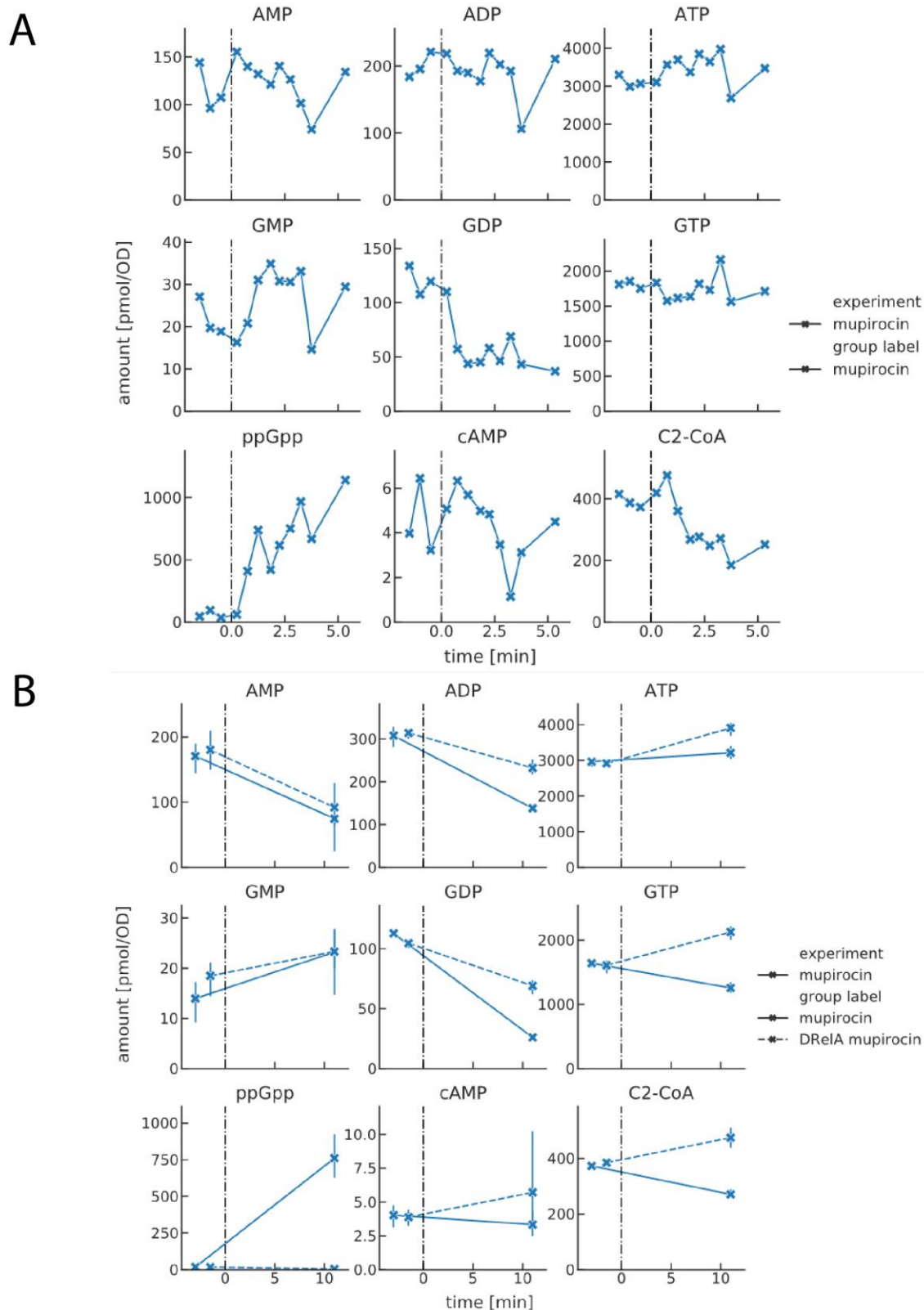
Supplemental Figure 5.1. Steady-state concentrations of acyl-ACP species within *E. coli* NCM3722 in six media (blue) and steady-state acyl-ACP concentrations in glucose cultures of *E. coli* pRelA* limited by excess ppGpp (magenta). ppGpp is titrated by inducing RelA* with increasing concentrations of inducer. Concentrations and PL fluxes are normalized to concentration and flux averages obtained across each strain as described in Figure 1. Error bars represent standard deviation of 3 sampling replicates.



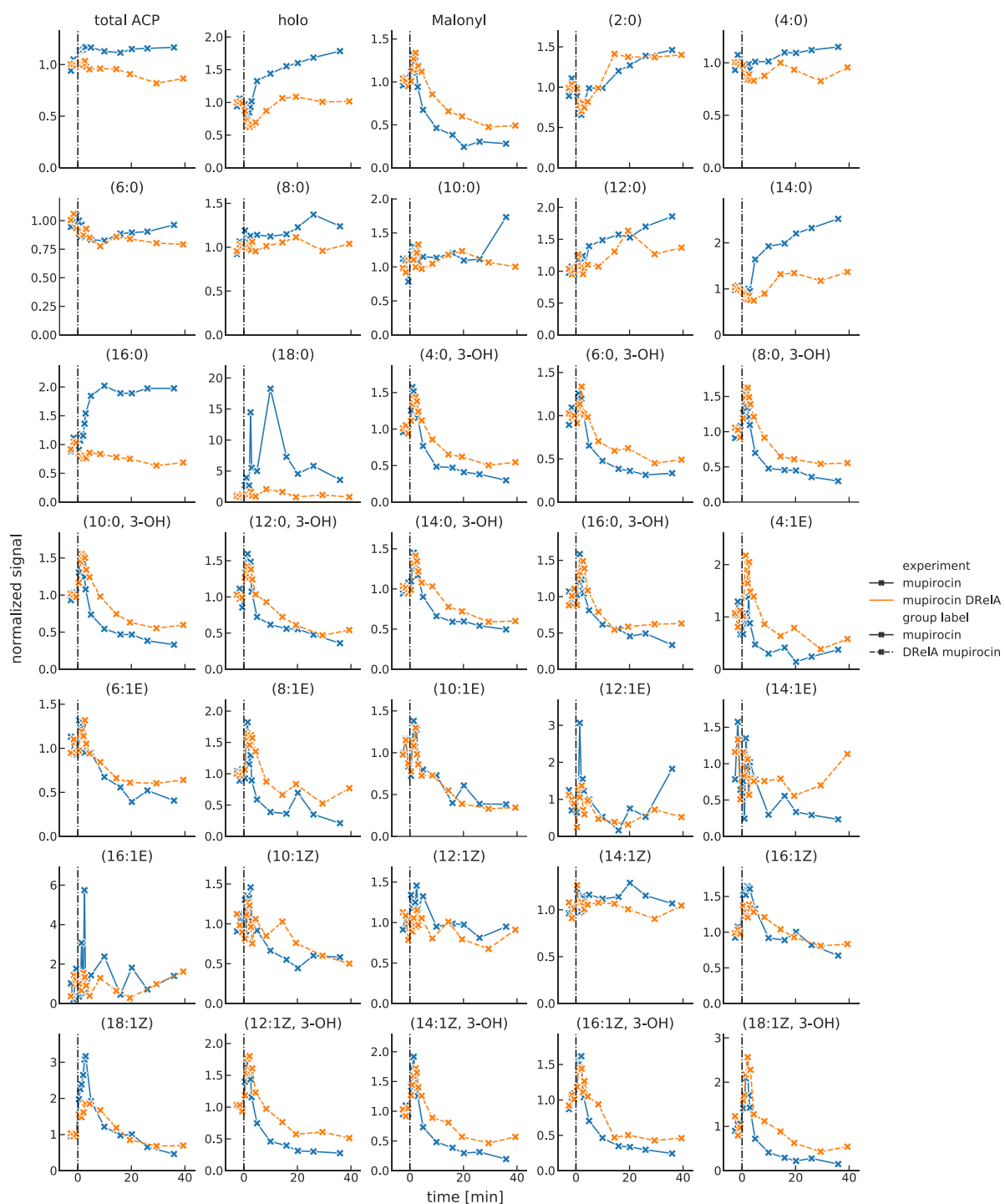
Supplemental Figure 5.2. Steady-state concentrations of nucleotides within *E. coli* NCM3722 in six media (blue). Overlaid are steady-state concentrations in glucose cultures of *E. coli* pRelA* limited by excess ppGpp (magenta). ppGpp is titrated by inducing RelA* with increasing concentrations of inducer. Error bars represent standard deviation of 3 sampling replicates.



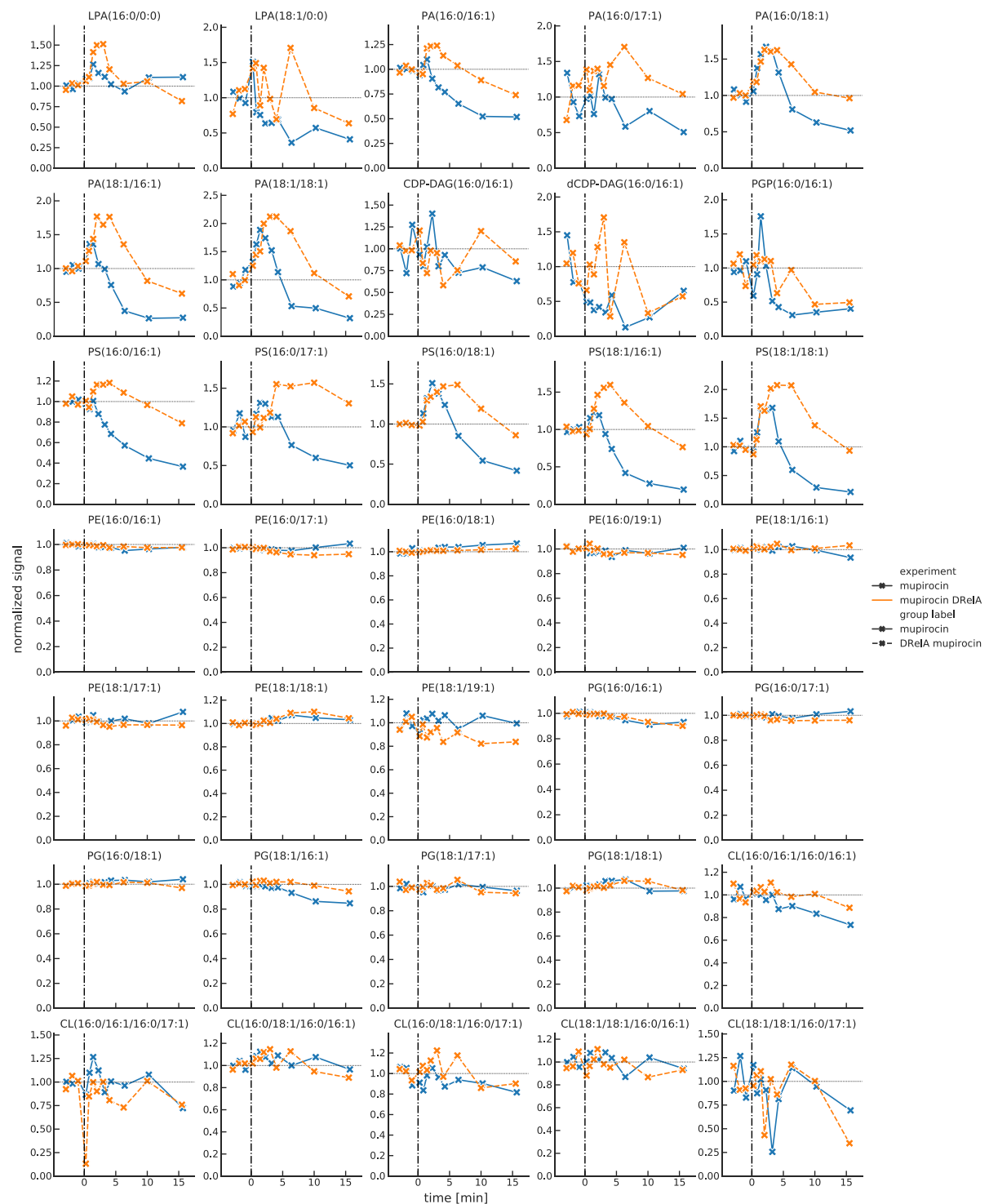
Supplemental Figure 5.3. Concentrations of enzymes in the fatty acid synthesis pathway during steady-state growth in carbon-limited (blue) in ppGpp-limited (magenta) cultures. Values are normalized as described in Figure 1. Error bars represent standard deviation of 3 sampling replicates.



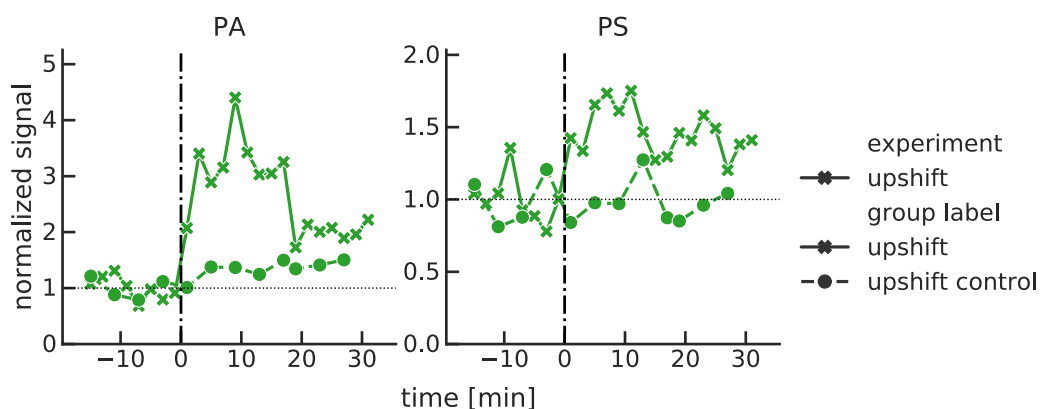
Supplemental Figure 5.4. A. Dynamics of nucleotide pools of wild-type *E. coli* after mupirocin addition (dashed line at $t=0$ minutes). Data points indicate individual measurements from a single culture. **B.** Response of nucleotide pools of wild-type and $\Delta relA$ strains to mupirocin, added at $t=0$. Error bars represent standard deviation of 3 sampling replicates.



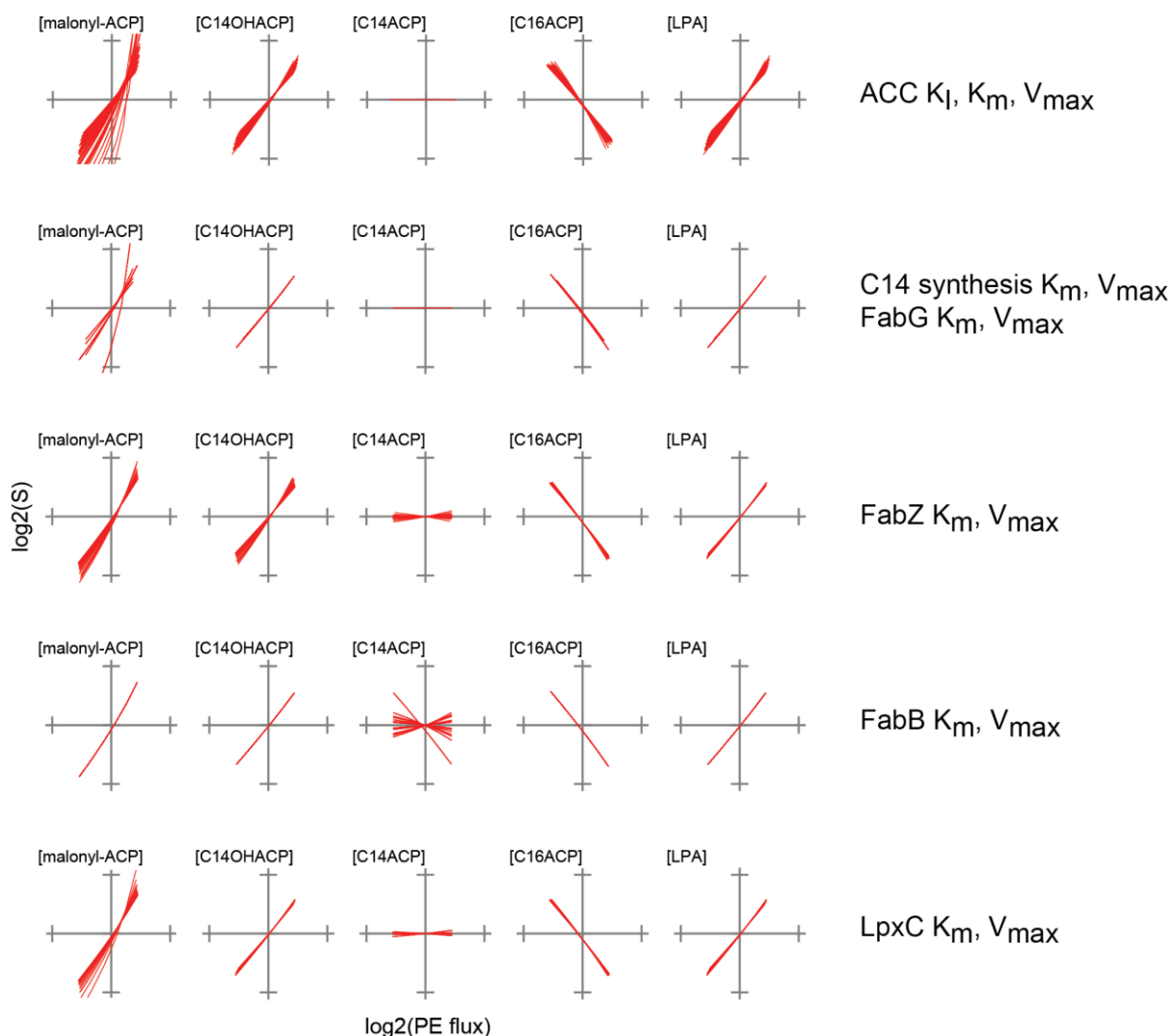
Supplemental Figure 5.5. Response of acyl-ACP species (counts per OD unit) to mupirocin at $t = 0$ in wild-type and $\Delta relA$ *E. coli*. Values are normalized such that the concentrations before $t = 0$ are averaged to 1. Data points indicate individual measurements from a single culture.



Supplemental Figure 5.6. Response of individual PL species (counts per total PE) to mupirocin at $t = 0$ in wild-type and $\Delta relA$ *E. coli*. Values are normalized such that the concentrations before $t = 0$ are averaged to 1. Data points indicate individual PE measurements from a single culture.



Supplemental Figure 5.7. Response of PL species (counts per total PE) to addition of glucose and amino acids at $t = 0$ to a glycerol culture of wild-type *E. coli*. Values are normalized such that the concentrations before $t = 0$ are averaged to 1. Data points indicate individual measurements from single cultures.



Supplemental Figure 5.8. Sensitivity analysis of the fatty acid and phospholipid synthesis model demonstrates that the steady-state metabolite concentration trends simulated from PlsB V_{max} variations are robust against variations in model parameters. Parameters were simultaneously varied across a 4-fold range centered around the model parameter used and PlsB V_{max} was varied as described in the main text.

Species	Pearson correlation coefficient (<i>r</i>)	Significance (<i>p</i> , two-tailed)
malonyl-ACP	0.84	0.04
G3P*	0.99	<0.01
C14:0-OH-ACP	0.99	<0.01
C16:0-ACP	-0.54	0.26
C16:1-ACP	0.43	0.40
C18:1-ACP	-0.25	0.63
LPA	0.95	<0.01
PA	0.99	<0.01
(d)CDP-DAG	0.89	0.02
PS	0.95	<0.01
PGP**	0.99	<0.01

*G3P: calculated with glycerol point excluded.

**PGP: calculated with glucose + Cas-amino acids point excluded.

Enzyme	Pearson correlation coefficient (<i>r</i>)	Significance (<i>p</i> , two-tailed)
PlsB	-0.52	0.29
PlsC	0.59	0.22
CdsA	0.86	0.03
PssA	-0.47	0.35
Psd	0.09	0.87
PgsA	-0.73	0.10
PgpA	0.94	0.01
AccA	0.69	0.13
AccB	0.35	0.50
AccC	0.51	0.30
AccD	-0.37	0.47
AcpP	0.02	0.98
FabA	0.38	0.46
FabB	0.45	0.38
FabD	0.53	0.28
FabF	0.75	0.09
FabG	0.63	0.18
FabI	0.81	0.05
FabZ	0.77	0.08
GpsA	-0.69	0.13

Supplemental Table 5.1. Pearson correlation coefficients and significance determined for PL flux and species abundance during steady-state growth in wild-type *E. coli*. Correlations were calculated from log(2) normalized concentrations and PL fluxes using the Descriptive Statistics function (OriginPro v. 2015). Shaded cells indicate $p < 0.05$.

Acknowledgements

We thank Michael Cashel for providing *E. coli* strain CF7974. We thank Christophe Danelon, Bertus Beaumont, and Frank Bruggeman for invaluable suggestions for improving the manuscript. This research was funded by a grant to GB from the Netherlands Organisation for Scientific Research (ALW Open 824.15.018) and an award from the Frontiers of Nanoscience program.

Conflict of Interest

The authors declare that they have no conflict of interest.

5.5 Materials and Methods

Culture conditions

Cultures were grown in 250-1000 mL Erlenmeyer flasks filled up to 10% of nominal volume with MOPS minimal medium (42) with 9.5 mM NH₄Cl or ¹⁵NH₄Cl and 0.2% (w/v) carbon source (acetate, succinate, malate, glycerol, glucose, U-¹³C-glucose (Cambridge Isotope Laboratories) or glucose supplemented with 0.1% Cas-amino acids). Culture flasks were placed in a Grant Instruments Sub Aqua Pro dual water bath at 37 °C and agitated by stirring with a 12 mm magnetic stir bar (VWR), coupled to a magnetic stir plate (2mag MIXdrive 1 Eco and MIXcontrol 20) set at 1200 rpm. Growth was monitored by optical density measurement at 600 nm using Ultrospec 10 Cell Density Meter (GE Healthcare). Samples for acyl-ACP, lipid analysis and proteomics were collected using cultures without isotopic labelling. Samples for nucleotide phosphate measurements were collected from U-¹⁵N-labeled cultures and samples for G3P measurements were collected from U-¹³C-labeled cultures.

Strains and plasmid pRelA*

All experiments were performed using *Escherichia coli* K-12 strain NCM3722 (CGSC# 12355) and its derivatives. NCM3722 *relA::kan* was constructed by P1 phage transduction using strain CF7974 (MG1655 Δlac (*rph*⁺) *relA255::kan*) as a donor. Plasmid pRelA* was created by cloning DNA encoding residues 1-455 from the *E. coli* RelA protein into BglBrick plasmid pBbS2k (43) (SC101* origin of replication, P_{Tet} promoter, kanamycin resistance). The fluorescent protein mVenus was fused by restriction-digestion to the C-terminus of RelA via a glycine-serine linker.

Metabolite sampling

Samples for acyl-ACP, proteomics and lipid analysis were acquired by fast quenching of 1 mL of culture sample into 250 μ L of ice-cold 10% trichloroacetic acid. After 10 min incubation at 0°C cells were pelleted by centrifugation and stored at -80°C until analysis. For nucleotide phosphates and polar metabolites analysis, samples were acquired by a modified fast vacuum filtration method (44). 1 mL of culture was

collected by vacuum on a pre-wetted 2.5 cm 0.45 μm HV Durapore membrane filter. After rapid collection the filter was immediately placed upside-down in quenching solution. For the measurement of nucleotide phosphates, 1 mL of ice-cold 2 M formic acid with 10 μL internal standards mix was used as a quenching solution, which was subsequently neutralized by 25 μL of 28% ammonium hydroxide. For G3P measurements, 1 mL of 50:30:20 (v/v/v) mixture of methanol, acetonitrile and water with 0.1% formic acid with 10 μL internal standard solution (cooled on dry ice) was used as a quenching solution. After 10 min incubation cells were washed from the filter, transferred to a tube and stored at -80°C until analysis.

Preparation of internal standards

Isotopically-labeled internal standards (IS) were used to control for sampling and measurement variation. For acyl-ACP and proteomics assays $\text{U-}^{15}\text{N}$ *E. coli* whole cell extracts were prepared using a MOPS minimal medium culture with $^{15}\text{NH}_4\text{Cl}$ as the sole nitrogen source. At OD of ~ 0.5 10% TCA was added 1:4 to the culture to facilitate quenching of metabolism. After 10 min incubation on ice 10 mL single-use IS aliquots were collected by centrifugation and stored at -80°C until the sample preparation. For the phospholipid measurement $\text{U-}^{13}\text{C}$ lipid extract was prepared using a culture grown in minimal MOPS medium with 0.2% $\text{U-}^{13}\text{C}$ glucose as the sole carbon source. At OD of ~ 0.5 10% TCA was added 1:4 to the culture and insoluble cell material was collected by centrifugation after 10 min incubation on ice. Pellets were resuspended in mixture consisting of 75 μL MeOH, 10 μL 15 mM citric acid/ 20 mM dipotassium phosphate buffer and 250 μL of methyl-t-butyl ether per 1 mL of initial culture volume. After vortexing and 10 min sonication phase separation was induced by addition of 70 $\mu\text{L}/1\text{mL}$ of 15 mM citric acid/ 20 mM dipotassium phosphate buffer. After further vortexing, sonication and 10 minutes of incubation at room temperature phases were separated by 10 min centrifugation at 4000 rpm at room temperature. Upper phase was collected to a glass vial and stored at -20°C until sample preparation.

Instrumentation

All LC/MS runs were performed using Agilent LCMS consisting of binary pump (G1312B), autosampler (G7167A), temperature-controlled column compartment (G1316A), and triple quadrupole (QQQ) mass spectrometer (G6460C) equipped with a standard ESI source, all operated using MassHunter data acquisition software (version 7.0). Mass spectrometer operated in dynamic MRM mode using transitions generated *in silico* by a script written in Python using RDkit library using chemical structures of target compound as input. Transitions for targeted proteomics assays were developed using Skyline (45) based on protein sequences from the Uniprot database. Details of transition setting are included in **Supplemental Tables 3-7**.

LC/MS quantification of acyl-ACP intermediates

Acyl-ACP were measured using a published method (18) with minor modifications. Lysis buffer was prepared by suspending appropriate number of frozen U-¹⁵N-labeled *E. coli* pellets in 10 mL of 50 mM potassium phosphate buffer, pH 7.2, 6 M urea, 10 mM N-ethyl-maleimide, 5 mM EDTA and 1 mM ascorbic acid. 1 mL of lysis buffer was added to each of TCA-quenched and pelleted cells and proteins were isolated by chloroform/methanol precipitation as described previously. Protein pellets were resuspended in 10 μ L of digestion buffer (4% 2-octyl-glucoside in 25 mM potassium phosphate buffer, pH 7.2) and after adding 10 μ L of 0.1 mg/mL GluC protease (Promega) incubated overnight at 37°C. After quenching by addition of 5 μ L MeOH, samples were centrifuged and 10 μ L was injected in LC/MS system. Separation was performed on 2.1 mm x 50 mm 1.7 μ m CSH C-18 column (Waters) held at 80°C using a binary gradient: 15% B, 3 minute ramp to 25%, 9 min increase to 95% and 1 minute hold at 95% B before 3 minute re-equilibration at starting conditions (A: 25 mM formic acid, B: 50 mM formic acid) at a flow rate of 0.6 mL/min.

LC/MS quantification of phospholipids

Phospholipids sample preparation procedure is a combination of an MTBE extraction method (46) and an established LC/MS method (47) Pelleted *E. coli* were resuspended in mixture containing 150 μ L of MeOH, 250 μ L of U-¹³C *E. coli* extract prepared as described above and 250 μ L MTBE. After vigorous vortexing and sonication 125 μ L of 15 mM citric acid/ 20 mM dipotassium phosphate buffer was added to homogenized pellets. Following further vortexing and 10 min incubation at room temperature, liquid phases were separated by centrifugation for 10 min at 20000g. 500 μ L of the upper phase was moved to a new tube and dried in a vacuum centrifuge (Labconco). Dried lipid films were resuspended in 10 μ L 65:30:5 (v/v/v) isopropanol/acetonitrile/H₂O, supplemented with 10 mM acetylacetone. After resuspension, 5 μ L H₂O was added to reduce the organic content of the buffer and 5 μ L of resulting mixture was injected into the LC/MS system. Separation was performed on 2.1 mm x 50 mm 1.7 μ m CSH C-18 column (Waters) at 60°C with a flow rate of 0.6 mL/min using the following binary gradient: 25% B, ramp to 56%B in 6 min followed by linear increase to 80% B in 6 min, 2 min hold at 100% B and 3 min re-equilibration (A: 0.05% NH₄OH in water, B: 0.05% NH₄OH in 80% isopropanol 20% ACN).

LC/MS quantification of nucleotide phosphates

Frozen cell extracts were defrosted by 1-2 minute incubation in a 37°C water bath and sonicated for 10 minutes in water ice slurry. After 10 minute centrifugation at 20000g, samples were loaded on 1 mL/30 mg Oasis Wax cartridge (Waters) preconditioned with 1 mL of MeOH and 1 mL 50 mM ammonium acetate buffer, pH 4.5. After washing with 1 mL ammonium acetate buffer, analytes were eluted with 200 μ L of 2.8% ammonium hydroxide in MeOH:ACN:H₂O 50:30:20 (v:v:v). After addition of 10 μ L of 5% trehalose and brief vortexing samples were dried down in a vacuum centrifuge

(Labconco). Dried trehalose-stabilized extracts were re-dissolved in 20 μ L of MeOH:ACN:H₂O 50:30:20 (v:v:v) and moved to an autosampler vial for analysis. Separation was performed on 2.1 mm x 100 mm 3.5 μ m iHilic column (HILICON) or SeQuant Zic-cHILIC, 2.1mm x 100 mm, 3 μ m (Merck) at 0.3 mL/min using the following binary gradient: 100% B, ramp to 85%B in 1.5 min followed by 10 min isocratic hold at 85% B and linear decrease 30% B in 3 minutes with 2 minute hold at 30% B and 8 minute re-equilibration at initial conditions. (A: 3.75 mM ammonium acetate, 1.25 mM acetic acid, 2 mM acetylacetone in MQ, B: 11.25 mM ammonium acetate, 3.75 mM acetic acid, 2 mM acetylacetone in 80% ACN). Injection volume was 2 μ L.

LC/MS quantification of G3P

Stored metabolite extracts were dried down in a vacuum centrifuge (Labconco), re-dissolved in 20 μ L of MeOH:ACN:H₂O 50:30:20 (v:v:v) and moved to an autosampler vial for analysis. Separation was performed on 2.1 mm x 100 mm 3.5 μ m iHilic column (HILICON) at 0.3 mL/min using the following binary gradient: 100% B, ramp to 80% B in 10 min followed by linear decrease to 30% B in 3 min, 2 min hold at 30% B and 8 min re-equilibration. Injection volume was 2 μ L.

LC/MS targeted protein quantification

Relative concentrations of enzymes were measured by targeted proteomics using a modified version of the acyl-ACP assay. Lysis buffer was prepared by suspending appropriate number of frozen U-¹⁵N-labeled *E. coli* pellets in 10 mL of 50 mM potassium phosphate buffer, pH 7.2 and 6 M urea. 1 mL of lysis buffer was added to each of TCA-quenched and pelleted cells and proteins were isolated by chloroform/methanol precipitation as described previously. Protein pellets were resuspended in 10 μ L of digestion buffer (4% 2-octyl-glucoside in 25 mM Tris buffer, pH 8.1 supplemented with 1 mM CaCl₂ and 5 mM TCEP). Alkylation of cysteine residues was performed by adding 3 μ L of 50 mM iodoacetamide followed by 15 minutes of incubation in darkness. Digestion was performed by adding 10 μ L of 0.2 mg/mL Trypsin Gold (Promega) and overnight incubation at 37°C. Samples were centrifuged and 10 μ L was injected in LCMS system. Separation was performed on 2.1 mm x 50 mm 1.7 μ m CSH C-18 column (Waters) held at 40°C using a binary gradient: 2% B, 20 minute ramp to 25% B, 4 min increase to 40% B, 0.5 ramp to 80% and 1 minute hold at 80% B before 3 minute re-equilibration at starting conditions (A: 25 mL formic acid, B: 50 mM formic acid) at a flow rate of 0.5 mL/min.

Data Analysis

All LC-MS data files were processed in Skyline versions 4.x using target list based on *in silico* generated transition list. Each target compound had matching isotopically-labeled internal standard (IS). Processed data were exported as target compounds and IS peak areas and processed further using a set of Python scripts. Growth rates were obtained from linear fits to log-transformed growth curves. OD-corrected data were obtained by dividing the signal by OD₆₀₀ value interpolated from growth curve at

the time of sampling. PE-corrected results were produced by dividing the signal by sum all of signals for all phosphatidyl-ethanolamine species from the same measurement (in case of phospholipids) or matching sample (in case of other assays). In nucleotide phosphate and G3P assay absolute concentrations were estimated based on amounts of internal standards in IS-spike solution assuming $RR = 1$ implies equimolar amounts of target compound and IS at the moment of quenching. Concentrations of IS in the spike mix are provided in the supplement.

Steady-state model description

The simplified pathway model was set up using COPASI as a series of irreversible Michaelis-Menten equations. Most reactions in the fatty acid pathway were excluded in order to determine whether the experimentally-observed trends in intermediate concentrations could be captured in a simplified model. Acetyl-CoA and C16:1-ACP concentrations were fixed at their initial values. For simplicity, V_{max} values and K_M parameters of each reaction were set to similar values (around 10 and 30 μM , full parameter set given below). For steady-state calculations, we do not claim that the model parameters reflect the exact *in vivo* values. However the values are useful in capturing the basic steady-state behaviours of the system. The simulated steady-state fluxes and metabolite concentrations depicted in Figure 5.2 were obtained using the “Parameter Scan” function in COPASI. The differential equations that determine the fluxes through each intermediate pool are defined below.

The strong flux control exerted by PIsB is a consequence of its use of a substrate (C16:0-ACP) that strongly inhibits its own synthesis (i.e. inhibits ACC), as predicted by metabolic control analysis. Although acyl-ACP species are predicted from experiments to exhibit mixed inhibition of *E. coli* ACC with respect to acetyl-CoA (49), we use competitive inhibition to minimize the number of parameters in the model. Changes in concentrations of other substrates (e.g. ATP, bicarbonate) or allosteric regulators of ACC (e.g. GlnB) would be expected to exert a similar influence on ACC activity and fatty acid synthesis as variations in ACC V_{max} .

Differential equation definitions

Steady-state fluxes are defined as follows. Note that ppGpp inhibition of PlsB was not considered in steady-state calculations (i.e. ppGpp was set to 0 μM).

$$\begin{aligned}
 \frac{d([\text{"malonyl-ACP"}] \cdot V_{\text{compartment}})}{dt} &= +V_{\text{compartment}} \cdot \left(\frac{50 \cdot [\text{"acetyl-CoA"}]}{300 + [\text{"acetyl-CoA"}] + \frac{300 \cdot [\text{C16ACP}]}{1}} \right) \\
 &\quad -V_{\text{compartment}} \cdot \left(\frac{10 \cdot [\text{"malonyl-ACP"}]}{30 + [\text{"malonyl-ACP"}]} \right) \\
 &\quad -V_{\text{compartment}} \cdot \left(\frac{20 \cdot [\text{C14ACP}] \cdot [\text{"malonyl-ACP"}]}{30 \cdot 30 + [\text{C14ACP}] \cdot 30 + [\text{"malonyl-ACP"}] \cdot 30 + [\text{C14ACP}] \cdot [\text{"malonyl-ACP"}]} \right) \\
 \frac{d([\text{C16ACP}] \cdot V_{\text{compartment}})}{dt} &= +V_{\text{compartment}} \cdot \left(\frac{10 \cdot [\text{C16OHACP}]}{30 + [\text{C16OHACP}]} \right) \\
 &\quad -V_{\text{compartment}} \cdot \left(\frac{10 \cdot [\text{C16ACP}]}{30 + [\text{C16ACP}] \cdot \left(1 + \frac{[\text{ppGpp}]}{200} \right)} \right) \\
 \frac{d([\text{LPA}] \cdot V_{\text{compartment}})}{dt} &= +V_{\text{compartment}} \cdot \left(\frac{10 \cdot [\text{C16ACP}]}{30 + [\text{C16ACP}] \cdot \left(1 + \frac{[\text{ppGpp}]}{200} \right)} \right) \\
 &\quad -V_{\text{compartment}} \cdot \left(\frac{20 \cdot [\text{LPA}] \cdot [\text{C161ACP}]}{30 \cdot 30 + [\text{LPA}] \cdot 30 + [\text{C161ACP}] \cdot 30 + [\text{LPA}] \cdot [\text{C161ACP}]} \right) \\
 \frac{d([\text{PA}] \cdot V_{\text{compartment}})}{dt} &= +V_{\text{compartment}} \cdot \left(\frac{20 \cdot [\text{LPA}] \cdot [\text{C161ACP}]}{30 \cdot 30 + [\text{LPA}] \cdot 30 + [\text{C161ACP}] \cdot 30 + [\text{LPA}] \cdot [\text{C161ACP}]} \right) \\
 &\quad -V_{\text{compartment}} \cdot \left(\frac{10 \cdot [\text{PA}]}{30 + [\text{PA}]} \right) \\
 \frac{d([\text{CDPDAG}] \cdot V_{\text{compartment}})}{dt} &= +V_{\text{compartment}} \cdot \left(\frac{10 \cdot [\text{PA}]}{30 + [\text{PA}]} \right) \\
 &\quad -V_{\text{compartment}} \cdot \left(\frac{10 \cdot [\text{CDPDAG}]}{30 + [\text{CDPDAG}]} \right) \\
 \frac{d([\text{PS}] \cdot V_{\text{compartment}})}{dt} &= +V_{\text{compartment}} \cdot \left(\frac{10 \cdot [\text{CDPDAG}]}{30 + [\text{CDPDAG}]} \right) \\
 &\quad -V_{\text{compartment}} \cdot \left(\frac{10 \cdot [\text{PS}]}{30 + [\text{PS}]} \right) \\
 \frac{d([\text{C14BKACP}] \cdot V_{\text{compartment}})}{dt} &= +V_{\text{compartment}} \cdot \left(\frac{10 \cdot [\text{"malonyl-ACP"}]}{30 + [\text{"malonyl-ACP"}]} \right) \\
 &\quad -V_{\text{compartment}} \cdot \left(\frac{10 \cdot [\text{C14BKACP}]}{30 + [\text{C14BKACP}]} \right) \\
 \frac{d([\text{C14OHACP}] \cdot V_{\text{compartment}})}{dt} &= +V_{\text{compartment}} \cdot \left(\frac{10 \cdot [\text{C14BKACP}]}{30 + [\text{C14BKACP}]} \right) \\
 &\quad -V_{\text{compartment}} \cdot \left(\frac{10 \cdot [\text{C14OHACP}]}{30 + [\text{C14OHACP}]} \right) \\
 &\quad -V_{\text{compartment}} \cdot \left(\frac{10 \cdot [\text{C14OHACP}]}{30 + [\text{C14OHACP}]} \right) \\
 \frac{d([\text{C14ACP}] \cdot V_{\text{compartment}})}{dt} &= -V_{\text{compartment}} \cdot \left(\frac{20 \cdot [\text{C14ACP}] \cdot [\text{"malonyl-ACP"}]}{30 \cdot 30 + [\text{C14ACP}] \cdot 30 + [\text{"malonyl-ACP"}] \cdot 30 + [\text{C14ACP}] \cdot [\text{"malonyl-ACP"}]} \right) \\
 &\quad +V_{\text{compartment}} \cdot \left(\frac{10 \cdot [\text{C14OHACP}]}{30 + [\text{C14OHACP}]} \right) \\
 \frac{d([\text{C16BKACP}] \cdot V_{\text{compartment}})}{dt} &= +V_{\text{compartment}} \cdot \left(\frac{20 \cdot [\text{C14ACP}] \cdot [\text{"malonyl-ACP"}]}{30 \cdot 30 + [\text{C14ACP}] \cdot 30 + [\text{"malonyl-ACP"}] \cdot 30 + [\text{C14ACP}] \cdot [\text{"malonyl-ACP"}]} \right) \\
 &\quad -V_{\text{compartment}} \cdot \left(\frac{10 \cdot [\text{C16BKACP}]}{30 + [\text{C16BKACP}]} \right) \\
 \frac{d([\text{C16OHACP}] \cdot V_{\text{compartment}})}{dt} &= +V_{\text{compartment}} \cdot \left(\frac{10 \cdot [\text{C16BKACP}]}{30 + [\text{C16BKACP}]} \right) \\
 &\quad -V_{\text{compartment}} \cdot \left(\frac{10 \cdot [\text{C16OHACP}]}{30 + [\text{C16OHACP}]} \right)
 \end{aligned}$$

Values used in mathematical model of fatty acid and PL synthesis pathways. No relationship between simulated values and actual *in vivo* values is implied.

Initial Species Values	Species	Concentration	
	acetyl-CoA	300 $\mu\text{mol/l}$	
malonyl-ACP	0 $\mu\text{mol/l}$		
C16ACP	0 $\mu\text{mol/l}$		
LPA	0 $\mu\text{mol/l}$		
ppGpp	0 $\mu\text{mol/l}$		
PA	0 $\mu\text{mol/l}$		
CDPDAG	0 $\mu\text{mol/l}$		
PS	0 $\mu\text{mol/l}$		
C161ACP	30 $\mu\text{mol/l}$		
C14BKACP	0 $\mu\text{mol/l}$		
C14OHACP	0 $\mu\text{mol/l}$		
C14ACP	0 $\mu\text{mol/l}$		
C16BKACP	0 $\mu\text{mol/l}$		
C16OHACP	0 $\mu\text{mol/l}$		
Kinetic Parameters	Reaction	Parameter	Value
	acetyl-CoA carboxylase	Km	300 μmol
	V	50 $\mu\text{mol/s}$	
	Ki	1 μmol	
C14 synthesis	Km	30 μmol	
	V	10 $\mu\text{mol/s}$	
LPA synthesis	Km	30 μmol	
	V	10 $\mu\text{mol/s}$	
	Ki	200 μmol	
PA synthesis	vmax	20 $\mu\text{mol/s}$	
	Kma	30 μmol	
	Kmb	30 μmol	
CDPDAG synthesis	Km	30 μmol	
	V	10 $\mu\text{mol/s}$	
PS synthesis	Km	30 μmol	
	V	10 $\mu\text{mol/s}$	
PE synthesis	Km	30 μmol	
	V	10 $\mu\text{mol/s}$	
C14 reduction	Km	30 μmol	
	V	10 $\mu\text{mol/s}$	
LPS initiation	Km	30 μmol	
	V	10 $\mu\text{mol/s}$	
C14 dehydration	Km	30 μmol	
	V	10 $\mu\text{mol/s}$	
C14 elongation	vmax	20 $\mu\text{mol/s}$	
	Kma	30 μmol	

	K _{mb}	30 μmol
C16 reduction		
	K _m	30 μmol
	V	10 μmol/s
C16 dehydration		
	K _m	30 μmol
	V	10 μmol/s

Sensitivity analysis

The V_{max} values of PlsB and other enzymes were varied over a 4-fold range and new steady-state values for fluxes and metabolites obtained. The stability of the model was assessed by a sensitivity analysis in which the K_I, K_M, and V_{max} values of each individual enzyme were simultaneously varied over a 4-fold range centered around the values used in the main model (Supplemental Figure 5.8). Values for the “C14 synthesis” pseudo-reaction and the C14 reduction (FabG) were varied together.

Kinetic modelling of PlsB inhibition by ppGpp

For kinetic simulation of ppGpp inhibition, the model described by the above differential equations was used, aside from the LPA synthesis rate, described by equation 1 below. The kinetics of ppGpp response were first obtained by simulating mRNA synthesis and decay, RelA translation and protein dilution, and ppGpp synthesis and decay, and adjusting parameters until simulated kinetics of ppGpp accumulation closely matched the observed values. ppGpp inhibition of PlsB was simulated using the standard Michaelis-Menten equation multiplied by an empirical inhibition term (equation 1):

$$\text{LPA synthesis rate} = V_{max} \times \left(\frac{[\text{C16:0-ACP}]}{K_M + [\text{C16:0-ACP}]} \right) \times \left(\frac{K_I}{K_I + [\text{ppGpp}]} \right) \quad (1)$$

The K_I parameter was varied until the simulated output agreed with the initial PA and PS data points (from 0 to 25 minutes, Figure 5.4C), as this timescale is more likely to reflect the fast-acting post-translational response to ppGpp. We cannot explain the subsequent drop in PS concentrations after 25 minutes, though we note that PA slightly accumulates beginning with the drop in PS. We note that PS synthase PssA has been found to possess PS hydrolase activity, generating PA (50). Further studies will be needed to understand PS dynamics during growth transitions.

Author contributions

MN and GB designed the experiments. MN, FB, NvdB, NS, and GB performed experiments. MN, NvdB, and NI developed analytical methods. MN and GB analysed the data. GB supervised the research, constructed the mathematical model, and wrote the manuscript.

References

1. Kamio Y, Nikaido H (1976) Outer Membrane of Salmonella Typhimurium: Accessibility of Phospholipid Head Groups to Phospholipase C and Cyanogen Bromide Activated Dextran in the External Medium. *Biochemistry* 15(12):2561–2570.
2. Funahara Y, Nikaido H (1980) Asymmetric localization of lipopolysaccharides on the outer membrane of Salmonella typhimurium. *J Bacteriol* 141(3):1463–1465.
3. Suzuki H, et al. (1978) Murein-lipoprotein of Escherichia coli: A protein involved in the stabilization of bacterial cell envelope. *MGG Mol Gen Genet* 167(1):1–9.
4. Dowhan W (2013) A retrospective: use of Escherichia coli as a vehicle to study phospholipid synthesis and function. *Biochim Biophys Acta* 1831(3):471–494.
5. Scott M, Gunderson CW, Mateescu EM, Zhang Z, Hwa T (2010) Interdependence of cell growth and gene expression: Origins and consequences. *Science (80-)*. doi:10.1126/science.1192588.
6. Chubukov V, et al. (2013) Transcriptional regulation is insufficient to explain substrate-induced flux changes in Bacillus subtilis. *Mol Syst Biol* 9. doi:Artn 70910.1038/Msb.2013.66.
7. Hackett SR, et al. (2016) Systems-level analysis of mechanisms regulating yeast metabolic flux. *Science (80-)* 354(6311). doi:10.1126/science.aaf2786.
8. Raetz CR, Larson TJ, Dowhan W (1977) Gene cloning for the isolation of enzymes of membrane lipid synthesis: phosphatidylserine synthase overproduction in Escherichia coli. *Proc Natl Acad Sci U S A* 74(4):1412–1416.
9. Ohta A, Waggoner K, Louie K, Dowhan W (1981) Cloning of genes involved in membrane lipid synthesis. Effects of amplification of phosphatidylserine synthase in Escherichia coli. *J Biol Chem*.
10. Ganong BR, Raetz CR (1982) Massive accumulation of phosphatidic acid in conditionally lethal CDP-diglyceride synthetase mutants and cytidine auxotrophs of Escherichia coli. *J Biol Chem* 257(1):389–394.
11. Heacock PN, Dowhan W (1987) Construction of a lethal mutation in the synthesis of the major acidic phospholipids of Escherichia coli. *J Biol Chem* 262(27):13044–13049.
12. Increased synthesis of phosphatidylserine decarboxylase in a strain of Escherichia coli bearing a hybrid plasmid. Altered association of enzyme with the membrane. (1979) *J Biol Chem* 254(3):627–633.
13. Dennis PP, Bremer H (2008) Modulation of Chemical Composition and Other Parameters of the Cell at Different Exponential Growth Rates. *EcoSal Plus* 3(1). doi:10.1128/ecosal.5.2.3.
14. Sud IJ, Schaechter M (1964) Dependence of the content of cell envelopes on the growth rate of Bacillus megaterium. *J Bacteriol* 88(6):1612–1617.
15. Ballesta JPG, Schaechter M (1972) Dependence of the Rate of Synthesis of Phosphatidylethanolamine and Phosphatidylglycerol on the Rate of Growth of Escherichia coli. *J Bacteriol* 110(1):452–453.
16. Schulman H, Kennedy EP (1977) Relation of turnover of membrane phospholipids to synthesis of membrane derived oligosaccharides of Escherichia coli. *J Biol Chem* 252(12):4250–4255.

17. Harris LK, Theriot JA (2016) Relative rates of surface and volume synthesis set bacterial cell size. *Cell* 165(6):1479–1492.
18. Noga MJ, et al. (2016) Mass-Spectrometry-Based Quantification of Protein-Bound Fatty Acid Synthesis Intermediates from *Escherichia coli*. *J Proteome Res* 15(10):3617–3623.
19. Gerhardt ECM, et al. (2015) The Bacterial signal transduction protein GlnB regulates the committed step in fatty acid biosynthesis by acting as a dissociable regulatory subunit of acetyl-CoA carboxylase. *Mol Microbiol* 95(6):1025–1035.
20. Davis MS, Cronan J (2001) Inhibition of *Escherichia coli* acetyl coenzyme A carboxylase by acyl-acyl carrier protein. *J Bacteriol*. doi:10.1128/JB.183.4.1499-1503.2001.
21. Wahl A, My L, Dumoulin R, Sturgis JN, Bouveret E (2011) Antagonistic regulation of *dgkA* and *plsB* genes of phospholipid synthesis by multiple stress responses in *Escherichia coli*. *Mol Microbiol* 80(5):1260–1275.
22. Rhodius VA, Suh WC, Nonaka G, West J, Gross CA (2006) Conserved and variable functions of the σ Essence response in related genomes. *PLoS Biol*. doi:10.1371/journal.pbio.0040002.
23. Schreiber G, et al. (1991) Overexpression of the *relA* gene in *Escherichia coli*. *J Biol Chem* 266(6):3760–3767.
24. Heath RJ, Jackowski S, Rock CO (1994) Guanosine Tetraphosphate Inhibition of Fatty-Acid and Phospholipid-Synthesis in *Escherichia coli* Is Relieved by Overexpression of Glycerol-3-Phosphate Acyltransferase (*PlsB*). *J Biol Chem* 269(42):26584–26590.
25. Sorensen PG, et al. (1996) Regulation of UDP-3-O-[R-3-hydroxymyristoyl]-N-acetylglucosamine Deacetylase in *Escherichia coli*: THE SECOND ENZYMATIC STEP OF LIPID A BIOSYNTHESIS. *J Biol Chem* 271(42):25898–25905.
26. Merlie JP, Pizer LI (1973) Regulation of phospholipid synthesis in *Escherichia coli* by guanosine tetraphosphate. *J Bacteriol* 116(1):355–366.
27. Nunn WD, Cronan Jr. JE (1976) Regulation of membrane phospholipid synthesis by the *relA* gene: dependence on ppGpp levels. *Biochemistry* 15(12):2546–2550.
28. Larson TJ, Dowhan W (1976) Ribosomal-Associated Phosphatidylserine Synthetase from *Escherichia coli*: Purification by Substrate-Specific Elution from Phosphocellulose Using Cytidine 5'-Diphospho-1,2-diacyl-sn-glycerol. *Biochemistry* 15(24):5212–5218.
29. Eichel J, Chang YY, Riesenber D, Cronan JE (1999) Effect of ppGpp on *Escherichia coli* cyclopropane fatty acid synthesis is mediated through the RpoS sigma factor ($\sigma(S)$). *J Bacteriol* 181(2):572–576.
30. Hofmeyr JHS, Cornish-Bowden A (2000) Regulating the cellular economy of supply and demand. *FEBS Lett*. doi:10.1016/S0014-5793(00)01668-9.
31. Li SJ, Cronan JE (1993) Growth rate regulation of *Escherichia coli* acetyl coenzyme A carboxylase, which catalyzes the first committed step of lipid biosynthesis. *J Bacteriol* 175(2):332–340.
32. Davidi D, Milo R (2017) Lessons on enzyme kinetics from quantitative proteomics. *Curr Opin Biotechnol* 46:81–89.
33. Ogura T, et al. (1999) Balanced biosynthesis of major membrane components through regulated degradation of the committed enzyme of lipid A

- biosynthesis by the AAA protease FtsH (HflB) in *Escherichia coli*. *Mol Microbiol* 31(3):833–844.
34. Emiola A, Andrews SS, Heller C, George J (2016) Crosstalk between the lipopolysaccharide and phospholipid pathways during outer membrane biogenesis in *Escherichia coli*. *Proc Natl Acad Sci* 113(11):3108–3113.
 35. Crowfoot PD, Esfahani M, Wakil SJ (1972) Relation Between Protein Synthesis and Phospholipid Synthesis and Turnover in *Escherichia coli*. *J Bacteriol* 112(3):1408–1415.
 36. Lueking DR, Goldfine H (1975) The involvement of guanosine 5-diphosphate-3-diphosphate in the regulation of phospholipid biosynthesis in *Escherichia coli*. Lack of ppGpp inhibition of acyltransfer from acyl-ACP to sn-glycerol 3-phosphate. *J Biol Chem* 250(13):4911–4917.
 37. Nunn WD, Kelly DL, Stumfall MY (1977) Regulation of fatty acid synthesis during the cessation of phospholipid biosynthesis in *Escherichia coli*. *J Bacteriol* 132(2):526–531.
 38. Gully D, Bouveret E (2006) A protein network for phospholipid synthesis uncovered by a variant of the tandem affinity purification method in *Escherichia coli*. *Proteomics* 6(1):282–293.
 39. Carty CE, Ingram LO (1981) Lipid synthesis during the *Escherichia coli* cell cycle. *J Bacteriol* 145(1):472–478.
 40. May KL, Silhavy TJ (2018) The *Escherichia coli* phospholipase PldA regulates outer membrane homeostasis via lipid signaling. *MBio* 9(2). doi:10.1128/mBio.00379-18.
 41. Hermansson M, Hokynar K, Somerharju P (2011) Mechanisms of glycerophospholipid homeostasis in mammalian cells. *Prog Lipid Res* 50(3):240–257.
 42. Neidhardt FC, Bloch PL, Smith DF (1974) Culture Medium for Enterobacteria. *J Bacteriol* 119(3):736–747.
 43. Lee T, et al. (2011) BglBrick vectors and datasheets: A synthetic biology platform for gene expression. *J Biol Eng* 5(1):12.
 44. Link H, Kochanowski K, Sauer U (2013) Systematic identification of allosteric protein-metabolite interactions that control enzyme activity in vivo. *Nat Biotechnol* 31(4):357–361.
 45. MacLean B, et al. (2010) Skyline: An open source document editor for creating and analyzing targeted proteomics experiments. *Bioinformatics* 26(7):966–968.
 46. Matyash V, Liebisch G, Kurzchalia T V, Shevchenko A, Schwudke D (2008) Lipid extraction by methyl-tert-butyl ether for high-throughput lipidomics. *J Lipid Res* 49(5):1137–1146.
 47. Susanto O, et al. (2017) LPP3 mediates self-generation of chemotactic LPA gradients by melanoma cells. *J Cell Sci* 130(20):3455–3466.
 48. Hoops S, et al. (2006) COPASI - A COmplex PATHway Simulator. *Bioinformatics* 22(24):3067–3074.
 49. Davis MS, Cronan J (2001) Inhibition of *Escherichia coli* acetyl coenzyme A carboxylase by acyl-acyl carrier protein. *J Bacteriol*. doi:10.1128/JB.183.4.1499-1503.2001.
 50. Larson TJ, Dowhan W (1976) Ribosomal-Associated Phosphatidylserine Synthetase from *Escherichia coli*: Purification by Substrate-Specific Elution from Phosphocellulose Using Cytidine 5'-Diphospho-1,2-diacyl-sn-glycerol. *Biochemistry* 15(24):5212–5218.

Summary

Bacteria have been an integral part of human life since the ancient times either as cooperative tenants living in and around us or as constant threats to our health and wellbeing. Since prehistoric times we unknowingly used them as tools of fermentation and fought against them with haphazardly discovered natural remedies. Today, after more than 3 centuries since they were first observed with a microscope, our understanding of their functions has increased immensely along with our ability to alter it. We have discovered on a molecular level how life stores and transfers information, how this information is used to build biochemical machines with a myriad of functions, namely proteins, and how these proteins undertake their functions. Along with a better understanding came the ability to alter the biological information within DNA and to create new proteins that does not occur in nature.

An increased understanding of life at a molecular level led to the design of new strains of bacteria and other microorganisms to produce chemicals and enzymes for industrial purposes such as biofuels and insulin. Better drugs targeting specific molecular machinery were developed to help combat against bacterial diseases. We are even developing bacteria to achieve tasks that we do not need yet such as mining on the moon. However even with all the progress, our knowledge and abilities are limited compared to the complexity of life. Central questions such as how bacteria respond to changing environments, how they manage the inevitable stochasticity at the molecular level, how they cooperate with us and other life forms and many more are active areas of research. Unique biochemistry and functions are being discovered every year along with new species of bacteria and microorganisms. So, there is quite a lot to still learn about life at the molecular level.

In chapter 2 we reviewed how stochasticity affects the lives of bacteria. Our ability to observe single cells has increased significantly in the last decade with new live cell microscopy techniques involving flow cells to trap and feed bacteria. This led to a massive increase in the single cell data available to scientists and allowed observation of differences between individual bacteria with the same genetic code. This showed that bacteria, while being one of the simplest life forms, is dealing with a fundamental problem, stochasticity. Biochemical reactions are inherently stochastic in nature meaning whether a reaction will happen depends partially on “chance”. Since the basis of all life is biochemistry, all life forms have evolved alongside this inherent stochasticity. Bacterial cells have evolved hundreds of known regulatory pathways which control biochemistry of the cell to achieve damping of stochasticity. Some of these are well known and understood. However, the debate is still ongoing about how much stochasticity affects bacterial cells overall; is it a simple nuisance, a massive problem or just a part of their lives they co-evolved with to take advantage of?

Research in the recent years showed that it's a bit of all. For some reactions there are so many substrates and enzymes involved that the randomness averages over many reactions and is not even observable, like flipping a coin 1000 times and getting around 500 heads and 500 tails. However, for biological functions which depend on a small number of reactants, fluctuations in these numbers were shown to lead to growth rate differences. For example, unlucky cells were slowing down due to not having enough of a crucial component. For other biochemical functions a long list of different enzymes are needed to carry out several in between steps. It was shown that an unlucky fluctuation in one of the components can cause inefficiencies down the line effectively decreasing fitness. However, some bacteria evidently use the inherent randomness to generate heterogeneous populations where some of the members are less fit to the current environment. When the environment changes however, the less fit members could be more prepared to the new environment allowing the genetic information of the population to survive. A non-stochastic population would simply die off when a negative environmental factor appears while a heterogenous population could survive. Furthermore, this allows lucky members in the population to grow much faster under favourable conditions and increase the population average growth, increasing population fitness. So, stochasticity appears to be an integral part of how bacteria function and this is an active area of research promising to understand more about the effects of randomness on biology.

In chapter 3 we focused on one of the stochasticity dampening mechanism namely cell size control. All bacteria start their lives as a small daughter cell from a mother which has just divided. However as mentioned, life at the molecular level is stochastic which leads to various possibilities for our new daughter cell. Its mother might have divided a bit later or earlier than required leading to bigger or smaller daughters, or the division might not have been perfectly at the middle and now one of the daughters would be smaller while other is larger. If these effects are not corrected somehow by the new cell, eventually the population would have giant and tiny cells which is not what is observed. It was recently shown that bacteria achieve this by the “adder mechanism” where every cell tries to add the same amount of length to itself before dividing. Even if one is borne large or small it adds the same length to itself and divides. This allows next generation to be closer to the population average and dampens heterogeneity and stochasticity. However how bacteria manage to measure the length that they added to decide on when to divide is not known. Furthermore, bacteria size changes according to the growth rate. In an environment where growth is faster cell size is larger compared to a slow growth environment. So, bacteria not only manage to keep size homeostasis in stable environments but is also able to adjust the average size if the growth rate changes. How this is done is also not understood.

There is a signalling molecule called guanosine-tetraphosphate (ppGpp). Level of ppGpp reversely correlates with growth and controls growth rate and many growth dependent processes. If growth is fast, ppGpp is low, if it is slow ppGpp is high. It has many other functions such as stress response under growth arresting conditions

where ppGpp concentrations increase dramatically. However, these are mostly well understood, what it does at concentrations where growth is still permitted on the other hand is not clear. In this chapter we show that the level of ppGpp control not only growth rate but also cell size. A sudden increase in ppGpp levels triggered by production of an engineered enzyme resulted in cell size decreasing rapidly while growth rate takes much longer to stabilize. Indicating that the connection between ppGpp and cell size is growth rate independent. Furthermore, we observed that in order to decrease cell size rapidly, cells transiently decrease their cycle durations. Dividing earlier than they should allow them to become smaller, while growth rate is still high. Later as growth slows down cycle duration also increases to match the new growth regime. These rapid changes to the cycle duration by ppGpp manipulation suggests a link between division machinery and ppGpp which suggest that ppGpp is a link between growth rate and division to regulate average size in a given growth rate.

In chapter 4 we describe our efforts to create a light activated ppGpp hydrolysis enzyme. In wild type bacteria, ppGpp levels respond within couple minutes to a change in the environment. Our method to change ppGpp levels from chapter 3 does not create as fast of a change. This is because it takes time for an induced enzyme to be produced and start to produce or hydrolyse ppGpp. Therefore, in order to answer some questions regarding the effects of rapid ppGpp changes which bacteria normally experience, we need a faster system. To this aim light activated enzymes can be used as they allow instant activation of enzymes. In particular a newly discovered plant enzyme domain called LOV2, can be engineered to fuse with another enzyme to regulate its activity. LOV2 domain has a protein structure called alpha-helix at the end of the enzyme. These helices are structures which occur when specific amino acids are placed in a row in the protein sequence and these then fold onto each other to create a helix. The helix in LOV2 changes localization when correct wavelength of light interacts with the domain. If a target enzyme has an alpha-helix at the beginning, LOV2's end helix can be fused to the target enzyme's and create a continuous alpha helix. This allows the localization change upon light to alter the shape and thus activity of the target enzyme.

A newly discovered ppGpp hydrolysis enzyme from fruit flies called Mesh1 has an alpha helix at the beginning. We tried various different fusion locations to find a version which would change activity under light. One of the constructs that we tried appeared to hydrolyse ppGpp only in light. We tested this by overexpressing a ppGpp synthesis enzyme. In a cell with no other modification, this leads to growth stopping due to ppGpp accumulation. When we added our light activated construct, cells could grow in light but not in dark. Because in light the construct is active and hydrolyses the excess ppGpp allowing growth, however in dark this does not happen as the enzyme is inactive. We further improved this construct by changing some amino acids at the shared helix to increase stability. This led to a better variant where activity in dark was much less.

In chapter 5 we revealed a direct inhibitory role of ppGpp on phospholipid (PL) synthesis. Phospholipids are the building blocks of microbial membranes and their production is directly linked to growth rate. In our work we show that the concentration of the enzyme which diverts resources towards PL synthesis called PlsB does not change with growth rate. Cells always have the same concentration of PlsB, however at slower growth ppGpp inhibits PlsB and diverts resources away from PL production. This allows cells to rapidly increase their PL production upon an improvement to the nutrient condition. If cells were responding slowly by changing the concentration of PlsB enzyme in order to regulate resource flow towards PL synthesis, they would not be able to respond rapidly when the environment improves.

This shows that ppGpp's general role as a transcriptional regulator is only a part of the full story. This molecule can control various enzyme levels directly, responds rapidly to changing environments and balances not only metabolism but also cell size with growth rate. We hope that future developments in visualizing ppGpp at the single cell level along with better control methods such as our efforts in chapter 4 will allow uncovering of the intricate details of bacteria's lives.

Samenvatting

Sinds de oudheid zijn bacteriën een integraal deel van het menselijke bestaan, hetzij als coöperatieve huurders die in en om ons heen wonen, hetzij als een constante bedreiging voor onze gezondheid en ons welzijn. In het begin gebruikten we ze onbewust als hulpmiddelen voor fermentatie en bestreden we ze met lukraak ontdekte natuurlijke remedies. Vandaag de dag, meer dan 3 eeuwen sinds we bacteriën voor het eerst waarnamen, is ons begrip van hun functies enorm toegenomen, samen met ons vermogen om deze functies aan te passen. We hebben op moleculair niveau ontdekt hoe het leven informatie opslaat en overdraagt, hoe deze informatie wordt gebruikt om veelzijdige biochemische machines te bouwen die eiwitten worden genoemd en hoeveel van deze eiwitten hun functies uitoefenen. Samen met een beter begrip kwam het vermogen om de biologische informatie opgeslagen in het DNA aan te passen en om nieuwe eiwitten te creëren die niet in de natuur voorkomen.

Door een beter begrip van het leven op moleculaire schaal waren we in staat om nieuwe bacteriestammen en andere micro-organismen te ontwerpen om chemicaliën en enzymen voor ons te produceren, zoals biobrandstoffen en insuline. Er werden betere geneesmiddelen ontwikkeld die gericht zijn op specifieke moleculaire machines om te helpen bij de bestrijding van bacteriële ziekten. We ontwikkelen zelfs bacteriën om taken uit te voeren die we nog niet nodig hebben, zoals mijnbouw op de maan. Maar zelfs met alle vooruitgang zijn onze kennis en mogelijkheden beperkt in vergelijking met de enorme complexiteit van het leven. Kernvragen zoals hoe bacteriën reageren op een veranderende omgeving, hoe ze omgaan met de onvermijdelijke stochasticiteit op moleculair niveau, hoe ze met ons en andere levensvormen samenwerken en nog veel meer zijn actieve onderzoeksgebieden. Ieder jaar worden nieuwe unieke biochemie en functies ontdekt net als nieuwe soorten bacteriën en micro-organismen. Er valt dus nog veel te leren over het leven op moleculair niveau.

In hoofdstuk 2 hebben we gekeken naar de effecten van stochasticiteit. Het vermogen om individuele cellen te observeren is de afgelopen tien jaar aanzienlijk toegenomen met nieuwe microscopie technieken voor levende cellen waarbij *flow cells* (Eng. Stromingscellen) worden gebruikt om bacteriën op te vangen en te voeden. Dit heeft geleid tot een enorme toename van data over individuele cellen die beschikbaar zijn voor wetenschappers en maakte het mogelijk om verschillen tussen individuele bacteriën met dezelfde genetische code te observeren. Dit toonde aan dat bacteriën, hoewel ze een van de eenvoudigste levensvormen zijn, te maken hebben met een fundamenteel probleem, namelijk de stochasticiteit. Biochemische reacties zijn inherent stochastisch van aard, wat betekent dat de vraag of een reactie zal gebeuren gedeeltelijk afhangt van "toeval". Aangezien de basis van al het leven de biochemie is, zijn alle levensvormen in de aanwezigheid van deze inherente

stochasticiteit geëvolueerd. Bacteriële cellen hebben honderden regulerende paden ontwikkeld die de biochemie van de cel controleren om de stochasticiteit te dempen. Sommige daarvan zijn welbekend en begrepen. Echter, het debat over tot in welke mate stochasticiteit een effect heeft op de bacteriële cellen hebben, is nog steeds gaande; is het simpelweg hinderlijk, een enorm probleem of is het slechts een deel van hun leven waarnaast ze zijn geëvolueerd om er voordeel uit te halen?

Onderzoek in de afgelopen jaren heeft aangetoond dat het een beetje van allemaal is. Bij sommige reacties zijn er zoveel substraten en enzymen betrokken dat de willekeurigheid gemiddeld over veel reacties heen gaat en niet eens waarneembaar is, zoals 500 kop en 500 keer munt krijgen bij 1000 potjes kop of munt. Voor biologische functies die afhankelijk zijn van een klein aantal reactanten is echter aangetoond dat fluctuaties in deze aantallen leiden tot verschillen in de groeisnelheid. Zo vertraagden ongelukkige cellen omdat ze niet genoeg van een cruciaal component hadden. Voor andere biochemische functies is een lange lijst van verschillende enzymen nodig om een aantal tussenstappen uit te voeren. Er werd aangetoond dat een ongelukkige schommeling in een van de componenten kan leiden tot inefficiënties in de rest van de kettingreactie, waardoor de fitness effectief afneemt. Sommige bacteriën maken echter duidelijk gebruik van de inherente willekeurigheid om heterogene populaties te genereren waar sommige van de leden minder geschikt zijn voor de huidige omgeving. Maar wanneer de omgeving verandert, kunnen de minder passende leden beter voorbereid zijn op de nieuwe omgeving waardoor de genetische informatie van de populatie kan overleven. Een niet-stochastische populatie zou eenvoudigweg afsterven wanneer een negatieve omgevingsfactor verschijnt terwijl een heterogene populatie zou kunnen overleven. Bovendien kunnen de gelukkige leden van de populatie hierdoor veel sneller groeien onder gunstige omstandigheden en de gemiddelde groei van de populatie verhogen, wat de fitheid van de populatie ten goede komt. Stochasticiteit blijkt dus een integraal onderdeel te zijn van hoe bacteriën functioneren en een beter begrip van alle effecten hiervan is nog steeds een actief onderzoeksgebied.

In hoofdstuk 3 hebben we ons gericht op een van de stochasticiteitsdempende mechanismen, namelijk de regeling van de celgrootte. Alle bacteriën beginnen hun leven als een kleine dochtercel van een moeder die zich net heeft gedeeld. Maar zoals eerder gezegd, is het leven op moleculair niveau stochastisch, wat leidt tot verschillende mogelijkheden voor onze nieuwe dochtercel. Het kan zijn dat de moeder zich iets later of vroeger heeft opgesplitst dan nodig is, wat leidt tot grotere of kleinere dochters, of dat de verdeling niet perfect in het midden is geweest en dat nu één van de dochters kleiner is, terwijl de andere groter is. Als deze effecten niet worden gecorrigeerd door de nieuwe cel, zou de populatie uiteindelijk reusachtige en kleine cellen vertonen die niet worden waargenomen. Onlangs werd aangetoond dat bacteriën dit bereiken door het "adder mechanisme" waarbij elke cel probeert dezelfde hoeveelheid lengte aan zichzelf toe te voegen voordat hij zich deelt. Zelfs als men groot of klein wordt gedragen, voegt het dezelfde lengte aan zichzelf toe en verdeelt

het zich. Hierdoor kan de volgende generatie dichter bij het bevolkingsgemiddelde komen en wordt de heterogeniteit en stochasticiteit gedempt. Het is echter onbekend hoe bacteriën erin slagen om de lengte te meten die ze hebben toegevoegd om te beslissen wanneer ze moeten delen. Bovendien verandert de grootte van de bacteriën afhankelijk van de groeisnelheid. In een omgeving waar de groeisnelheid hoger ligt, zijn cellen groter dan in een omgeving met een langzame groei. Dus bacteriën slagen er niet alleen in om celgrootte te reguleren in een stabiele omgeving, maar zijn ook in staat om de gemiddelde grootte aan te passen als de groeisnelheid verandert. Hoe dit gebeurt, is ook nog niet bekend.

Er is een signaalmolecuul genaamd guanosine-tetrafosfaat (ppGpp). Het niveau van ppGpp hangt tegenovergesteld samen met de groei en controleert de groeisnelheid en vele processen afhankelijk van groei. Als de groei snel is, is ppGpp laag en als het langzaam is, is ppGpp hoog. Het heeft nog menig andere functies zoals bij de stressrespons onder groeiremmende omstandigheden waarbij de ppGpp-concentraties dramatisch toenemen. Deze reacties zijn echter grotendeels bekend, daarentegen wat het doet bij concentraties waar groei nog wel mogelijk is, is onduidelijk. In dit hoofdstuk laten we zien dat het niveau van ppGpp niet alleen de groeisnelheid controleert, maar ook de celgrootte. Een plotselinge toename van de ppGpp-niveaus, veroorzaakt door de productie van een gemanipuleerd enzym, leidde tot een snelle afname van de celgrootte, terwijl het veel langer duurde voordat de groeisnelheid zich stabiliseerde. Dit geeft aan dat het verband tussen ppGpp en de celgrootte onafhankelijk is van de groeisnelheid. Bovendien zagen we dat om de celgrootte snel te verminderen, cellen tijdelijk hun cyclusduur verminderen. Door eerder te delen dan nodig is het mogelijk om kleiner te worden, terwijl de groeisnelheid nog steeds hoog is. Later, als de groei vertraagt, neemt ook de duur van de cyclus toe om aan te sluiten bij het nieuwe groeiregime. Deze snelle veranderingen in de cyclusduur door ppGpp-manipulatie suggereert een verband tussen het delingsmechanisme en ppGpp, wat suggereert dat ppGpp een schakel is tussen groeisnelheid en deling om de gemiddelde celgrootte in een bepaalde groeisnelheid te reguleren.

In hoofdstuk 4 beschrijven we onze inspanningen om een licht geactiveerd ppGpp hydrolyse enzym te creëren. Bij wild-type bacteriën reageren de ppGpp-niveaus binnen enkele minuten op een verandering in de omgeving. Onze methode om de ppGpp-niveaus uit hoofdstuk 3 te veranderen, doet dit niet snel genoeg. Dit komt omdat het tijd kost om een geïnduceerd enzym te produceren en te beginnen met het produceren of hydrolyseren van ppGpp. Om enkele vragen te beantwoorden over de effecten van de snelle ppGpp-veranderingen die bacteriën in normale omstandigheden ervaren, hebben we een sneller systeem nodig. Hiervoor kunnen lichtgevoelige enzymen worden gebruikt, omdat ze een ogenblikkelijke activering van enzymen mogelijk maken. Een nieuw ontdekt planten-enzym domein genaamd LOV2 kan worden ontworpen om te fuseren met een ander enzym om de activiteit ervan te reguleren. Het LOV2-domein heeft een eiwitstructuur aan het einde die een alfa-helix

wordt genoemd. Deze alfa-helices zijn structuren die ontstaan wanneer specifieke aminozuren op een rij in de eiwitsequentie worden geplaatst en deze vervolgens in elkaar vouwen om een helix te creëren. De helix in LOV2 verandert van locatie als licht van de juiste golflengte het domein raakt. Als een *target* (Eng: doelwit) eiwit een alfa-helix aan het begin bevat, kan de eind-helix van LOV2 worden gefuseerd met het *target* enzym waarbij een onafgebroken alfa helix wordt gecreëerd. Hierdoor kan de locatieverandering van de alfa-helix van LOV2 ook de vorm van het *target* enzym veranderen en daarmee de functionaliteit.

Een nieuw ontdekt ppGpp-hydrolyse-enzym uit fruitvliegjes genaamd Mesh1 heeft een alfa-helix aan het begin. We hebben verschillende fusie-locaties geprobeerd om een versie te vinden waar de enzymatische activiteit onder licht zou veranderen. Een van de constructies die we probeerden leek ppGpp alleen in licht te hydrolyseren. Dit hebben we getest door een ppGpp-synthese-enzym over te produceren. In een cel zonder extra modificatie leidt dit tot het stoppen van de groei door ppGpp-accumulatie. Bij toevoeging van ons licht-geactiveerde construct bleken de cellen in het licht groeien, maar niet in het donker. Dit komt doordat het construct actief is in het licht en dan overschot aan ppGpp afbreekt, waardoor groei mogelijk is, maar in het donker gebeurt dit niet omdat het construct dan inactief is. We hebben dit construct verder verbeterd door een aantal aminozuren op de gedeelde helix te veranderen om de stabiliteit te verhogen. Dit leidde tot een betere variant waarbij de activiteit in het donker gereduceerd was.

In hoofdstuk 5 hebben we een directe remmende rol van ppGpp op de fosfolipidesynthese onthuld. Fosfolipiden zijn de bouwstenen van microbiële membranen en de productie hiervan is direct gekoppeld aan de groeisnelheid. In ons werk tonen we aan dat de concentratie van het enzym dat de toestroom van middelen richting de fosfolipideproductielijn regelt, PlsB genaamd, niet varieert met de groeisnelheid. De concentratie van PlsB in cellen is constant, echter bij tragere groei heeft ppGpp een remmende werking op PlsB en wordt de toevoer van grondstoffen weggeleid van de fosfolipideproductielijn. Dit stelt cellen in staat om hun fosfolipideproductie snel te verhogen bij een verbetering van de aanwezige voedingsstoffen. Als cellen langzaam zouden reageren door de concentratie van het PlsB enzym te wijzigen om de stroom van grondstoffen richting fosfolipidesynthese te reguleren, zouden ze niet snel kunnen reageren wanneer de omstandigheden verbeteren.

Dit laat zien dat de algemene rol van ppGpp als transcriptie-regulator slechts een deel van het verhaal is. Dit molecuul kan het niveau van verschillende enzymen direct controleren, reageert snel op veranderende omstandigheden en brengt niet alleen het metabolisme in balans, maar ook de celgrootte door middel van de groeisnelheid. We hopen dat toekomstige ontwikkelingen in het visualiseren van ppGpp op individueel celniveau in combinatie met betere controlemethoden, zoals onze inspanningen in hoofdstuk 4, het mogelijk zullen maken om de fijne kneepjes van het leven van bacteriën bloot te leggen.

Acknowledgements

After 4 years and a half of hard work, stress, uncertainty and failures here we are at the end of my PhD thesis. This path while riddled with bumps and obstacles was some of the most exciting times of my life, where I have learned so much and conducted research that I couldn't imagine doing back when I was an aspiring student. For that I am proud. However more so I am grateful, for all the friendship, help and knowledge I have received from people I worked with. Work described in this thesis would not have been possible without knowledge centuries in the making and help from experts who I call friends.

First of all, I'd like to thank both my supervisors **Greg Bokinsky** and **Sander Tans**. At the beginning for having a sense of equality and not foregoing my application which was sent to AMOLF and forgotten along with applications of others'. Throughout my project you both were there to discuss any potential issues, provide guidance, criticize mistakes and praise hard work. During our numerous discussions I've never felt overlooked nor ignored and what I had to say always seemed to be important. After hearing so many stories of "horrible" supervisors from other PhD's and PostDoc's I was a bit nervous at the beginning but you both made sure we were in a professional environment where my skills and knowledge were important. Hope to keep in touch after this and collaborate in the future with both of you.

Being in 2 different groups simultaneously was mostly an advantage as I got to meet many skilful people, befriend and learn from them. Here's a thank you all in no particular order. To **Nicole Imholz** for showing me that no matter how hard things get, one should find the energy to conduct their work and rise above challenges. Cannot list here all the things I asked you for help with but we both now they were numerous. You were always easy to talk with and I've never felt like I was annoying you (even though I'm sure I was sometimes), Thanks also for agreeing to be one of my paranymphs, I'm hoping that you won't have to fist fight anyone. To **Rebecca McKenzie** for being an awesome teammate who I never had issues with somehow with all the equipment sharing. Thanks for all the help in cleaning the microscope setup, copying data, fixing stuff and much more. We have synergized perfectly in our use of the microscope and I hope I can find such colleagues in the future. Thanks also for being the other one of my paranymphs. To **Marek Noga** for being a solid friend. I hate making new friends but after 5 minutes of talking to you during my interview I knew that you'd be one rapidly. Who else could I discuss orbital mechanics, medieval sieging techniques and computer games with, inside of the same 10 min conversation? All your biochemistry knowledge which I have taken advantage of numerous times cannot be listed in this short text, but you should know that I am grateful for all. To **Martijn Wehrens** for all the help with microscopy and PDMS chip stuff. We have built the flow cell -*which I believe was the first in the Netherlands!* - together with frustration, sweat and anger. It would not have been

possible without you. Our discussions on politics and economics were also a refreshing change in between all the science. To **Helena Shomar Monges** not only for all the information and help regarding cloning and anything microbiology/genetics, but also for being an energetic group member pushing for new things for the lab. Your insightful comments on how science works these days will certainly be remembered and taken into account in my future directions. To **Vanda Sunderlikova**, for all the strains and small requests I had throughout my project. Even though I spent most my time in Delft, when I was in AMOLF you were always friendly and involved. To **Niels van den Broek** and **Nicole Scherer** for running the Mass Spec and allowing our measurements to go on. To **Elena Fueyo** for all the confidence boosting chats and questions which made me feel useful.

Special thanks to all the students whose projects I've supervised. **Liliana Sokol** for being meticulous in the lab and managing to clone all the required variants within a short period of time. You were quick to learn our techniques and become useful. To **Cindy Geerlings** for your hard work on improving the variants we've made with Liliana. Within 3 months you've managed so much. I hope your skills are recognized throughout your life. To **Sammie Yam** for the extremely small error bars from a colorimetric assay. While I don't condone your decision to move to music as a profession, I think science has lost some good hands. To **Otto Mulleners** and **Maya Louage**, I wish the COVID-19 pandemic did not hit the world while you both were still conducting your projects. You both are amazing in the lab which was demonstrated in the small amount of time you could spend in there. I'm sure you both will manage this process as best as you can and still produce something amazing.

At last I'd like to thank my family. To my parents **Siyaset** and **Ertan** for supporting me in every possible way throughout my education. If not for you I could not be here today. Throughout my PhD, while you were physically far, thanks to technology I could whine and complain about life all the way till my late 20s. To my brother **Onur** for all the hours of chats and gameplay, you are a significant reason my mental health is not in shambles. And lastly to my wife **Cansu**, I can only imagine how annoying I was throughout my PhD. Thanks for putting up with all my many different moods and life choices. Your presence was always soothing and without you I would not be standing where I am today.

Publications

1- **Büke F**, Grilli J, Cosentino Lagomarsino M, Bokinsky G and Tans S. ppGpp is a regulator in bacterial cell size homeostasis. (Manuscript Submitted)

2- Wehrens M, **Büke F**, Nghe P, Tans SJ. Stochasticity in cellular metabolism and growth: Approaches and consequences. *Curr Opin Syst Biol.* 2018;8(March):131-136. doi:10.1016/j.coisb.2018.02.006

3- Noga MJ, **Büke F**, van den Broek NJ, et al. Post-translational control is sufficient to coordinate membrane synthesis with growth in Escherichia coli. *bioRxiv.* 2019:728451. doi:10.1101/728451 (Manuscript Submitted)

4-Willemse J, **Büke F**, van Dissel D, Grevink S, Claessen D, van Wezel GP. SParticle, an algorithm for the analysis of filamentous microorganisms in submerged cultures. *Antonie van Leeuwenhoek, Int J Gen Mol Microbiol.* 2018;111(2):171-182. doi:10.1007/s10482-017-0939-y

Curriculum vitae

Ferhat Büke was born in Bursa/Turkey on August 10th, 1991. He spent most of his pre-university life in Istanbul/Turkey where he attended high school in Kabatas Anatolian Highschool with a major in science and maths. His fascination for evolution and the general complexity of life led to a university preference with biology as the major. After a successful university entry exam, he was granted scholarships from the government and the Bilkent University to attend the Molecular Biology and Genetics program. During his studies in the university he discovered a curiosity and talent for computer programming and specifically automated image analysis. He undertook several projects in Bilkent and University of Zurich where his image analysis skills became valuable for analysing bacterial remains or bird eggs. However, after spending much time in front of the screen he decided that he wanted to do more hands-on work in the lab. So, after graduating from his bachelors, he attended an MSc. program in Leiden University/Netherlands starting 2013. The program's focus was on Microbial Biotechnologies and health however even though his main projects were focused on laboratory work, several image analysis projects were also conducted during his internships. One of the projects was eventually published where he developed from scratch an imageJ based automated image analysis software to identify and measure *Streptomyces* pellets. In 2015 he graduated from his master's program. Now with some lab-work under his belt, he applied and was accepted for his PhD candidateship in the same year for a shared project between 2 institutes, AMOLF and TU Delft with 2 co-promoters. His work during his PhD which is described in this thesis included genetically modifying bacteria, building microfluidic flowcells to trap and observe said bacteria and engineering a chimeric enzyme whose chemical activity could be altered by light.